

Instituto Tecnológico y de Estudios Superiores de Monterrey

Campus Monterrey

School of Engineering and Sciences



Bearing Fault Diagnosis in Spindles using Vibration and Acoustic  
Emission

A thesis presented by

Oscar Darío Tamayo Pazos

Submitted to the

School of Engineering and Sciences

in partial fulfillment of the requirements for the degree of

Master of Science

In

Manufacturing Systems

Monterrey, Nuevo León, October 8<sup>th</sup> 2018



Instituto Tecnológico y de Estudios Superiores de Monterrey

Campus Monterrey

School of Engineering and Sciences

The committee members, hereby, certify that have read the dissertation presented by Oscar Darío Tamayo Pazos and that it is fully adequate in scope and quality as a partial requirement for the degree of Master of Science in Manufacturing Systems.



Dr. Rubén Morales Menéndez  
Tecnológico de Monterrey  
Advisor



Dr. David Ibarra Zarate  
Tecnológico de Monterrey  
Co Advisor



Dr. Antonio Jr. Vallejo Guevara  
Tecnológico de Monterrey  
Committee Member



Dr. Rubén Morales Menéndez  
Dean of Graduate Studies  
School of Engineering and Sciences

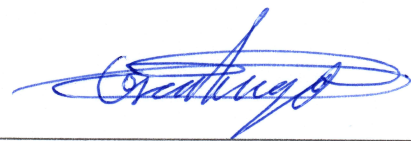
Monterrey, Nuevo León, October 8<sup>th</sup> 2018



## Declaration of Authorship

I, Oscar Darío Tamayo Pazos, declare that this dissertation titled, *Bearing Fault Diagnosis in Spindles using Vibration and Acoustic Emission* and the work presented in it are my own. I confirm that:

- This work was done wholly or mainly while in candidature for a research degree at this University.
- Where any part of this dissertation has previously been submitted for a degree or any other qualification at this University or any other institution, this has been clearly stated.
- Where I have consulted the published work of others, this is always clearly attributed.
- Where I have quoted from the work of others, the source is always given. With the exception of such quotations, this dissertation is entirely my own work.
- I have acknowledged all main sources of help.
- Where the dissertation is based on work done by myself jointly with others, I have made clear exactly what was done by others and what I have contributed myself.



---

Oscar Darío Tamayo Pazos  
Monterrey, Nuevo León  
October 8<sup>th</sup> 2018

@2018 by Oscar Darío Tamayo Pazos  
All rights reserved

# Dedication

I dedicate this work mainly to my family, to my parents for all their unconditional support, their example and their guidance which have helped me to fulfill the goals I set for myself in life.

To my brothers who have been a personal and professional role model that have taught me to be a better person.

To the people of Mexico for making their beautiful country a second home for me during my stay.

To God for giving me the opportunities I have had in my life, the strength to overcome all the adversities and the fortune of knowing so many good people in my life.

Dedico este trabajo principalmente a mi familia, a mis padres por todo su apoyo incondicional, su ejemplo y su guía los cuales me han ayudado a cumplir las metas que me propongo en la vida.

A mis hermanos los cuales han sido un modelo a seguir tanto en lo personal como en lo profesional que me han enseñado a ser mejor persona.

Al pueblo de México por hacer su bello país un segundo hogar para mí durante mi estadía.

A Dios por darme las oportunidades que he tenido en mi vida, la fortaleza para superar todas las adversidades y la fortuna de conocer tantas buenas personas en mi vida.





# Acknowledgements

I would like to express my deepest gratitude to Tecnológico de Monterrey for the tuition support and giving me the life changing opportunity to study in such a wonderful institution.

I thank the Automotive Consortium and BOCAR SA de CV for the given experience to participate in the project *Monitoring and Diagnosis of High Speed Machining Spindles*.

I want to thank to my thesis advisor, Dr. Rubén Morales Menéndez for his guidance and support during this work. I would like to express my deepest thanks to my co advisor Dr. David Isaac Ibarra Zarate for their support, guidance and patience during this work that helped me to achieved the objectives of this research. I would like to express my most sincere thanks to the committee member Dr. Antonio Jr. Vallejo Guevara for the given recommendations and his valuable time and support for the development of this thesis.

Finally, i want to thank CONACyT for the financial support during my studies.



# Bearing Fault Diagnosis in Spindles using Vibration and Acoustic Emission

By

Oscar Darío Tamayo Pazos

## Abstract

In modern automated manufacturing processes, machinery has become more flexible and automatic but also more susceptible to conditions in different parts like spindles. The main conditions affecting them are focused in the shaft and bearings. To successfully detect and identify each condition, methodologies based on new transforms and sensors are used in controlled environments, in order to recognize the conditions effects in vibration and sound.

To detect machining conditions there are two important factors: (1) The feature extraction method and (2) the type of sensor used. In feature extraction methods reviewed, Cepstrum Pre-Whitening (CPW) is remarkable useful for vibration. Its main feature is suppress the shaft speed waveform of the motor in rotational machine systems and help to detect bearing faults. The main sensor used is the accelerometers to acquire vibration, but recently acoustic emission (AE) acquired from transducers are studied to improve the diagnosis along with accelerometers. In this study, an experimental system was built to acquire vibration and AE signals from faulted bearings and a methodology based on *CPW*, tested for vibration signals, was applied for both type of signals to compare and enhance results on machining condition monitoring.

A methodology proposed using *CPW*, envelope spectrum, trend removal, compression and RMS limit filters (the last two just for *AE*) was applied to 9 vibration and 9 *AE* signals taken from the experimental system with the purpose of diagnosing bearing faults in the inner race (*IR*), outer race (*OR*) and rolling element (*RE*) in low frequencies for both signals and high frequencies in *AE*. For the 18 analyzed signals, in 5 the identification of fault components were easily made, in 12 signals the fault identification was possible; but there were peaks with similar amplitudes of the fault components and in 1 signal the identification of fault components was unsatisfactory because there was no peak that matches the bearing fault frequencies. The comparison between vibration and *AE* showed that in 6 from 9 tests, vibration have a better result diagnosing bearing faults than *AE*, specifically in the *IR* and *RE*, for the remaining 3 tests that correspond to *OR*, *AE* have a better result than vibration. Finally, the high frequencies in *AE* revealed that just *RE* faults had high frequency components in one of the three analyzed tests that can be related to remarkable faults in the ball.



# Contents

<b>1</b>	<b>Introduction</b>	<b>1</b>
1.1	Motivation . . . . .	1
1.2	Problem Description . . . . .	2
1.3	Research Question . . . . .	5
1.4	Solution Overview . . . . .	5
1.5	Main Contribution . . . . .	6
1.6	Disertation . . . . .	6
<b>2</b>	<b>State of the Art</b>	<b>7</b>
2.1	Literature Review . . . . .	7
2.1.1	Rolling Element Bearings Monitoring . . . . .	8
2.1.2	Shaft Faults Monitoring . . . . .	10
2.1.3	Methodology approach . . . . .	11
2.2	Theoretical Background . . . . .	11
2.2.1	Rotating Machines Vibration . . . . .	11
2.2.2	Bearings . . . . .	12
2.2.3	Monitoring Systems Sensors . . . . .	13
2.3	Signal Processing and Analizing Methods . . . . .	14
2.3.1	Fast Fourier Transform . . . . .	15
2.3.2	Short Time Fourier Transform . . . . .	15
2.3.3	Cepstrum Pre–Whitening Transform . . . . .	16
2.3.4	Envelope Spectrum . . . . .	17
<b>3</b>	<b>Proposal</b>	<b>18</b>
3.1	Introduction . . . . .	18
3.2	Methodology . . . . .	18
3.2.1	Data Acquisition . . . . .	18
3.2.2	RMS limit filter . . . . .	19
3.2.3	Compression filter (Companding tool) . . . . .	20

3.2.4	Cepstrum Pre-Whitening (CPW) . . . . .	21
3.2.5	Signal envelope . . . . .	21
3.2.6	Trend Removal . . . . .	22
3.2.7	Fast Fourier Transform (FFT) . . . . .	23
3.2.8	Normalization . . . . .	23
3.2.9	Diagnosis . . . . .	24
<b>4</b>	<b>Experimental System</b>	<b>26</b>
4.1	Introduction . . . . .	26
4.2	Experimental System . . . . .	26
4.2.1	Bearing faults diameters . . . . .	27
4.2.2	Design of experiments in test rig . . . . .	28
4.3	Case Western Reserve University database . . . . .	29
<b>5</b>	<b>Results</b>	<b>32</b>
5.1	Introduction . . . . .	32
5.2	<i>CWRU</i> Database for validation . . . . .	32
5.3	Experimental System Database application . . . . .	33
5.3.1	Experimental System Vibration Results . . . . .	34
5.3.2	Experimental System Acoustic Results . . . . .	38
5.4	Results discussion . . . . .	45
5.4.1	Experimental system discussion . . . . .	45
<b>6</b>	<b>Conclusions</b>	<b>47</b>
6.1	Contributions . . . . .	48
6.2	Publications . . . . .	48
6.3	Future work . . . . .	48
	<b>Bibliography</b>	<b>50</b>
<b>A</b>	<b>Acronyms and Variables Descriptions</b>	<b>54</b>
<b>B</b>	<b>Experimental system additional results</b>	<b>56</b>
B.1	Defects measurements . . . . .	56
B.2	Experimental results . . . . .	60
<b>C</b>	<b>Window size selection</b>	<b>62</b>
C.1	<i>CWRU</i> Database . . . . .	62
C.2	Experimental System Database . . . . .	62

C.2.1	Vibration . . . . .	63
C.2.2	Acoustic Emission . . . . .	64
C.2.3	Conclusions about window size selection . . . . .	67
<b>D</b>	<b><i>CWRU</i> Database validation</b>	<b>68</b>
D.1	<i>CWRU</i> Results . . . . .	69
<b>E</b>	<b>Additional results</b>	<b>72</b>
E.1	Experimental system vibration results . . . . .	72
E.2	Experimental system acoustic results . . . . .	73
<b>F</b>	<b>Developed code</b>	<b>75</b>
<b>G</b>	<b>Published papers</b>	<b>92</b>
	<b>Curriculum Vitae</b>	<b>94</b>





# List of Figures

1.1	Spindle system architecture from [SKF, 2018]. . . . .	3
1.2	Spindle monitoring architecture . . . . .	3
1.3	Feature extraction and selection process [Bhuiyan and Choudhury, 2014] . . . . .	5
2.1	State of art division . . . . .	8
2.2	Raw and envelope signals for bearings faults. Modified from [Attoui <i>et al.</i> , 2017]. . . . .	12
2.3	<i>STFT</i> window's distribution. . . . .	16
3.1	Proposed methodology flowchart . . . . .	19
3.2	a) and b) <i>AE</i> raw signal with RMS and time limits c) Signal trimmed d) Compression and e) Expansion examples . . . . .	20
3.3	Compression characteristics (a) $\mu$ -law (b) A-law. . . . .	21
3.4	<i>CPW</i> pre-processing example using <i>AE</i> and vibration signals . . . . .	22
3.5	Envelope example using <i>AE</i> and vibration signals . . . . .	22
3.6	Signal's trend removal process . . . . .	23
3.7	<i>FFT</i> of <i>AE</i> and vibration signals original and normalized . . . . .	24
3.8	Bearing defects spectrum zones . . . . .	25
4.1	Experimental system . . . . .	27
4.2	Experimental system DoE data acquisition example . . . . .	29
4.3	<i>CWRU</i> experimental system [ <i>CWRU</i> , 2018] . . . . .	30
5.1	Vibration signals . . . . .	33
5.2	<i>AE</i> signals before using the compression filter . . . . .	34
5.3	Normal state test:2 vibration signal. . . . .	35
5.4	Experimental System vibration signals after applying the methodology . . . . .	36
5.5	<i>IR</i> Test:2 vibration signal. . . . .	36
5.6	<i>OR</i> Test:1 vibration signal method comparison. . . . .	37
5.7	<i>RE</i> Test:1 vibration signal. . . . .	38
5.8	Normal state test:2 <i>AE</i> signal. . . . .	38
5.9	Experimental System <i>AE</i> signals after applying the <i>CPW</i> methodology . . . . .	39

5.10	<i>IR</i> Test:2 <i>AE</i> signal. . . . .	40
5.11	<i>OR</i> Test:1 <i>AE</i> signal . . . . .	41
5.12	<i>RE</i> Test:4 <i>AE</i> signal method comparison. . . . .	42
B.1	<i>RE</i> condition comparison . . . . .	57
B.2	<i>OR</i> condition comparison . . . . .	57
B.3	<i>IR</i> condition comparison . . . . .	57
B.4	<i>RE</i> vertical defects measurement . . . . .	58
B.5	<i>RE</i> horizontal defects measurement . . . . .	58
B.6	<i>OR</i> 1st defects measurement . . . . .	59
B.7	<i>OR</i> 2nd defects measurement . . . . .	59
B.8	<i>IR</i> defects measurement . . . . .	59
B.9	Normal state <i>AE</i> and vibration signals . . . . .	60
B.10	Inner race <i>AE</i> and vibration signals . . . . .	60
B.11	Outer race <i>AE</i> and vibration signals . . . . .	61
B.12	Rolling element <i>AE</i> and vibration signals . . . . .	61
C.1	Experimental system, <i>OR</i> vibration fault signal at window of 10 revolutions . . . . .	63
C.2	Experimental system, <i>OR</i> vibration fault signal at window of 100 revolutions . . . . .	64
C.3	Experimental system, <i>OR AE</i> fault signal at window of 10 revolutions . . . . .	65
C.4	Experimental system, <i>OR AE</i> fault signal at window of 100 revolutions . . . . .	65
D.1	<i>CWRU</i> analyzed signals used to validate the methodology . . . . .	68
D.2	<i>CWRU</i> signals after applying the proposed methodology . . . . .	69
D.3	<i>IR (Y)</i> category signal method comparison ( <i>CWRU</i> ) . . . . .	70
D.4	<i>OR (Y)</i> category signal method comparison ( <i>CWRU</i> ) . . . . .	70
D.5	<i>RE (Y)</i> category signal method comparison ( <i>CWRU</i> ) . . . . .	71
E.1	<i>IR</i> vibration signals . . . . .	72
E.2	<i>OR</i> vibration signals . . . . .	73
E.3	<i>RE</i> vibration signals . . . . .	73
E.4	<i>IR AE</i> signals . . . . .	73
E.5	<i>OR AE</i> signals . . . . .	74
E.6	<i>RE AE</i> signals . . . . .	74

# List of Tables

2.1	Sensor monitoring systems comparison . . . . .	14
2.2	Feature extraction methods for signal processing . . . . .	14
4.1	Data Acquisition parts for the experimental system . . . . .	27
4.2	6204-2Z SKF Bearing specifications. . . . .	27
4.3	Mechanical parts of the experimental system . . . . .	28
4.4	Experimental system areas of available faults . . . . .	28
4.5	6203-2RS JEM SKF Bearing specifications. . . . .	30
4.6	<i>CWRU</i> diameters and areas of available faults . . . . .	30
4.7	Categorization of <i>CWRU</i> diagnosis results . . . . .	31
5.1	Bearing fault frequency features for experimental system @3858 RPM . . . . .	34
5.2	Bearing fault results for experimental system's database . . . . .	44
5.3	Experimental System results comparison . . . . .	45
5.4	High frequencies found in <i>AE</i> signals for <i>RE</i> fault . . . . .	46
A.1	Acronyms Definitions . . . . .	54
A.2	Algorithms. Variables Descriptions . . . . .	55
B.1	<i>CWRU</i> diameters and areas of available faults . . . . .	56
C.1	<i>Experimental system</i> envelope resolution based on shaft rev. and $F_s = 25,6$ kHz . . . . .	63
C.2	Experimental system <i>OR</i> vibration signals computational times at 10, 25, 50, 100 revs . . . . .	64
C.3	Experimental system <i>IR</i> vibration signals computational times at 10, 25, 50, 100 revs . . . . .	64
C.4	Experimental system <i>RE</i> vibration signals computational times at 10, 25, 50, 100 revs . . . . .	65
C.5	Experimental system <i>OR AE</i> signals computational times at 10, 25, 50, 100 revs . . . . .	66
C.6	Experimental system <i>IR AE</i> signals computational times at 10, 25, 50, 100 revs . . . . .	66
C.7	Experimental system <i>RE AE</i> signals computational times at 10, 25, 50, 100 revs . . . . .	66
D.1	Bearing fault results for <i>CWRU</i> database . . . . .	71



# Chapter 1

## Introduction

It is important to know and recognize the Mexico's role in automotive manufacture. According to the ProMéxico 2018 [México, 2018] report, investment in Mexico's automotive industry represent the 7,17% of the total investment in the first six months of the year and the percentage of money income from exports in Mexico corresponding to the automotive industry is 9.6% in the same lapse of time. Thus, having a better production in the automotive industry and their parts can increase the productivity, profitability and consumption of them worldwide.

To achieve that improvement the process by which these parts are made (e.g. Machining, Milling) should be improved and monitored to get the best possible efficiency. Automotive companies invests big sums of money in the latest technology machinery expecting to have the best performance, but avoiding faults in the equipment is essential to achieve this goal. An unexpected fault can cause accidents, downtimes or stops in processes or even heavy damages in machinery that can cause break downs and financial losses for the companies.

### 1.1 Motivation

Nowadays, machining is one of the most important and widely used process in manufacturing industry instead of forming, molding, and casting processes. Generally, machining can be defined as a process of removing material from a workpiece in the form of chips. In modern automated manufacturing processes, machinery has to become more flexible and automatic [Deris *et al.*, 2011]. Some reviews [Cohen, 1989] have shown that the effective machining time of a machine tool can be increased from 10% to 65% with machines condition monitoring and control systems. In order to increase productivity, enhance quality and reduce costs, spindle and machine tools have to work in the best environment and with the least possible error. Spindle's fault detection and diagnosis like Unbalance (*UB*), Misalignment (*MA*), Bent Shaft (*BS*) or rolling element bearings faults, have always been a challenge in rotating machining monitoring. To face these challenges, new machin-

ing monitoring systems are always being developed for improving machining performance using sensors different from the usual ones and/or new fault recognition algorithms. The intention of this research is to develop a methodology, using this fault recognition algorithms, to detect spindle's faults with better results over the traditional algorithms specially focused in the analysis of vibration and *AE* (Acoustic Emission) signals to diagnose those faults.

## 1.2 Problem Description

The machining processes can be divided in two types: conventional machining, where non automated machines are used to manufacture products like regular lathe and milling machines, and modern machining, where *CNC* (Computer Numerical Control) machines are used to manufacture products with higher precision. Machining centers tend to fail in two specific parts of them, the spindle and tool, which affects directly the process efficiency. Thus, machining monitoring different approaches are focused into tool and spindle conditions to identify and prevent failures.

Both, spindle and tool condition monitoring, get information from different aspects of the same process and analyze that information expecting for a common result, reducing the process overall cost and prevent machine failures. But in spindle monitoring case the specific focus is to prevent spindle failures and extend the spindle's useful life as much as possible. The spindle system is composed by: tool holder, spindle nose, housing, shaft, bearings and pulleys as Fig. 1.1 shows, where the housing hold bearings that allow the free rotational movement of the system. Successful application of machining technology is highly dependent on spindles operating free of faults without overloading the angular load of contact bearings [Cao and Altintas, 2007].

Spindle monitoring architecture has three main different elements or characteristics as Fig. 1.2 shows. The first characteristic allows to identify the type of failure in the spindle; bearing conditions in the Inner Race (*IR*), Outer Race (*OR*), Rolling Element (*RE*) or cage (*C*); the shaft mechanism like *UB*, *MA* or *BS*; or in other housing elements like washers. The second is the sensor used to measure the condition consequence which can be a transducer for *AE*, an accelerometer for vibration, temperature sensors for energy and entropy and an amperemeter for electrical current. The third is the signal processing method, which includes the feature extraction, feature selection and decision making methods that will reveal, classify and control every diagnosable spindle condition respectively.

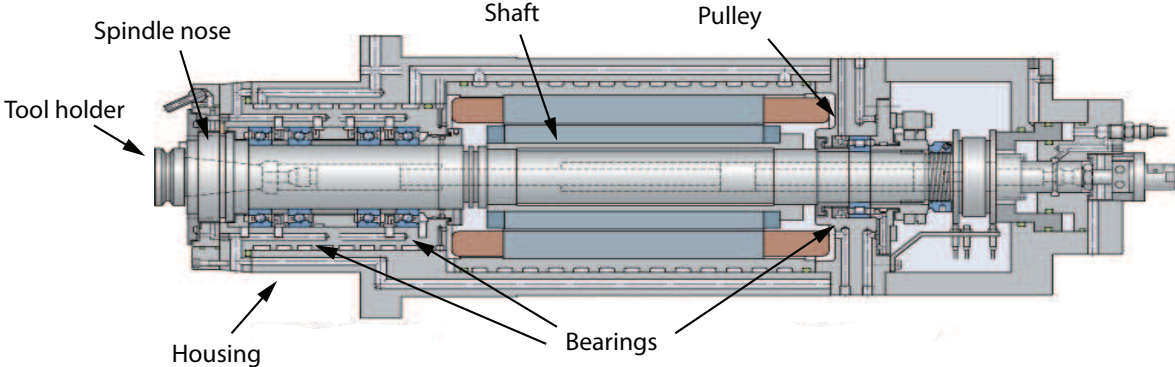


Figure 1.1: Spindle system architecture from [SKF, 2018].

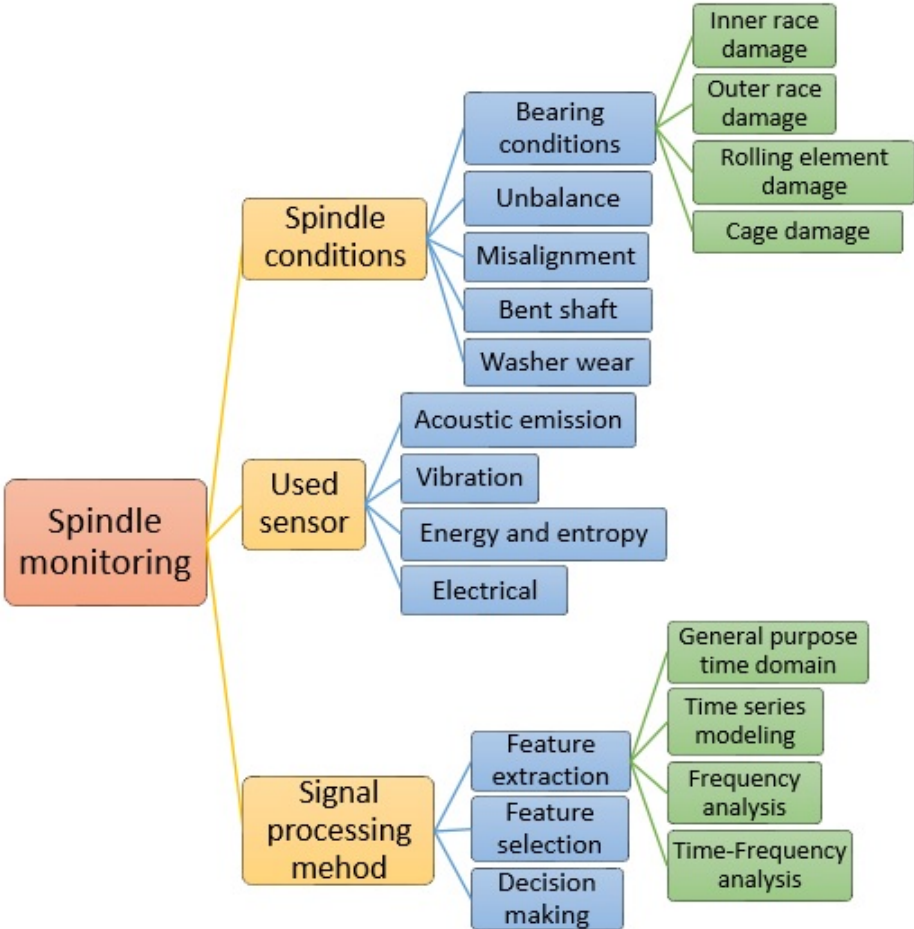


Figure 1.2: Spindle monitoring architecture

The most typical faults in the rolling element bearings are produced by localized wear in the *IR*, *OR*, or the ball. Localized defects include cracks, pits and spalls on the rolling surface, although the dominant fault mode is race spalls. When the *RE* strikes the defect, a shock is produced, exciting high frequency resonances of the structure. The presence of such a defect causes a significant increase in the vibration level [Bediaga *et al.*, 2013]. Those vibration levels can be detected by multiple kind of forms using different sensors as shown in Fig. 1.2, but the most commonly used sensor in spindle monitoring is the accelerometer to measure vibration. On the other hand, *AE* has proven its effectiveness in detecting bearing faults too. Unlike vibration, the *AE* is less affected by noise and by structural vibration e.g. a bearing installed in a mechanical system where the resonance frequencies of the structure between the bearings and the transducers exist at high-frequency resonant bands have more difficulty in detecting bearing faults using vibration than *AE* [McFadden and Smith, 1984].

In spindles, the raw vibration or acoustic signals are illegible and demand signal processing to extract the significant features out of them. Several signal parameters are used to correlate the *UB* level, bearing conditions, *MA* level, washer wear and other occurrences involved in machining with the captured signal such as *RMS* (Root Mean Square), Kurtosis, Peak to Peak (*PTP*) values among others. Usually, the pattern recognition analysis is used to characterize the signal pattern and thus to monitor the spindle performance. But, the most common signal processing method presented in Fig. 1.2 uses feature extraction methods in several domains like time, frequency and time-frequency to detect the occurrences features.

A complete signal processing example process is shown in Fig. 1.3. It begins with an analog signal (Vibration or *AE*) obtained from a data acquisition system, then it gets preprocessing by a filtering system or an *A/D* segmentation to clear noise; after that, the feature extraction method is applied using a time, frequency or time-frequency domain method. In time signals there are some general purpose time domain analyses that reveal the intensity level of occurrences like *RMS*, Kurtosis or *PTP* values. On the other hand, the main frequency domain transformation used is the *FFT* (Fast Fourier Transform); but, when there is noise or difficulty of pattern recognition, other transforms are used like the *CPW* (Cepstrum Pre-Whitening), *STFT* (Short-Time Fourier Transform), *HT* (Hilbert Transform) or *WT* (Wavelet Transform). Finally, with the known signal features, the feature selection method correlate and link those features with previously known ones taught or determined using algorithms like neural networks-based systems ([He and He, 2017], [Hwang *et al.*, 2009]), Neuro-Fuzzy logic ([Attoui *et al.*, 2017], [Yan *et al.*, 2011]), Support Vector Machines ([Guo *et al.*, 2009], [Gowid *et al.*, 2015]), among others. In more complex systems, there are a decision-making method, which takes control of the process settings to solve the abnormal features problem of the signal and therefore resolve the occurrence in the process.



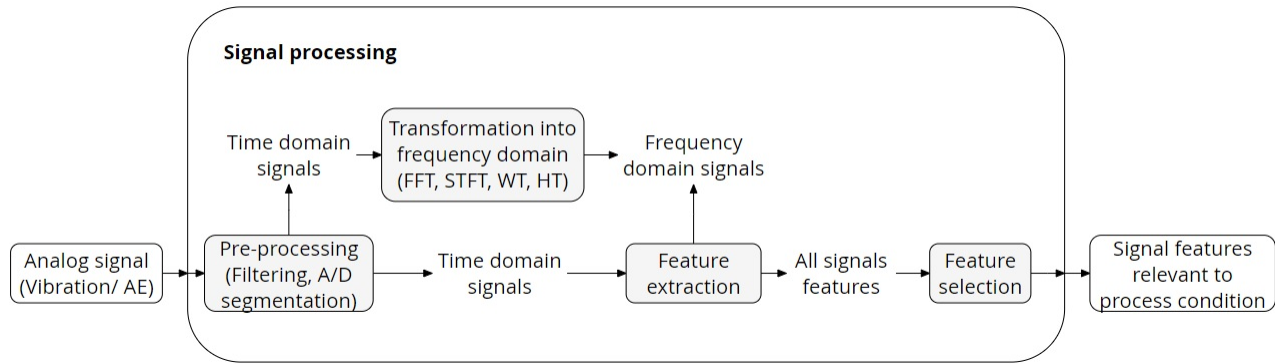


Figure 1.3: Feature extraction and selection process [Bhuiyan and Choudhury, 2014]

### 1.3 Research Question

In machining manufacturing, the main goal is to obtain a machined part with the desired characteristics using the least possible material, energy and time. With this objective, machining condition monitoring is implemented to diagnose any spindle fault and help increase the efficiency of the process. Using this approach, the hypothesis of this proposal is the feasibility of diagnose a bearing spindle fault using a machining condition monitoring system that uses vibration and/or *AE* signals acquired in real time, processed using a frequency domain feature extraction method to recognize and classify the specific condition in the bearing.

Using the aforementioned hypothesis, the purpose of this study divides in two parts:

- To propose a methodology using *CPW* transform to diagnose spindle bearing conditions in the inner, outer race and rolling element of bearing using both vibration and *AE* signals.
- To apply the proposed methodology in bearing fault signals (faults in *IR*, *OR* and *RE* of bearing) obtained from an experimental system with two types of sensors (vibration and *AE*) specially made for this study and diagnose each specific fault using visual inspection in the frequency spectrum obtained from the methodology application, in order to compare vibration and *AE* efficiency to diagnose bearing faults using this methodology.

### 1.4 Solution Overview

The purpose of this study is to propose a methodology using *CPW* and other pre-processing methods like Trend removal, Companding filter and Envelope spectrum to get an easily diagnosable spindle monitoring system using both vibration and *AE* signals. The road to this purpose can be achieved by the application of the proposed methodology in vibration and *AE* signals obtained specially from an experimental system constructed to simulate bearing faults in the *IR*, *OR* and *RE*.

This in order to test the efficiency and reliability of the vibration and *AE* signals using a well know diagnose method like *CPW* and comparing it with some basic methods like *FFT* and Envelope Analysis. The study can help to identify the main advantage and disadvantages of each type of sensor to help as starting point in the hybrid sensor monitoring systems development to diagnose spindle conditions.

## 1.5 Main Contribution

The main contribution of this study is focused on the application of the methodology with *CPW* and other pre-processing methods like trend removal and companding filter in the vibration and *AE* signals obtained from an experimental system to diagnose bearing faults, with the purpose of study the *CPW* algorithms in *AE* signals and compare their efficiency with vibration signals from the same tests. Also, a dual (vibration and *AE*) sensor monitoring system could be developed with this study to increase data acquisition systems performance with the inclusion of transducers (eg. microphones) that help to diagnose parts of the spindle that are hard to reach without modifying spindle architecture.

## 1.6 Disertation

This thesis is structured as follows:

- **Chapter 2** introduces the state of art for different approaches of signal analysis in bearing fault detection emphasizing the Cepstrum Pre-Whitening method and vibration/*AE* research done. Also, this chapter includes theoretical background of Bearing faults, Fast Fourier Transform, Short-Time Fast Fourier Transform, Cepstrum Pre-Whitening and Envelope Spectrum.
- **Chapter 3** introduces the proposed methodology for each type of signal (vibration and *AE*) with a detailed description of each part.
- **Chapter 4** introduces two case studies used for validate the methodology: Case Western Reserve University bearing database, Experimental system database including construction of test rig and *DoE* (Design of Experiment).
- **Chapter 5** shows the results produced by the proposed methodology and a comparison with other traditional methods.
- **Chapter 6** presents the conclusions, contributions made with this work, published articles during this research and introduces future work.

# Chapter 2

## State of the Art

### 2.1 Literature Review

The machining condition monitoring research can be done using multiple signals of the machine (e.g Vibration, Acoustic Emission, Current) for diagnose *UB*, Rolling element bearings faults, *MA*, *ML*, etc. These machine signals are processed using several methods in the literature; the best know method in frequency spectrum signal processing is the *FFT*, nevertheless is the method most susceptible to noise, for this reason different methods, using *FFT* as its base, are proposed in the literature to clean different kind of noises.

In the literature review done in this study the main approaches were finding out vibration and *AE* based experiments that use *FFT* (Fast Fourier Transform), *STFT* (Short-Time Fourier Transform) or *CPW* (Cepstrum Pre–Whitening). Any other work that uses other approaches like *WT* (Wavelet Transform) or *HHT* (Hilbert–Huang Transform) were used as state of art for vibration and *AE* signal processing. Its important to say that most of the works reviewed have industrial equipment or test rigs that runs on rotational speeds lower than 10,000 RPM, except [Gowid *et al.*, 2015] that worked with an air blower with a rotational speed of 15,650 RPM, in order to train an algorithm to diagnose bearing faults on its system. The sensor signals division is illustrated in Fig. 2.1a, where the total of works are 21 and there are works that used both *AE* and vibrations signals. In the other hand, the fault approach has a wider classification because it can be about bearing faults: Inner Race (*IR*), Outer Race (*OR*) or Rolling Element (*RE*). Or fault faults: misalignment (*MA*), mechanical looseness (*ML*), unbalance (*UB*) among others. Fig. 2.1b shows the literature review fault approach classification where same as Fig. 2.1a, there are 21 works and there are works that study all bearing faults, some bearing faults, *UB* and *MA*, just *UB* or just *MA* among others.

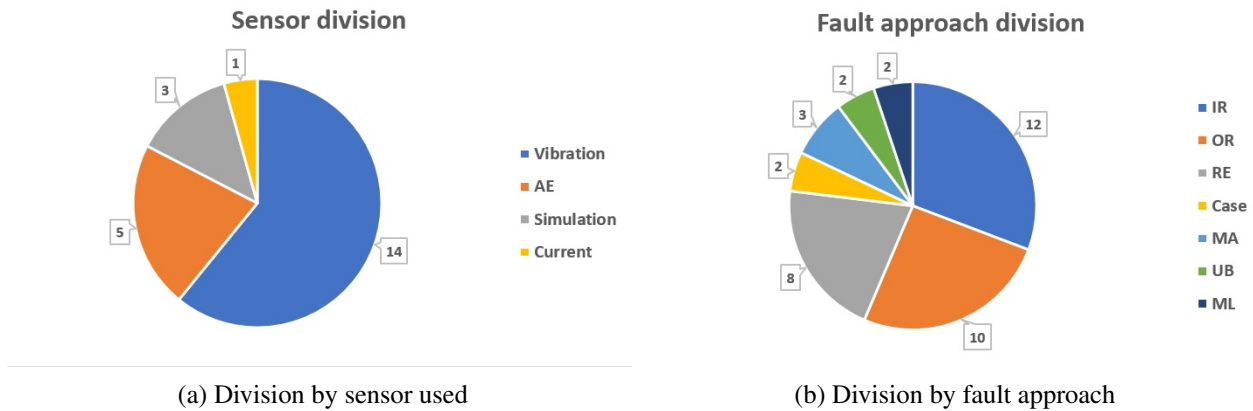


Figure 2.1: State of art division

### 2.1.1 Rolling Element Bearings Monitoring

The bearing condition based monitoring is the principal focus of this study. For this reason most of the works despite of not being fully focused into spindle bearings monitoring, a good approach can be achieved using the current literature focused in general rotating machines bearing diagnose. A lot of works have a *FFT* analyses as base reference of bearing condition monitoring performance like [Bediaga *et al.*, 2013], [Bujoreanu *et al.*, 2013], [Boudiaf *et al.*, 2016] [Gowid *et al.*, 2015], [Phadatare and B., 2016]. As Fig. 2.1b shows, the main bearing faults that are studied in the literature are *IR*, *OR* and *RE* faults; most of them using the Case Western Reserve University (*CWRU*) database like in [Attoui *et al.*, 2017], [Boudiaf *et al.*, 2016], [Quiroga *et al.*, 2012] and [Smith and Randall, 2015]. In the others, experimental test rigs where implemented using electric motors, industrial equipment or simulated signals. In terms of feature extraction methods used to diagnose bearing faults, the three main methods reviewed were: *FFT*, *STFT*, and Cepstrum Analysis (*CA*) and for each one different works were reviewed and analyzed focusing into database used, fault detection approach and results obtained:

- *FFT*

[Bediaga *et al.*, 2013] used four different methods to diagnose bearing faults in a test bench with two different fault diameters: 2.5 and 4.5 mm; the method used were *FFT*, *CA*, *HT* and *AD* (Amplitude Demodulation); the approach of this investigation was the comparison of traditional signal processing algorithms to diagnose bearing faults and the results using *FFT* corresponding to  $\phi 2.5mm$  were non distinguishable and for  $\phi 4.5mm$  the results were that high amplitudes at the resonance frequencies show the presence of the fault but not at low amplitudes. [Boudiaf *et al.*, 2016] used four different methods to diagnose bearing faults in *CWRU* vibration signals; the methods used were *FFT*, *CA*, Envelope Analysis (*EA*), and *WT*. As [Bediaga *et al.*, 2013], the approach of

this investigation was to make a comparative study of newer methods of bearing fault diagnosis. The results using *FFT* were that it allows the detection of the fault but a strong disadvantage is the inability of the method to determine the component of bearing which is defective. [Gowid *et al.*, 2015] used *FFT* to diagnose bearing faults using *AE* signals in an industrial air blower simulating faults in the *OR*; the rotational speed of the experiments were 15,650 RPM which can be considered as *HSM*. Finally the approach of this work was the classification of the datasets obtained using a Support Vector Machine (*SVM*).

[Quiroga *et al.*, 2012] used *FFT*, *EA* and *CA* to diagnose bearing faults in a test rig using vibration signals and validating the method with *CWRU* signals too, his objective was carrying out a comparative study of them. The results obtained with the *FFT* were not the best because the algorithm had natural frequencies interference of the system; compared to the other two methods studied in this work at diagnose bearing faults, it was not the best algorithm. [Guo *et al.*, 2009] used *FFT* along with *EA* to diagnose bearing faults in a test rig using vibration signals with the objective of classify them using *SVM* algorithm. In their work, before using the *EA*, they filtered the signal with a band-pass filter to obtain frequencies between 1 to 5 KHz, then the *EA* is applied using the *HT* and the *SVM* algorithm is used to classify the signals.

- ***STFT***

[Attoui *et al.*, 2017] used *WPT* and *STFT* to diagnose bearing faults in *CWRU* signals; where *WPT* decompose the signal into four data sets and the *STFT* is applied to the lower frequency data set with 10 windows and no overlap to eliminate the redundancy of information; finally they are classified using a Linear Discriminant Analysis (*LDA*). [He *et al.*, 2016] used a *STFT* and Manifold Analysis based methodology to diagnose bearing faults using *AE* signals in a test rig; the Manifold Analysis approach is extract the variation among the manifolds to reflect the condition states of a mechanical system rather than abstracting a feature by averaging all points with the time evolution. The tests were did at several rotational speeds (120, 240, 360, 480 and 600 RPM) were the better results obtained were in 240 and 360 RPM showing a better separation of faults than the other speeds.

- ***CA***

*CA* was used by [Bediaga *et al.*, 2013] to diagnose bearing faults in a test bench with two different fault diameters: 2.5 and 4.5 mm; the results using this methods were bad for  $\phi 2.5mm$  and  $\phi 4.5mm$  due to the need of exact spacing frequency to the algorithm work properly. [Boudiaf *et al.*, 2016] also used *CA* to diagnose bearing faults in *CWRU* database. The results using *CA* were that it can detect the fault and identify its nature with a certain amount of confidence but its main disadvantage is that it generates many undesired large peaks near the zero point; which makes the output a little difficult to interpret. [Choi and Kim, 2007] used a variation of the *CA* called

Minimum Variance Cepstrum (*MVC*) which uses a band-pass filter to detect the fault striking other bearing elements as impulses convolved with a periodic impulse train; the approach of this study was studying the feasibility of *MVC* in bearing fault detection using a test bench and bearing fault simulated by an electric drill pen and a sharp file with fault dimensions of 6x0.34 mm for *OR* and 6x0.42 mm for *IR*. The results were successful for 3 of 4 signals presented using this methodology but it is important to say that the analyses were made just in the time domain.

[Fan and Li, 2015] used another variation of the *CA* called Cepstrum Pre-Whitening (*CPW*) which is a method for separate the discrete components and random components of a signal. The main interest in the signals from a faulty bearing is the random part rather than the deterministic, so its a wise choice to filter all the deterministic components to facilitate bearing diagnosis. It is important to mention that *CPW* remove both harmonics and modulation sidebands of a signal when applied [Randall and Sawalhi, 2011]. This investigation approach was the bearing diagnosis using vibration signal acquired from a planetary bearing gearbox using an hybrid methodology based on *CPW*, Minimum Entropy Deconvolution (*MED*) as filtering methods and *EA* as the feature extraction method. The results obtained from this work divided in two parts: *IR* and *OR*. For the *OR* the diagnosis results were successful in different tests with variable load of 30, 50 and 70 Nm and variable location of the sensor putting it in the external or internal part of the gearbox. On the other hand, the *IR* the diagnosis results were mixed where all the different load signals with the sensors in the external part was non diagnosable and the internal sensor location in all the load were successfully diagnosable.

[Smith and Randall, 2015] used three different methodologies to compare their efficiency in diagnose bearing faults using *CWRU* database, one of the methodologies is based in the *CPW*. The methodologies used by them were based on: (1) *EA*, (2) *CPW* + *EA* and (3) Discrete/random separation (*DRS*) + Spectral Kurtosis (*SK*) + *EA*. From all of these methodologies the results were reported in three different types of diagnosable signal: (*Y*) for easily diagnosable, (*P*) for partially diagnosable and (*N*) for non-diagnosable; a full description of this classification can be seen further in section 4.3. The comparison made between the methodologies were done based on the difficulty of diagnose where the first methodology was better for partial and non diagnosable signals, the second for easy diagnosable and the third had the better results for non and easy diagnosable.

## 2.1.2 Shaft Faults Monitoring

Other machine faults like *UB*, *MA*, and *ML* are also studied widely using the previous mentioned methods in 2.1.1 but using less elaborated methods because the unbalance condition is measured in the shaft speed and its harmonics which are located in low frequencies. From the works reviewed in this study there are four that focused their investigation into shaft faults:

[Chandra, 2016] studied shaft fault detection in rotor bearing systems using time frequency techniques like *STFT*, *CWT* and *HHT* in a simulated model system where the faults diagnosed were

*UB* and *MA* and Shaft Crack (*SC*) where *STFT* can detect *UB* and *MA* with lower performance compared to the other methods and in *SC* it cannot detect the fault. [Hwang *et al.*, 2009] used *CA* to diagnose bearing faults but with shaft approach (e.g *UB*, *MA* and *ML* in rotating bearing systems) and used an *ANN* to classify them. The feature extraction method used in this study was specifically Cepstrum - coefficient extraction method which is a time domain extraction method to compare signal's coefficient to normal state and reveal faults.

### 2.1.3 Methodology approach

Literature review done in this study was focused into three specific feature extraction methods: *FFT*, *STFT* and *CA*. Most of them are widely applied into bearing and shaft fault diagnosis both in vibration and *AE*; but there is an specific variation of *CA* that is *CPW* analysis that was being studied just for vibration and there are no studies of this technique focused into *AE*. For that reason, the most solid methodology developed by [Smith and Randall, 2015] in their work using *CPW* and *EA* to diagnose bearing faults in vibration signals is proposed for *AE* applications to determine its feasibility.

## 2.2 Theoretical Background

The main theoretical background in this work is based on the vibration occurring in the spindle's machining centers, that can be detected using vibration and *AE* sensors, where and how they affect it but specially which parts of the spindle are the most compromised by these vibrations. The main spindle defects according to [Randall, 2011] are *MA*, *UB*, *BS*, *ML* and *RE* bearing defects. The main approaches of this work is *RE* bearing defects described in section 2.2.2. For monitoring and detecting those conditions there are specific purpose sensors described in section 2.2.3 and specialized methods presented in section 2.3. The vibrations and acoustic sound signals processing can be analyzed using Fast Fourier Transform (*FFT*), section 2.3.1, Short Time Fourier Transform (*STFT*), section 2.3.2, Cepstrum Pre-Whitening (*CPW*), section 2.3.3 or Wavelets Transform (*WT*) among others.

### 2.2.1 Rotating Machines Vibration

Rotating machines have dynamic components in their design, which when get damaged, cause vibrations. Those forces, produced by cyclic variations in the dynamic components of the cutting forces, usually start as small chatter responsible for the serrations on the finished surface of the machining piece and chip thickness irregularities, and progress to what has come to be commonly termed vibration. [Dimla, 2004] has measured the tool holder vibration and correlated them with

the tool wear. The observation has shown that at different cutting speed, the magnitudes of vibration signal spectra were higher along the z-axis and lower along the x-axis, which was observed to be significantly small along the y-axis. Vibration also tend to change with the speed and load of a machine, so for condition monitoring purpose the speed and load must be constant, which will be typically stationary and/or cyclo-stationary signals.

It is important to reduce those vibration as much as possible to ensure a long life-time of the rotating machine. They tend to change with the speed and load of a machine, so to guarantee a stationary vibration signals is recommended to work with constant speed and load.

## 2.2.2 Bearings

Bearings faults are the main machine's breakdown reason in rotating machines. The vibration generated by its faults are being widely studied using different methods like Wavelet Transform (*WT*), Short Time Fourier Transform (*STFT*), Wigner-Ville Transform (*WVD*) among others. Fig. 2.2 shows typical vibration signals of a rolling element bearing with localized faults in the main parts of it: *IR*, *OR* and *RE* as well as its envelope behavior respectively. In order to locate the defect frequencies the following kinematic formulas (2.1), (2.2) and (2.3) [Randall, 2011] are used based on the bearings characteristics:

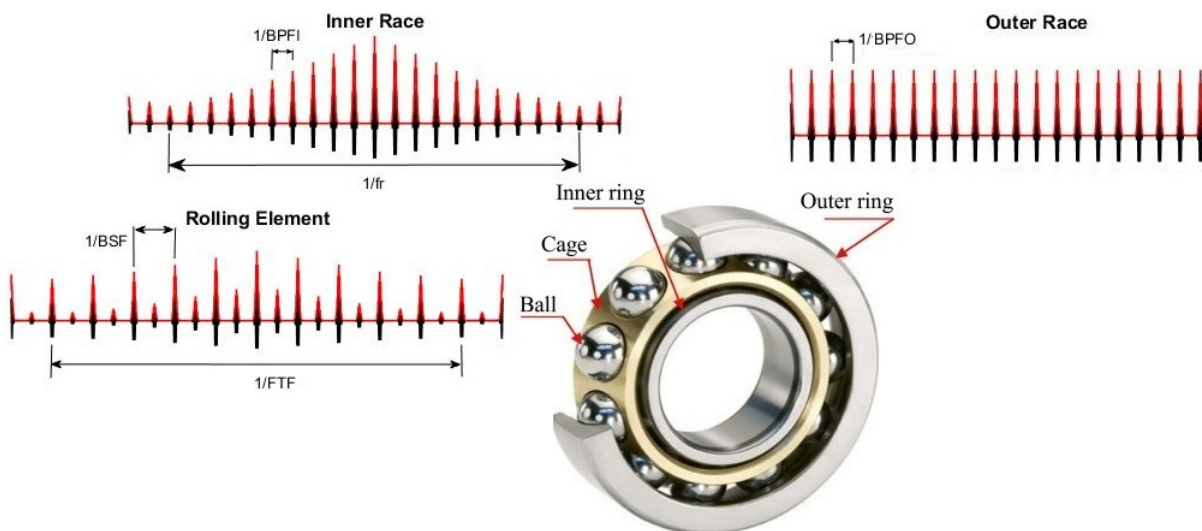


Figure 2.2: Raw and envelope signals for bearings faults. Modified from [Attoui *et al.*, 2017].



$$BPFO = \frac{n * f_r}{2} \left( 1 - \frac{d}{D} \cos(\alpha) \right) \quad (2.1)$$

$$BPFI = \frac{n * f_r}{2} \left( 1 + \frac{d}{D} \cos(\alpha) \right) \quad (2.2)$$

$$BSF = \frac{D * f_r}{2d} \left( 1 - \left[ \frac{d}{D} \cos(\alpha) \right]^2 \right) \quad (2.3)$$

where  $f_r$  is the shaft speed,  $n$  is the number of *RE*,  $d$  is the *RE* diameter,  $D$  is the pitch bearing diameter and  $\alpha$  is the angle of the load from the radial plane. It is important to mention that in *BSF* the ball strikes the same race (*IR* or *OR*) so in general there are two shocks in frequency spectrum per basic period. However, these frequencies are obtained assuming no slip, and in fact there is always be some slip because of the angle  $\alpha$ , which varies with the position of each *RE* in the bearing as the ratio of local radial or axial load changes, thus each rolling element has different rolling diameter and speed.

### 2.2.3 Monitoring Systems Sensors

Health's machine monitoring is mostly inspected using data acquisition systems based on vibration accelerometer sensors. But, there is a tendency in investigation which is the study of *AE* sensors on monitoring systems. As section 2.2.1 presents, vibration caused by machines faults in constant speed and load tends to get stationary or cyclo-stationary behavior which can be detected using accelerometers and common signal processing methods in modulated signals. In the opposite case when speed and load are variable through time the vibrations signals have a non-stationary behavior e.g. engine starts. But in the *AE* case there are studies, [Law *et al.*, 2012], that shows that *AE* also has modulations signals frequencies that represent faults generated by shaft and bearings conditions. Those frequencies are focused in the high frequency. Using [Abellan-Nebot and Subirón, 2010], and [Bhuiyan and Choudhury, 2014] sensor application reviews in machining monitoring systems and *TCM* (Tool Condition Monitoring) respectively, a sensors comparison for wear machining monitoring in cost, intrusive nature, signal reliability and other applications are presented in Table 2.1 where more checkmarks means a higher level of the feature e.g cost, intrusive nature.

Table 2.1: Sensor monitoring systems comparison

<i>Sensor</i>	<i>Cost</i>	<i>Intrusive nature</i>	<i>Signal reliability</i>	<i>Applications</i>
Dynamometer	✓✓✓	✓✓✓	✓✓	Tool wear (flank, crater, notch, and nose wear) monitoring; Machinability observation; Process monitoring
Accelerometer	✓✓	✓✓	✓✓✓	Process monitoring; Flank wear estimation
<i>AE</i>	✓✓	✓✓	✓✓	Chatter monitoring; Tool wear and breakage monitoring
Current/Power	✓	✓	✓	Tool (flank) wear monitoring

## 2.3 Signal Processing and Analyzing Methods

In machining condition monitoring the vibration signals are captured and recorded by the vibration/ *AE* sensor and then a feature extraction method is used, which is usually a general purpose time-domain method. There are two types of distributions patterns in a time vibration signal which are stationary and non-stationary. Stationary can also divided themselves into random and deterministic stationary signals. Most of vibrations signals for a one shaft rotating machine tends to be stationary deterministic signals which are signals made up entirely of discrete sinusoidal components. [Bhuiyan and Choudhury, 2014]’s review list and describe some signal pre and post processing method, specifically feature extraction methods are presented in Table 2.2.

Table 2.2: Feature extraction methods for signal processing

<i>General purpose time–domain</i>	<i>Time–series modeling</i>	<i>Frequency</i>	<i>Time–Frequency</i>
<i>RMS</i>	1st, 2nd, 3rd, 4th, 5th order AR.	<i>FFT</i>	<i>WT</i>
Variance	Moving average	<i>DFT</i>	<i>DWT</i>
Kurtosis	AR moving average	<i>STFT</i>	<i>WPT</i>
Signal power	<i>KLT</i>		<i>HHT</i>
PTP or PTV amplitude	Signal spectrum		<i>WVD</i>
Crest factor	Permutation entropy		
Ratio of signal increment			

*RMS* value is used to recognize if a signals is stationary because it represent the energy content of a vibration/*AE* signal. Same as Kurtosis which indicates the intensity level of occurrences present in those signals. Besides this, the frequency analyses methods like *FFT* can significantly expedite an existing spindle machine condition. The development of *FFT* allows the conversion of time-domain data into frequency spectra with ease with the objective of obtain a frequency

decomposition of the original signal in which abnormal features can be detected in a simpler way. On the other hand, Time-Frequency domain signals are used to represent the occurrences both in the time and frequency extent concurrently for non-stationary vibration signals. The *STFT* is a time-frequency analysis based on the *FFT* which is commonly used in the non-stationary signal processing. In vibration, previous knowledge of bearing or unbalance conditions can be used to assess a spindle condition or detect faults present in a machine and asses the fault severity. *AE* is still an experimental detection sensor approach, so there are no standards for machine condition detection that endorse the use of *AE* in the industry expect for tool breakage or stops due to machine failure which are simpler cases of machine conditions.

### 2.3.1 Fast Fourier Transform

*Fast Fourier Transform (FFT)* is one of the most used frequency method in the rotating machines diagnose for its ability to analyze stationary signals and obtain information of them using frequency spectrum. The *FFT* method is based on the *DFT*, being this one a more efficient version of *DFT* presented in equation (2.4) in terms of computational resources needed [Cao and Fan, 2011].

$$X_k = \sum_{n=0}^{N-1} x(n)e^{-jwn} \quad (2.4)$$

where  $x(n)$  is the discrete vibration signal and  $N$  is the total samples in  $x(n)$ . This version of the *DFT* when the signal is discrete and finite corresponds to the Fourier series in which the direct transform is divided by the length of the signal  $N$  to provide components of the Fourier series correctly scaled. *FFT* is good enough to describe a stationary signal behavior. However, when it's used with non-stationary signals, it averages the frequency composition over the duration of the signal; in result *FFT* will show an unaccurate frequency spectrum in non-stationary signals case. If *FFT* is used in random transient or stationary, the scaling must be adjusted according to the Nyquist criteria.

### 2.3.2 Short Time Fourier Transform

*Short Time Fourier Transform (STFT)* is a time-frequency *FFT* based distribution which is used because of its ability to analyze non-stationary signals. Traditionally, time-frequency distributions are used to reveal the bearing failure patterns evolution through time, which represent the energy of the failure frequency that correspond to a bearing failure[Lopez-Ramírez *et al.*, 2016]. The basic idea is to split the signal into segments with a short time window as Fig. 2.3 shows, and then apply *FFT* to each segment. The *STFT* of a signal is represented in equation (2.5):

$$X_{STFT}(w) = \sum_{n=0}^{\infty} x(n)h(n - mR)e^{-jwn} \quad (2.5)$$

where  $x(n)$  is the discrete vibration signal,  $h(n-mR)$  is the short time window and  $mR$  is the overlap between windows. Among the existing windows, the most used is the *Hanning* window, which considers a 50% overlap. This window has a better accuracy in frequency estimation compared to other windows, such as *rectangular*, [Yan *et al.*, 2011]. However, there is an inherent disadvantage in the *STFT*, the compensation between time and frequency resolutions, meaning that the higher the frequency resolution, the lower the time resolution and vice versa, [Gu *et al.*, 2002]. Unlike the *FFT*, the *STFT* can be used for the analysis of non-stationary signals, such as machining signals, where the shaft speed and the effort of the spindle vary with respect to time.

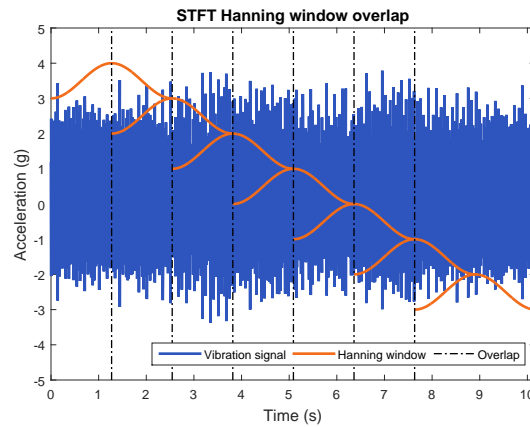


Figure 2.3: *STFT* window's distribution.

### 2.3.3 Cepstrum Pre–Whitening Transform

*Cepstrum Pre–Whitening (CPW)* is a pre processing method of the signal. It is based on the *Cepstrum* principle that allows highlighting the effects of bearing failures, removing shaft speed frequency, its harmonics and sidebands from unwanted components [Barbini *et al.*, 2016]. The *Cepstrum* contains information on the ratio of change of the components of the spectrum in frequency, so that a series of components separated at a constant distance in the spectrum is observed as a peak in the *Cepstrum* at the period of the base frequency. In the *CPW*, the *Cepstrum* is used to remove not wanted components and resonances, which is done by setting the real *Cepstrum* as a reference of the spectrum. It can be implemented using the equation (2.6):

$$x_{CPW} = \mathcal{F}^{-1} \left\{ \frac{\mathcal{F}(x)}{|\mathcal{F}(x)|} \right\} \quad (2.6)$$

where  $\mathcal{F}(x)$  is the *Fast Fourier Transform* of the signal and  $\mathcal{F}^{-1}(x)$  is the *Inverse Fast Fourier Transform*. Bearing failures cause cycle-stationary conditions which are not strictly periodic, so they are not affected by the algorithm of the *CPW*.

### 2.3.4 Envelope Spectrum

Envelope spectrum analysis using Hilbert Transform (*HT*) as a pre-processing method is widely used in the bearing fault detection ([Guo *et al.*, 2009],[Ho and Randall, 2000],[Sheen, 2007]). The envelope signal  $E(t)$  of a original signal  $s(t)$  can be obtained by taking the amplitude of the analytical signal formed from  $s(t)$  as the real part and its Hilbert transform as the imaginary part. Then the envelope spectrum can be obtained by taking the FFT of the envelope signal  $E(t)$ . Given the real time signal  $s(t)$ , the Hilbert Transform  $h(t) = H[s(t)]$  is defined as [Boashash, 1992] did in equation (2.7):

$$h(t) = H[s(t)] = \frac{1}{\pi} \int_{-\infty}^{\infty} \frac{s(\tau)}{t - \tau} d\tau = \frac{1}{\pi t} * s(t) \quad (2.7)$$

Therefore,  $h(t)$  is obtained as the convolution of the function  $\frac{1}{\pi t}$  and the original signal  $s(t)$ . Since the Fourier Transform of  $\frac{1}{\pi t}$  is defined in equation (2.8):

$$F\left(\frac{1}{\pi t}\right) = -j \operatorname{sgn}(f) = \begin{cases} -j & \text{if } f > 0 \\ j & \text{if } f < 0 \end{cases} \quad (2.8)$$

The Hilbert transform can be used as a filter of unitary amplitude and phase  $\pm 90$  depending on the sign of the frequency of input signal spectrum. The real signal  $s(t)$  and its Hilbert transform  $h(t)$  can form a new complex signal called the analytical signal defined in equation (2.9).

$$z(t) = s(t) + jh(t) \quad (2.9)$$

Finally, the envelope  $E(t)$  of the complex signal  $z(t)$  is shown in equation (2.10).

$$E(t) = |z(t)| = |s(t) + jh(t)| = \sqrt{s^2(t) + h^2(t)} \quad (2.10)$$

Doing the spectrum analysis using *FFT* to the envelope signal  $E(t)$ , the envelope spectrum can be obtained. When a fault is present in a rolling element bearing, some of the characteristic frequencies shown in 2.2.2 appear in the envelope spectrum. These frequencies according to [Ho and Randall, 2000] are quite clear using envelope spectrum and can be used as a reliable source for bearing diagnosis.

# Chapter 3

## Proposal

### 3.1 Introduction

A methodology proposed by [Smith and Randall, 2015] for bearing fault detection using *CPW* and *EA* with vibration is presented; this methodology was applied only for vibration and the specific method *CPW* has not been applied in *AE* so the application to audio signals is a new approach. First the signal is acquired by the acquisition system; then the kind of signal is selected among vibration and *AE* by a selection criteria. If the signal is *AE* two pre-processing filters are applied before the methodology, which are *RMS* limit filter and compression filter with the purpose of expanding the bearing fault transient hidden in the *AE* signal. If the signal is vibration then the methodology is directly applied. The methodology is based on *CPW* and *EA*, where its first step is perform the *CPW*, followed by the envelope spectrum of the signal, after this the trend and mean of the signal are eliminated to clear any offset from external sources and the *FFT* is performed to analyze the frequency spectrum. Finally a normalization is made to compare vibration and *AE* signals in an equal scale and the diagnose of the frequency spectrum is done.

### 3.2 Methodology

The methodology purpose is detect bearing faults (*IR*, *OR*, *RE*) and shaft faults (*UB*) by combining several filters and frequency techniques, Fig. 3.1. To execute the methodology *MATLAB* software was used. The steps of the methodology are described below:

#### 3.2.1 Data Acquisition

The signal to analyze must come from a sensor attached to the machine spindle (accelerometer for vibration), or close to it (transducer for *AE*). The sensor must have a sampling frequency high enough to detect the fundamental frequencies and first harmonics of the bearing's and shaft's faults.

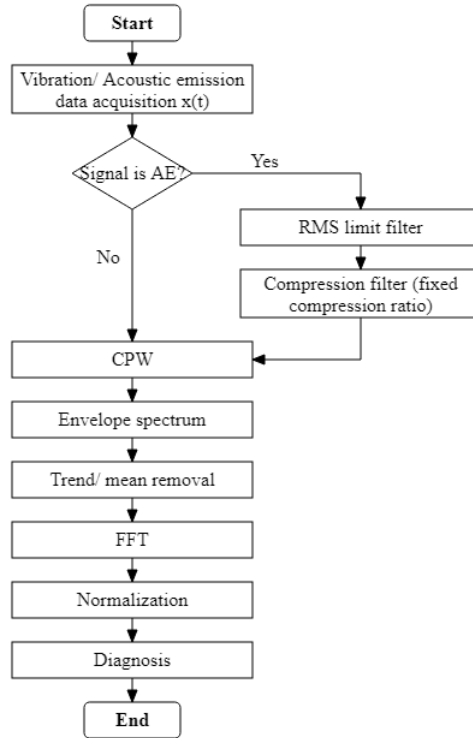


Figure 3.1: Proposed methodology flowchart

Then a simple selection criteria is applied where if the signal acquired is *AE* then two filters are applied before the methodology and if the signal is vibration then the methodology is applied directly.

### 3.2.2 RMS limit filter

The *RMS* limit filter is a tool used to limit the maximum values of the *AE* signals in order to obtain a proper threshold for applying the compression filter of the compandig tool. This filter takes all the values over a multiple of the *RMS* value of the signal and approximate them to that multiple to ensure that any value can not be higher than that *RMS* multiple.

$$if |x(t)| > |L * X_{RMS}| = \begin{cases} if x(t) < 0 & then x(t) = -|L * X_{RMS}| \\ if x(t) > 0 & then x(t) = |L * X_{RMS}| \end{cases} \quad (3.1)$$

where  $x(t)$  is the time signal to be filtered in time  $t$ ,  $L$  is the *RMS* multiple that will be the maximum limit for the magnitude value and  $X_{RMS}$  is the magnitude of the *RMS* value for the original signal. An example of the application is shown in Fig. 3.2 where a) and b) is the same *AE* signal with abnormal peaks and c) is the signal trimmed in magnitude to the fourth multiple of the *RMS* of the original signal.

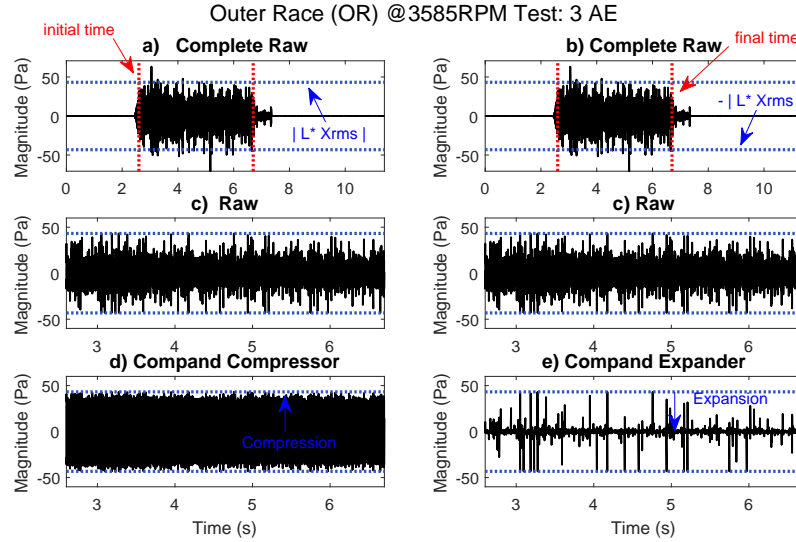


Figure 3.2: a) and b) AE raw signal with RMS and time limits c) Signal trimmed d) Compression and e) Expansion examples

### 3.2.3 Compression filter (Comanding tool)

The companding is a compression and expansion logarithmic audio tool used to reduce the dynamic range of an audio signal. It is mostly used to clear noise from audio signals in the PCM (Pulse Code Modulation) compression using a logarithmic threshold to compress any noise in magnitude down of the threshold and keep everything up to the threshold. [ITU, 1993] standard defines companding applications in 8-bit PCM digital telecommunication systems using two versions: u-law for North America and Japan and A-law for Europe. The main difference between both laws is that the -law algorithm provides a slightly larger dynamic range than the A-law at the cost of worse proportional distortions for small signals. The A-law and -law mathematic representation are shown in eqns. (3.2) and (3.3) respectively:

$$y = \begin{cases} x_{max} \frac{A(|x|/x_{max})}{1+\log_e A} \operatorname{sgn}x & 0 < \left(\frac{|x|}{x_{max}}\right) \leq \frac{1}{A} \\ x_{max} \frac{1+\log_e[A(|x|/x_{max})]}{1+\log_e A} \operatorname{sgn}x & \frac{1}{A} < \left(\frac{|x|}{x_{max}}\right) \leq 1 \end{cases} \quad (3.2)$$

$$y = x_{max} \frac{\log_e [1 + \mu(|x|/x_{max})]}{\log_e(1 + \mu)} \operatorname{sgn}x \quad \operatorname{sgn}x = \begin{cases} +1 & \text{for } x \geq 0 \\ -1 & \text{for } x < 0 \end{cases} \quad (3.3)$$

As shown in eqns. (3.2) and (3.3) both laws use a compression factor named A and  $\mu$  in each respectively law. Those factors are determined in the 8-bit PCM by the [ITU, 1993] standard as  $A=87.6$  and  $\mu=255$  but in [Sklar, 2001] a graphic representation of both laws are presented to get a better perception of compression and expansion rates. Those representation are shown in Fig. 3.3.



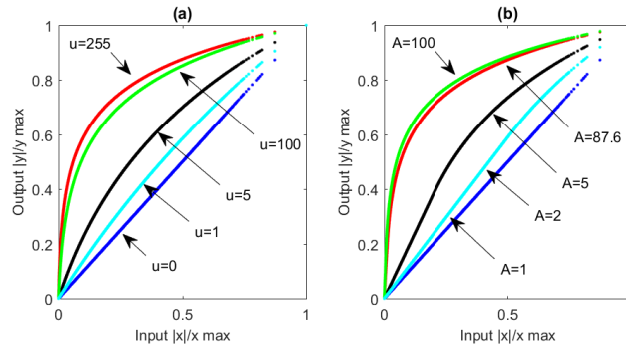


Figure 3.3: Compression characteristics (a)  $\mu$ -law (b) A-law.

where the input in the x axis is the original signal and the output is the resultant signal after applying the filter, the output scale  $|y|/y_{max}$  is the relationship between the actual output value  $y$  and the maximum output  $y_{max}$ , and the input scale  $|x|/x_{max}$  is the same relationship as the output. The curves in these graphics represent how the output of the filter change with respect to the input. During compression, which can be seen applied to an *AE* signal in Fig. 3.2 d), an analog signal is quantized to create a digital signal using unequal steps in order to amplify the quiet sounds while attenuating the loud ones. Conversely, at the expansion, which is applied to the same *AE* signal in Fig. 3.2 e), the digital signal is converted back to an analog signal after expansion, in which the low amplitude signals are amplified less when compared to higher ones. Using the compression filter part of this tool with the standard compression can expand the bearing fault's behavior hidden in the signal.

### 3.2.4 Cepstrum Pre-Whitening (CPW)

The Cepstrum Pre-Whitening *CPW* pre-processing is an algorithm developed to remove cyclical signal behaviors like the rotational shaft speed ones and keep the cyclo-stationary bearing faults behaviors. It is based in the *FFT* algorithm like subsection 2.3.3 presents. Fig. 3.4 a) present the same pre-processed *AE* signal in Fig. 3.2 d) using a compression filter, Fig. 3.4 b) present the raw vibration signal and Fig. 3.4 c) and d) show the *AE* and vibration signals respectively after applying the *CPW* algorithm.

### 3.2.5 Signal envelope

The envelope spectrum of a signal, explained in subsection 3.2.5, is applied to get the absolute value function to reveal the characteristic frequencies of bearing's faults according to [Ho and Randall, 2000]. It is important to mention that the envelope of a signal affects the signal adding a trend to it so its imperative to remove it after applying the envelope. In Fig. 3.5 a) and b) the *AE*

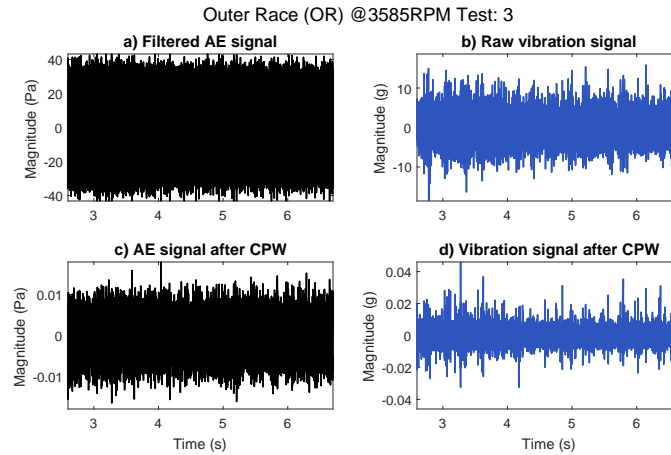


Figure 3.4: *CPW* pre-processing example using *AE* and vibration signals

and vibration signals from Fig. 3.4 c) and d) respectively after applying the *CPW* are presented and in Fig. 3.5 c) and d) their Envelope are presented.

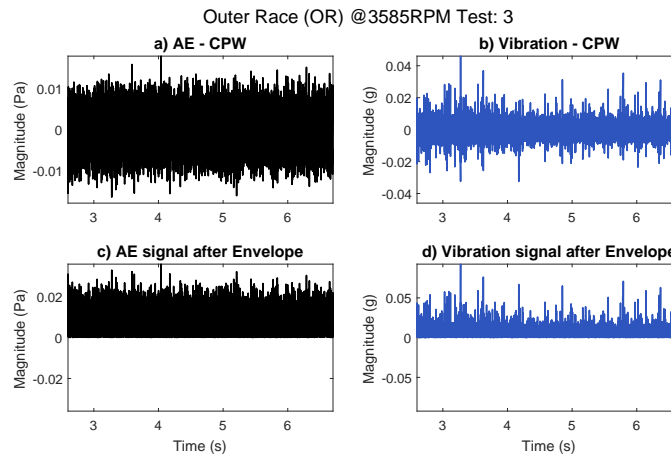


Figure 3.5: Envelope example using *AE* and vibration signals

### 3.2.6 Trend Removal

Vibration and *AE* signals acquired from any rotation machines are susceptible to background noise from its environment, specially in early faults. Therefore, the acquired signals must be pre-processed or post-processed to reduce this background noise and the errors from measurement systems. One technique to clear this is the trend removal. The Direct Current Component (*DCC*) present in any signal, also know as mean value, barely shows the relevant information from the mechanic faults of a machine because its behavior is constant [Lei, 2016]. Thus, the *DCC* should

be removed before analyzing the signal. To obtain the trend of a signal, a linear polynomial curve is fitted to the vibration/AE data using the command *fit* in matlab and the eqn. 3.4.

$$x(t) = p_1 * t + p_2 \quad (3.4)$$

where  $x(t)$  is the vibration/AE signal,  $t$  is the time and  $p_1$  and  $p_2$  are the polynomial values fitted to the line curve. Fig. 3.6 a) and b) shows the AE and vibration signals from Fig. 3.5 c) and d) respectively with the envelope applied. Also the trend is shown in each figure in red color. Below them, in Fig. 3.6 c) and d) the AE and vibration signals are presented without the trend and it is clear that the Gaussian noise is reduced using this post-processing.

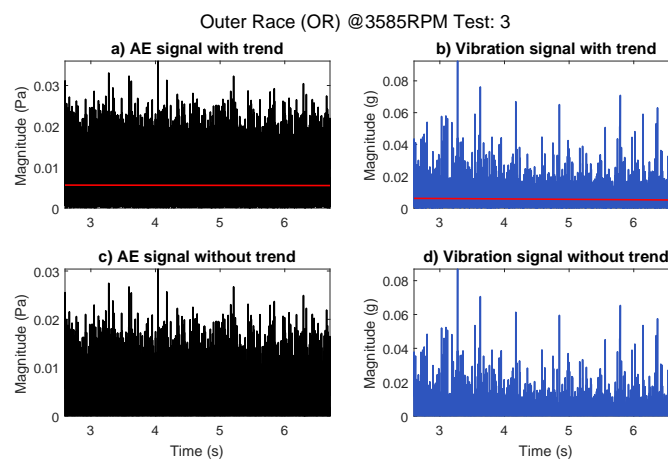


Figure 3.6: Signal's trend removal process

### 3.2.7 Fast Fourier Transform (FFT)

The *FFT* is a frequency domain transform based on the Discrete Fourier Transform (*DFT*) but with a better efficiency in terms of computational time. It is the most used transform for diagnose rotating machine conditions for its ability to analyze stationary signals and obtain information of them using frequency spectrum. This spectrum can be used to analyze the fundamental frequencies of bearing's and shaft's faults and its harmonics. The algorithm gives a frequency vs magnitude graphic that shows how much a signal changes over a range of frequencies. In Fig. 3.7a the AE and vibration frequency spectrum of the signals processed in Fig. 3.6 c) and d) are presented.

### 3.2.8 Normalization

In several methods used in this study to compare and validate the *CPW* efficiency, a threshold is needed; because of that a normalization method is applied. To do this, eqn. (3.5) is applied where

each value of the *FFT* spectrum is divided for the maximum value in the whole spectrum, ensuring that the values will be in the range from 0 to 1.

$$F_N(i) = \frac{F(i)}{\max(F)} \quad \text{for } i = 0, 1, 2, \dots, \text{length}(F) \quad (3.5)$$

where  $F_N(i)$  is the normalized magnitude value of the *FFT* in  $i$ ,  $F(i)$  is the current *FFT* magnitude value of  $i$  and  $\max(F)$  is the maximum magnitude in the whole *FFT* spectrum. At the end, the  $F$  spectra presented in Fig. 3.7a are normalized and presented in Fig. 3.7b; where a easier comparison can be made because both spectra have the same scale from 0 to 1. These normalization, in terms of different sensors used, is necessary because *AE* signals have a higher dynamic range than vibration ones.

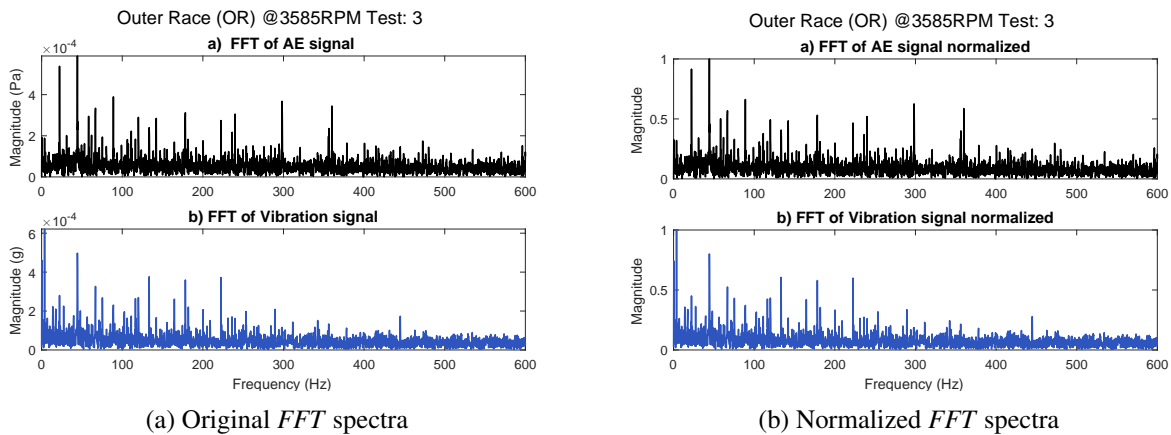


Figure 3.7: *FFT* of *AE* and vibration signals original and normalized

### 3.2.9 Diagnosis

The diagnosis of the frequency spectrum obtained from the methodology use different specifications and standards based on the position and magnitude of the frequency peaks of bearing faults and shaft rotational speed. For bearings faults, in vibration, the frequency spectrum according to [Scheffer and Girdhar, 2004] divides into four zones, where the changes in bearing wear notes as it increases. These zones are described as:

**Zone A:** Machine rotational speed and harmonics zone (0-5,000 RPM)

**Zone B:** Bearing defect frequencies zone (5,000-30,000 RPM)

**Zone C:** Bearing component natural frequencies zone (30,000-120,000 RPM)

**Zone D:** High-frequency detection (*HFD*) zone (beyond 120,000 RPM)

According to [Scheffer and Girdhar, 2004], zone B, defined as third stage, is where bearing defects are present. These faults are noticeable when the bearing have visible wear that may expand through to the edge of the bearing raceway. In this zone the fault frequencies defined using eqns. (2.1), (2.2) and (2.3) have visible peaks with and without side-bands. The literature review ([Hemmati *et al.*, 2016], [He *et al.*, 2016]) done for *AE* investigation of bearing fault diagnosis revealed that this zone division is the same for both kind of sensors with the difference that *AE* and vibration comparisons reveals that in *AE* most authors analyze high frequency peaks in zones like C and D. In Fig. 3.8 a graphic representation of all zones are presented, where Fig. 3.8 a) shows that *BPFO* appears without side-bands, Fig. 3.8 b) shows *BPFI* present with side-bands of RPM and Fig. 3.8 c) shows *BSF* present with side-bands of the Fundamental Train Frequency (*FTF*) of the bearing. It is important to say that fault frequencies have 1-2% deviation from the calculated value and as a random variation around the mean frequency [Randall, 2011].

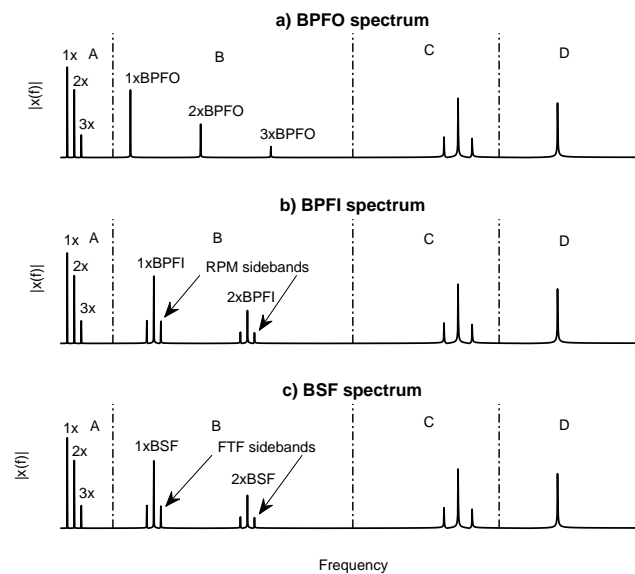


Figure 3.8: Bearing defects spectrum zones

# Chapter 4

## Experimental System

### 4.1 Introduction

This chapter presents the experimental system and the obtained vibration and *AE* signals from it. The full mechanical specifications and designs from the experimental system and the Design of Experiment (*DoE*) for the data obtained from it is presented with the purpose of applying the methodology defined in chapter 3. Also, the *CWRU* experimental system and database obtained from it are presented with [Smith and Randall, 2015] classification of them for validation purpose.

### 4.2 Experimental System

To develop a bearing fault methodology based on both vibration and *AE* signals, the best way to do it is comparing and analyzing them. Due to the need for a bearing faults database in which *AE* and vibration signals of the same fault can be compared, an experimental system was designed and manufactured. The experimental system is shown in Fig. 4.1 and consists of a data acquisition system described in Table 4.1 and the test rig where the data acquisition module is used to acquire both vibration and *AE* signals from the DeltaTron accelerometer and the GRAS 40PH microphone respectively.

The sensors are attached at the bearing base at a sample rate of 25.6 KHz using LabVIEW as the acquisition software. A second DeltaTron accelerometer was attached to the Emerson Electric motor to record its vibration. The test rig system consists of a two motor transmission using a toothed pulley-belt system to move a steel shaft which is placed using rolling element bearings (6204-2Z SKF) with the specifications shown in Table 4.2 and Table 4.3 where the Emerson Electric motor moves the whole system and the Dayton Gearmotor gear system works as the load of the system. The toothed pulleys have the same outer diameter to have the same rotational speed of the Emerson Electric motor into the test rig steel shaft.

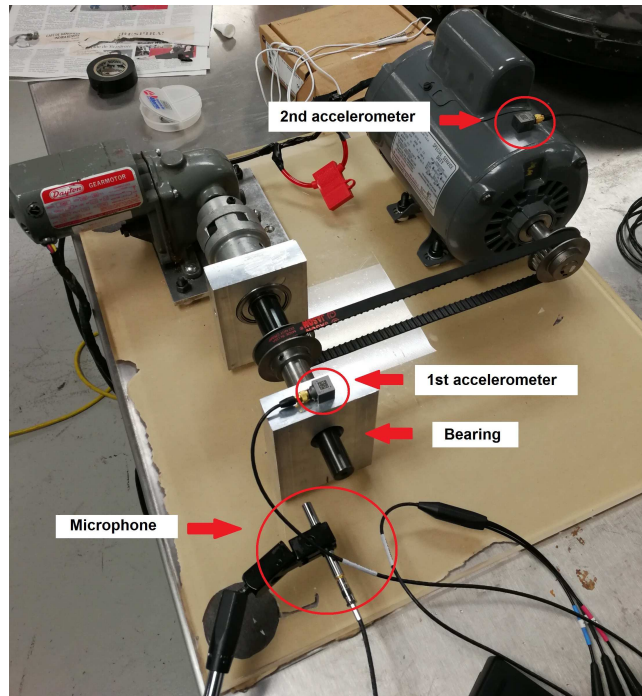


Figure 4.1: Experimental system

Table 4.1: Data Acquisition parts for the experimental system

Equipment	Model	Specifications	Number
Data Acquisition System Module	NI 9234- 4 channels	Sample rate: 51.2KHz/s/ch, Output: $\pm 5$ V	1
Triaxial Accelerometer	DeltaTron 4535-B	Frequency range: 0.3-10k Hz, Range: $\pm 714$ [g] Sensitivity: (X: 9.765 Y: 9.871 Z: 9.611) mV/g	2
Free-Field Array Microphone	GRAS 40 PH	Frequency range: 10-20k Hz, Range: 135 [dB] Sensitivity: 50 mV/Pa	1
Laptop	Dell Precision M4800	Processor: Intel(R) Core i7 2.9GHz, RAM:8 GB	1

Table 4.2: 6204-2Z SKF Bearing specifications.

Inner diameter	Outer diameter	Rolling element diameter	Pitch	# Rolling elements
0.787 in	1.85 in	0.3126 in	1.319 in	8

### 4.2.1 Bearing faults diameters

The bearings were damaged using a wide grain sandpaper, faults images can be appreciated in Appendix B. The faults were measured using a stereo microscope Zeiss Discovery V8 in a  $30^\circ$

Table 4.3: Mechanical parts of the experimental system

Equipment	Model	Specifications	Number
AC Gearmotor	Dayton 2z803	Power: 1/15 hp Speed: 100 RPM	1
AC Electric Motor	Emerson 0213	Power: 1/2 hp Speed: 3450 RPM	1
Coupling	NA	Diameter: 20 mm	1
Steel shaft	NA	1018 Steel	1
Aluminum bearing holders	NA	Height: 15 cm Width: 10 cm	2
Thoothed belt	Jason	Pitch: 1/5 inch Length: 25 inch	1
Thoothed pulley	Martin	Pitch: 1/5 inch Diameter: 2 inch	2

degree of inclination. To compare the experimental system faults with the *CWRU* ones, the *CWRU* faults were assumed to have a circular shape to get their areas presented in Table 4.6 in section 4.3. With the areas of *CWRU* faults, the comparison of them with the experimental system's ones is made using the area values obtained from figures analyzed in Appendix B and showed in Table 4.4. Experimental system's faults have horizontal shapes so in most cases the only measurements available are area and length, so in this case the comparison will be only in area to have an idea of the severity of the faults. Most of the values from *BD*, *IR*, and *OR* defects areas are between 0.007 and 0.014 inches diameters of faults from *CWRU* database, so it can be assumed that the fault approximated values are among 0.007 and 0.014 inches of diameter.

Table 4.4: Experimental system areas of available faults

	Area ( $\mu m^2$ )				
<b><i>BD</i></b>	90,638	78,577	35,298	35,241	23,485
<b>defect</b>	23,956	23,356	14,245	20,128	20,863
<b><i>IR</i></b>	43,969	16,0306	635,439		
<b>defect</b>					
<b><i>OR</i></b>	177,744	24,115	36,606	33,687	
<b>defect</b>					

### 4.2.2 Design of experiments in test rig

Data from tests made in the experimental system was recorded by two DeltaTron accelerometers at two places: one at the motor and other at the bearing's base; and a GRAS 40PH microphone near the experimental system. The accelerometers used in this system are tri-axial so they can record vibration in three axes, but the data acquisition system just had 4 channels and one of them



is used to record the audio, so the vertical perpendicular vibration of both accelerometer and the horizontal perpendicular vibration of the bearing were recorded. The experimental system motor have a 3850 RPM speed, measured by a Check-Line laser tachometer model: CDT-2000HD and use three bearing each one with a different fault, *IR*, *OR* and *RE*.

The tests were recorded for 10-11 seconds with a sampling rate of 25,600 samples/s; four different tests with each damaged bearing were recorded to get a total of 12 tests each one with 4 signals. Having a total of 48 signals available, 12 audio, 24 vibration from the bearing's base and 12 from the motor. Fig. 4.2 shows and example of the four signals that are acquired from the two DeltaTron accelerometers and the GRAS 40PH microphone.

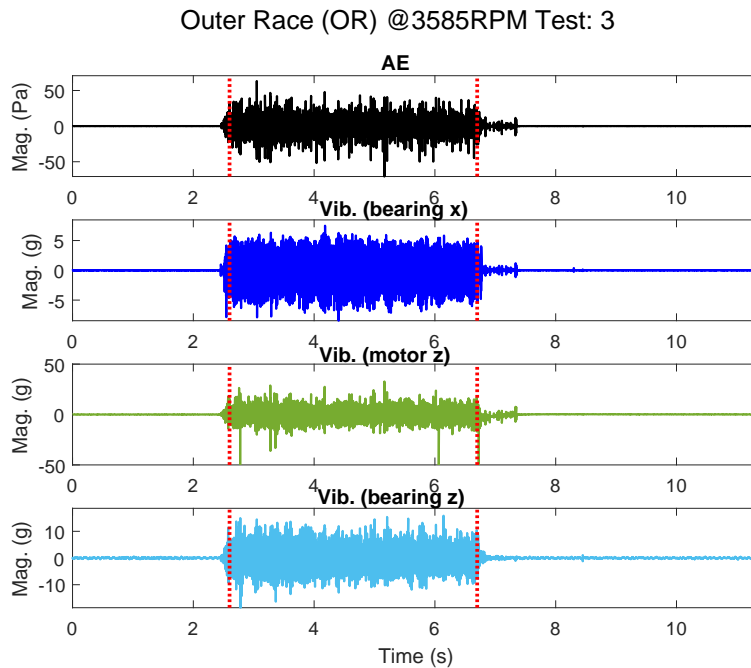


Figure 4.2: Experimental system DoE data acquisition example

### 4.3 Case Western Reserve University database

The database used to validate the methodology proposed in this study is the Case Western Reserve University (*CWRU*) Bearing Data Base which provides ball bearing test data for normal and faulty bearings. The experimental system used in this database is shown in Fig. 4.3 and consist of a 2 hp reliance electric motor, a dynamo-meter to apply loads to the shaft, accelerometers located to the side of the bearings and the base of the structure and bearings (6205-2RS JEM SKF and 6203-2RS JEM SKF) with the specifications shown in Table 4.5. The data acquisition was made using two different sample frequency of 12,000 and 48,000 Hz.

Table 4.5: 6203-2RS JEM SKF Bearing specifications.

Inner race diameter	Outer race diameter	Rolling element diameter	Pitch	# Rolling elements
0.9843 in	2.0472 in	0.3126 in	1.537 in	9

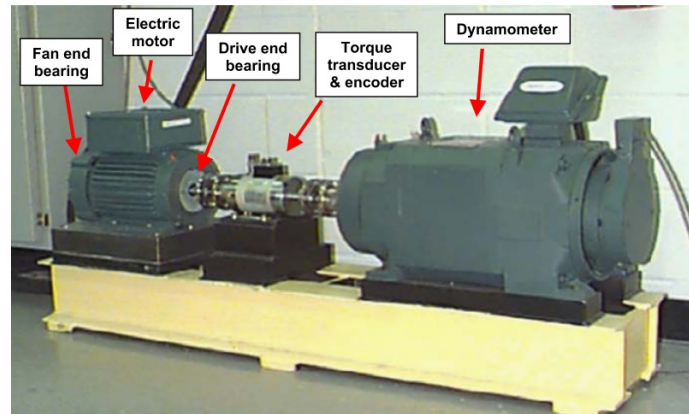


Figure 4.3: CWRU experimental system [CWRU, 2018]

Table 4.6: CWRU diameters and areas of available faults

Diameter (inch)	Diameter ( $\mu m$ )	Area ( $\mu m^2$ )
0.007	177.8	24,816
0.014	355.6	99,264
0.021	533.4	223,344
0.028	711.2	397,057

The motor bearings were seeded with faults using electro-discharge machining (*EDM*). Faults ranges go from 0.007 inches to 0.040 inches in diameter introduced separately at *IR*, *OR* and *RE*. Damaged bearings were used in several test and data was recorded for motor loads of 0 to 3 hp in motor speed of 1797 to 1720 RPM. For the data classification the [Smith and Randall, 2015] benchmark study of the CWRU data were used. There the signals were tested using three different methods, *FFT*, Envelope + *FFT* and *CPW*; and the results were classified using every method diagnose performance in order to get the following classification reproduced from [Smith and Randall, 2015] work in Table 4.7.

Table 4.7: Categorization of *CWRU* diagnosis results

<b>Diagnosis category</b>	<b>Diagnosis success</b>	<b>Explanation</b>
Y1	Yes	Data clearly diagnosable with classic characteristics for the given bearing fault in both time and frequency domains
Y2	Yes	Data clearly diagnosable but with non–classic characteristics in either or both of the time and frequency domains.
P1	Partial	Data probably diagnosable; e.g., envelope spectrum shows discrete components at the expected fault frequencies but they are not dominant in the spectrum.
P2	Partial	Data potentially diagnosable; e.g., envelope spectrum shows smeared components that appear to coincide with the expected fault frequencies
N1	No	Data not diagnosable for the specified bearing fault, but with other identifiable faults (e.g., <i>ML</i> )
N2	No	Data not diagnosable and indistinguishable from noise, with the possible exception of shaft harmonics in envelope spectrum

For the test and validation of certain methods, used in the current methodology, the *Y1* and *Y2* signals will be used. After this, the methodology will be tested using *P1* and *P2* signals in order to test the performance of the method and finally *N1* and *N2* signals, after a proper revision to see if the problem is noise and not data acquisition problems, will be the last phase of testing process of the methodology.

# Chapter 5

## Results

### 5.1 Introduction

This chapter presents the data analyzed from the experimental system's test rig using the proposed methodology described in Chapter 3. There are five sections in this chapter, *CWRU*, experimental system vibration, experimental system *AE* and *GROB* data where results are presented and analyzed and result discussion where the results are discussed.

### 5.2 *CWRU* Database for validation

For validation, the *CWRU* vibration database was used to analyze three types of fault signals, *IR*, *OR* and *RE*, in three levels of diagnose state: (*Y*) for easily diagnosable signals, (*P*) for partially diagnosable and (*N*) for no diagnosable signals following the criteria of [Smith and Randall, 2015] presented in Table 4.7. Every analysis done is described in Appendix D and the identification of fault components is summarized in Table D.1 with information of the identification of fault components in the *CWRU* signals including name of signals, difficulty of diagnose, maximum magnitude in the spectrum, which is the reference for the normalization, amplitude of the expected faults and its first harmonic, localization of the maximum magnitude and fault components found that were different from the expected fault. The analyzed signals were labeled according the difficulty of the diagnosis in the following way:

- Easy: The largest peaks coincide with the bearing fault frequencies. This does not consider the shaft speed frequency.
- Medium: High peaks coincide with the bearing fault frequencies; but, there are too many components with similar amplitude that are associated to the shaft frequency and their harmonics, or there are other components with high amplitude considered as noise.

- Hard: No peaks coincide with the bearing fault frequencies.

### 5.3 Experimental System Database application

The application of the proposed methodology in vibration, as in *AE*, for the experimental system's signals were analyzed. First, four tests were done using three different bearings with *IR*, *OR* and *RE* defects in the experimental system and three of the recorded signals were analyzed in vibration and *AE*; vibration signals are presented in Figs. 5.1 a), b) and c) correspond to *IR* fault selected tests 2, 3 and 4 respectively; where the three signals show signs of the *IR* waveform, but slightly noisy, the selected tests for *OR* fault were tests 1, 2 and 3 presented in Fig. 5.1 d), e) and f) respectively; where the signals also show the *OR* waveform slightly noisy. Finally, the selected tests for *RE* fault were tests 1, 3 and 4 presented in Fig. 5.1 g), h) and i) respectively; where the *RE* waveform is notable in the first two test at the first 0.5 seconds in Fig. 5.1 g), h) with some noise at the end but in Fig. 5.1 i) the waveform is hardly notable and overwhelmed by noise.

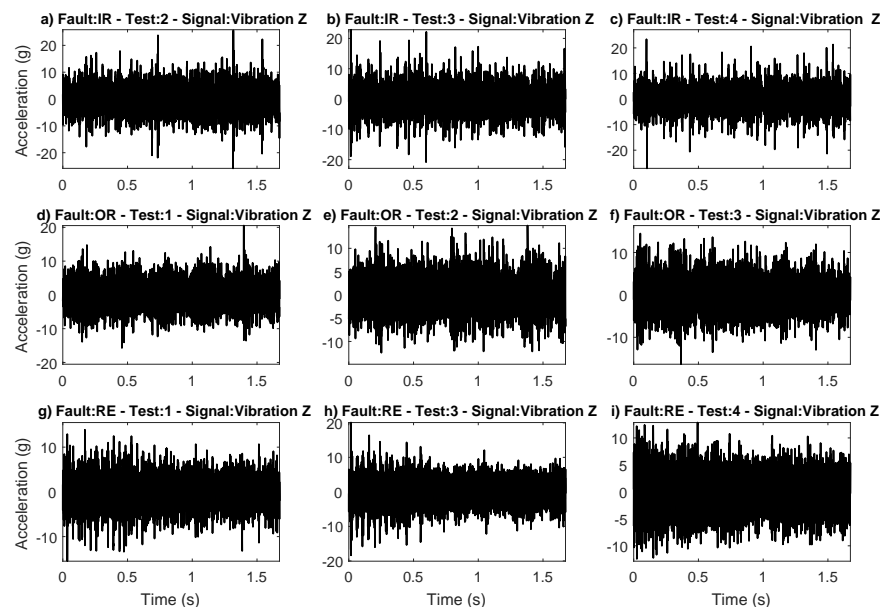


Figure 5.1: Vibration signals

The selected *AE* tests are the same for the vibration but in this case the waveform is remarkable in all cases before the use of the compression filter shown in subsection 3.2.3 but the frequency spectrum doesn't show the peaks according to the faults, for that reason the compression filter is used. Also, is clearly notable that *AE* signals shown in Fig. 5.2 have more ground noise than vibration ones shown in Fig. 5.1. For *IR* fault signals the waveform is remarkable in Figs. 5.2 a), b) and c) corresponding to tests 2, 3 and 4 respectively. For *OR* fault the waveform is clearly

visible in Fig. 5.2 d) and f) corresponding to tests 1 and 3; and slightly remarkable in Figure 5.2 e) for test 2. Finally, for *RE* fault signals the waveform is clearly notable in Fig. 5.2 g) and i) corresponding to test 1 and 4 and hardly remarkable in Fig. 5.2 h) for test 3. After the use of the compression filter most of the low magnitudes waveforms are amplified, but in the frequency spectrum the peaks corresponding to low magnitudes must be identified and discriminated as faults or noise.

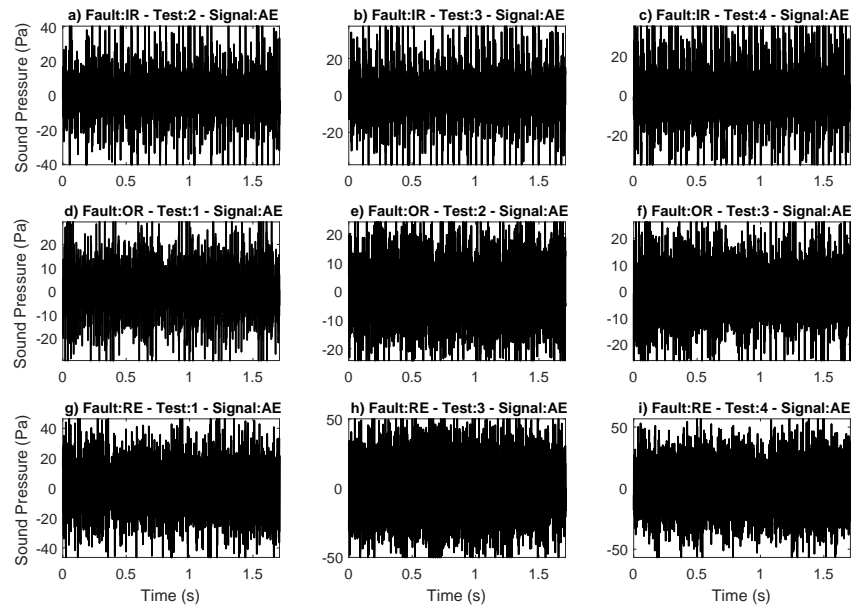


Figure 5.2: *AE* signals before using the compression filter

For every frequency analysis made further Table 5.1 present the numerical value of every fundamental frequency for shaft rotational speed (RPM), *BPFI*, *BPFO* and *BSF* in Hertz, the graphic representation in every frequency domain figure and the color of it.

Table 5.1: Bearing fault frequency features for experimental system @3858 RPM

Feature	Frequency (Hz)	Graphic representation	Color
RPM	59.75	.....	Cyan
BSF	118.9758	.-.-.-.-	Green
BPFO	182.3575	.-.-.-.-	Yellow
BPFI	295.6425	.-.-.-.-	Red

### 5.3.1 Experimental System Vibration Results

The analysis of the vibration signals from the experimental system begin with the analysis of the Normal State (*NM*) of the machine in Fig. 5.3 where the result of the methodology showed only

frequencies in the rotational speed of the shaft at 1x, 3x, 6x and 9x RPM and a peak in 1x *BPFO* with a magnitude approximately of 0.4 that can be explained due to the fixation of the bearing in the base using a bolt to press the bearing in its position.

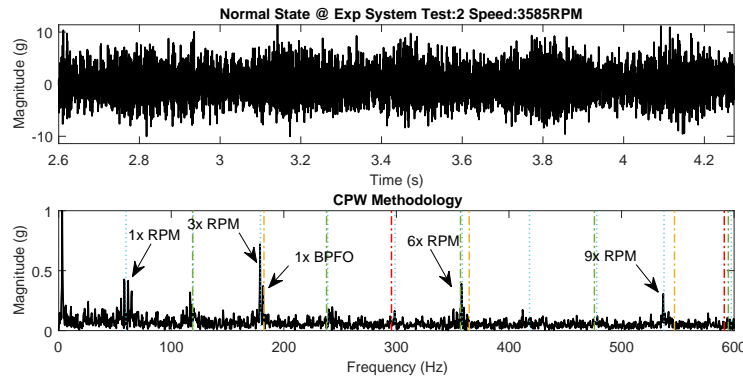


Figure 5.3: Normal state test:2 vibration signal.

Figure 5.4 show the results of the methodology applied to the 9 vibration signals selected in Fig. 5.1 from the experimental system database, where only the fault frequencies will be analyzed because as [Barbini *et al.*, 2016] mentioned, the *CPW* removes not only the shaft rotational information but the sidebands too. Also, two other transforms were compared to the *CPW* methodology for the *OR* case in Fig. 5.6a, using the current methodology only applying *FFT* is one of them and applying *FFT* + envelope is the other one, with the purpose of measure the maximum peaks values in each transform and compare their efficiency. In this section only some spectrum are presented, the remaining results can be found in Appendix E section E.1.

**IR signals:** First, the results from the *IR* fault signal corresponding to test 2 shown in Fig. 5.5 was deeply analyzed using the *CPW* methodology and the presence of a peak in 1x *BPFI* with a magnitude approximately of 0.5 is remarkable in addition of some harmonics of the rotational speed at 1x and 2x; but there is noise at low frequencies (22 Hz approx.) that overwhelm the spectrum but the fault peak is present; also its important to remark that a peak close to 2x *BSF* is present, with a exact value of 239.8 Hz which is at 2% of difference of the calculated harmonic frequency of 234.3 Hz but its out of the 1% tolerance permitted by [Randall, 2011] so it can be taken as noise. The second signal analyzed using the methodology was from test 3 shown in Fig. 5.4 b) where the presence of 1x *BPFI* is remarkable, also a peak in a half harmonic of the rotational speed is present at 1.5x which means there are presence of shaft faults, specifically *ML*, in this test; same as the last signal there is noise at low frequencies non related to the rotational speed that overwhelm the spectrum. Finally, the last signal analyzed using the *CPW* methodology was from test 4 shown in Fig. 5.4 c) where the presence of 1x *BPFI* is hardly remarkable because there are other peaks related and non-related to the rotational speed, where the only ones that can be identified are 1x and 2x harmonics; this signal can be taken as a partially diagnosable case.

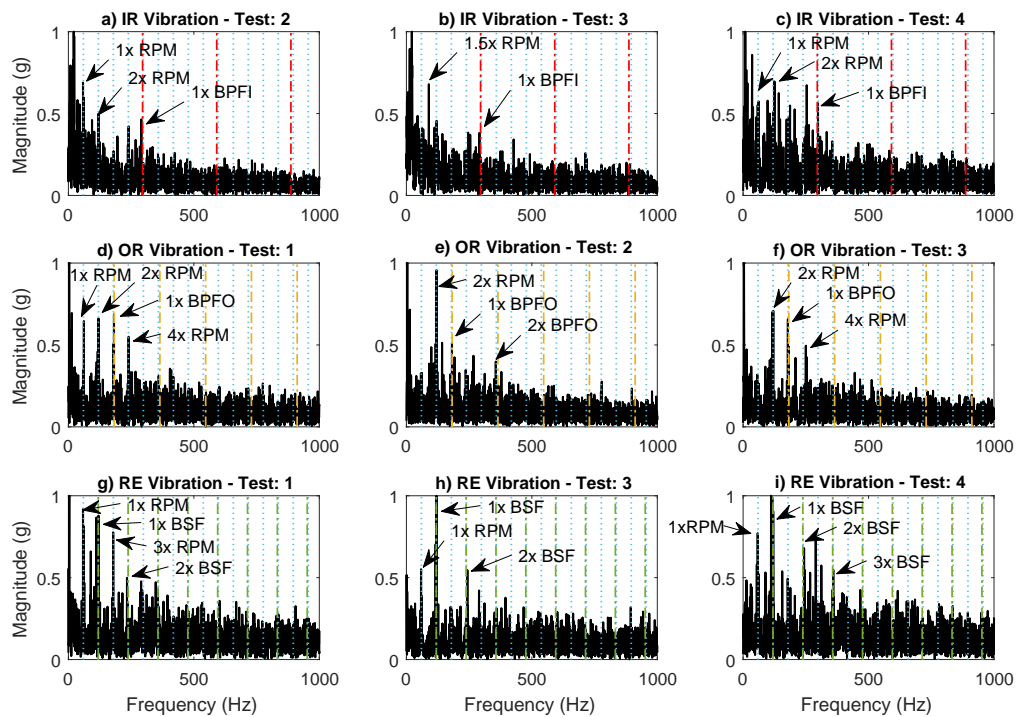


Figure 5.4: Experimental System vibration signals after applying the methodology

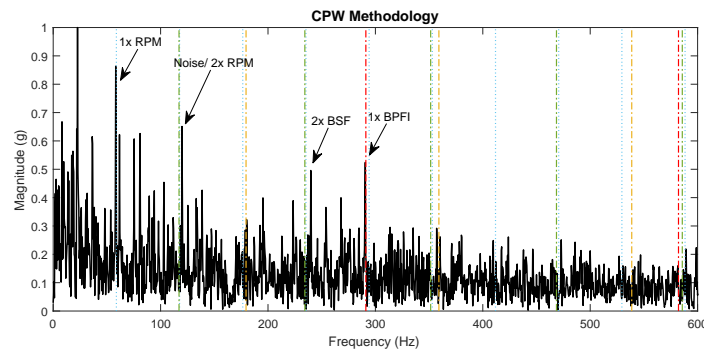


Figure 5.5: *IR* Test:2 vibration signal.

**OR signals:** The result from the *OR* fault signal corresponding to test 1 shown in Fig. 5.4 d) was analyzed using the methodology and the presence of multiple peaks are notable, specially in rotational speed harmonics 1x, 2x and 4x and 1x *BPFO* with a magnitude around 0.7 which means the *OR* fault is successfully diagnosable in this signal. The second signal analyzed using the methodology was from test 2 shown in Fig. 5.4 e) where there are three notable peaks, the second harmonic of the rotational speed, 1x and 2x of *BPFO* with lower magnitude than in the last signal. Finally, the third signal analyzed using the methodology was from test 3 shown in Fig. 5.4 f) where there are also three notable peaks corresponding to the second and fourth



harmonic of the rotational speed and 1x of *BPFO*, in this special case the *OR* fault is one of the most relevant peaks in the spectrum so the fault is diagnosable in this case. Finally, a comparison between the *CPW* methodology, envelope + *FFT* and *FFT* spectra explained at the beginning of section 5.3.1 is presented in Fig. 5.6a, for efficiency purpose, using the signal from test 1 where the maximum peak value for 1x *BPFO* is compared in the three spectra; at first sight the magnitude of the peak is higher in the *FFT* than the methodology and envelope spectra, but using focusing the image to the area of the specific frequency present in Fig. 5.6b it can be seen better that the highest peak in the *FFT* spectrum correspond to the third harmonic of the rotational speed and 1x of *BPFO* have almost the same magnitude than in the methodology which is an improvement at the moment of diagnose a bearing fault. Also, in the methodology spectrum of Fig. 5.6a the fourth harmonic of the rotational speed first detected can also correspond with 2x of *BSF* which means the presence of a *RE* fault in the test. In general the noise at low frequencies are related to the *CPW* method because in the Envelope and *FFT* is clear that the trend was removed.

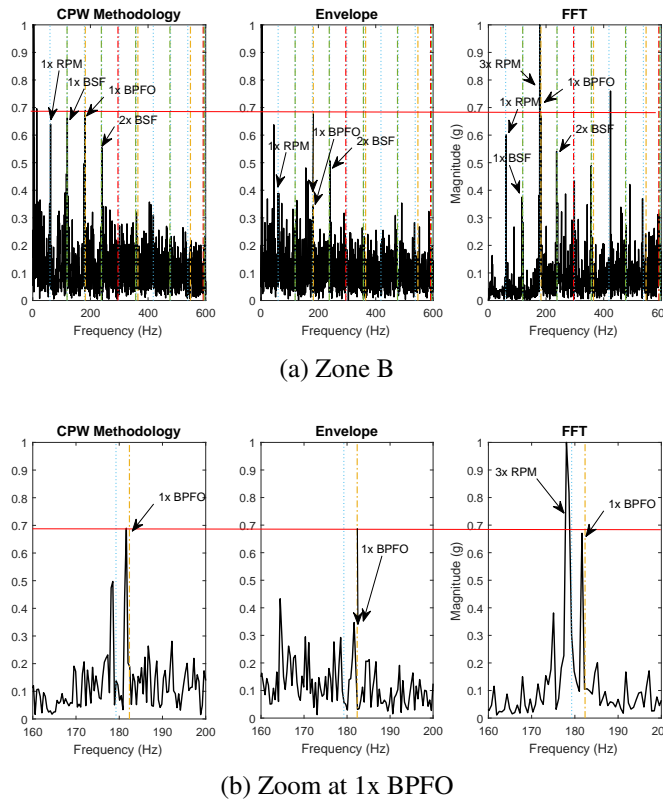


Figure 5.6: *OR* Test:1 vibration signal method comparison.

**RE signals:** The results from the *RE* fault signal corresponding to test 1 shown in Fig. 5.7 was analyzed in detail using the *CPW* methodology and the presence of multiple peaks is notable in this specific case, specifically at 1x *BPFO* and 1x and 2x of *BSF*; this signals is a clear example of a noisy signal which need a more complete analysis of the bearing. The second signal analyzed

using the methodology was from test 3 shown in Fig. 5.4 h) where there are three notable peaks corresponding to the first harmonic of the rotational speed and 1x and 2x of *BSF* where the first harmonic of it is the predominant frequency in the spectrum. As said before, *RE* faults in vibration can be analyzed in the even harmonics of *BSF* [Randall, 2011]; so this means that there is a fault in the *RE* in this test. Finally, the third signal analyzed using the methodology was from test 4 shown in Fig. 5.4 i) where there are multiple peaks in frequency related to known and unknown effects, the predominant ones are identified as the first harmonic of the rotational speed and 1x, 2x and 3x of *BSF* which means there are a diagnosable fault at *RE*.

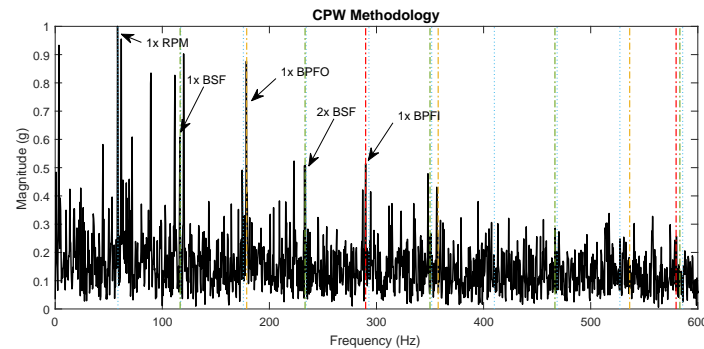


Figure 5.7: *RE* Test:1 vibration signal.

### 5.3.2 Experimental System Acoustic Results

Same as in vibration signals, the analysis of the *AE* signals from the experimental system begin with the analysis of the *NM* of the machine in Fig. 5.8 where the results of the methodology showed multiple peak in frequencies corresponding to rotational speed harmonics at 0.5x, 1x, 3x, 5x, 6x and 9x of RPM and the same peak in 1x *BPFO* that vibration showed is present in *AE* signals.

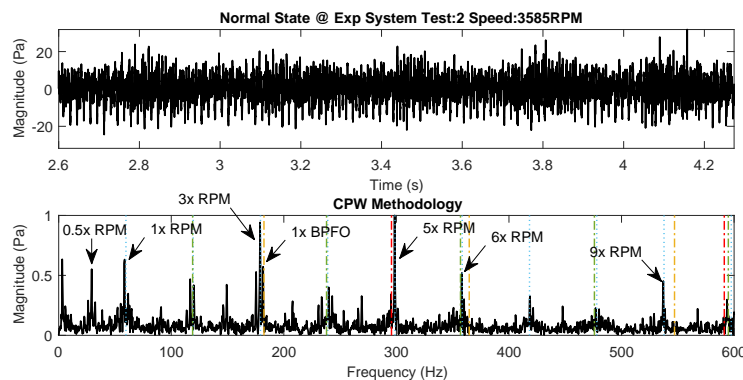


Figure 5.8: Normal state test:2 *AE* signal.

Figure 5.9 show the results of the *CPW* methodology applied to the 9 Acoustic emission signals selected in Fig. 5.2 from the experimental system database. Also, *FFT* and envelope + *FFT* methodologies spectra explained in the beginning of section 5.3.1 were compared for the *RE* signal to the *CPW* methodology in Fig. 5.12a to measure the maximum peaks values in each transform and compare their efficiency. The same frequencies for *BPFI*, *BPFO* and *BSF* analyzed in vibration will be analyzed in *AE* which correspond to the zone B according to subsection 3.2.9 and the zone D will be also analyzed to find any relevant high frequency peak related to any of the aforementioned frequencies. In this section only some spectrum are presented, the remaining results can be found in Appendix E section E.2.

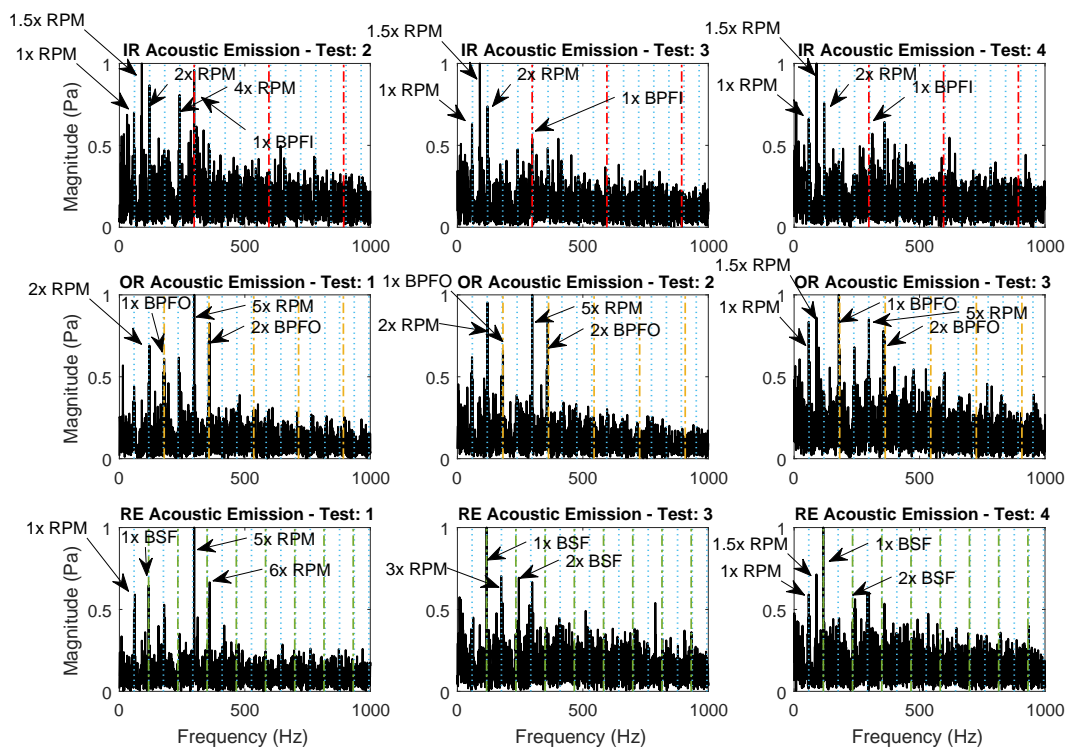
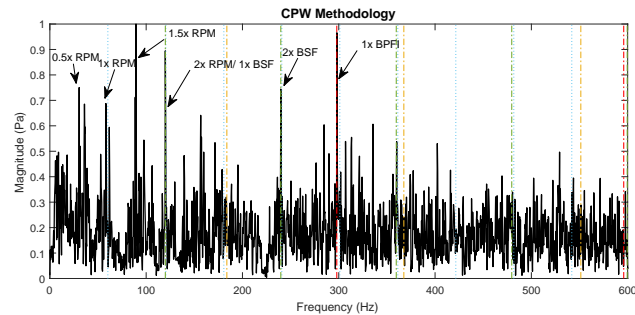


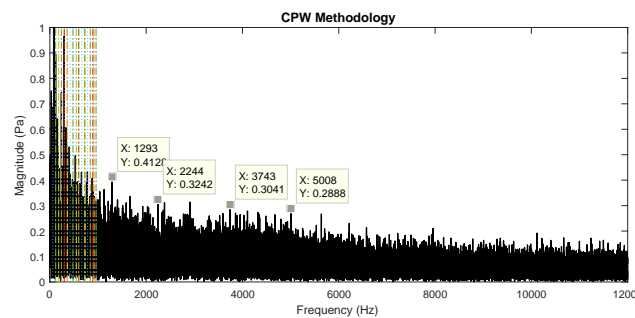
Figure 5.9: Experimental System *AE* signals after applying the *CPW* methodology

**IR signals:** First, the results from the *IR* fault signal corresponding to test 2 shown in Fig. 5.10a was analyzed in detail using the *CPW* methodology, specifically in zone B (5k to 30k RPM or 83.33 to 500 Hz), and the presence of multiple peaks is notable; the most relevant were identified as 1x, 1.5x, 2x and 4x harmonics of the rotational speed and 1x of *BPFI* which means there is presence of *UB* since 2x and 4x RPM are greater than 1x RPM, *ML* because of the presence of 1.5x RPM and fault in the *IR* because of 1x *BPFI*; the predominant frequency in this test was 1.5x RPM. After this, an analysis in zone D (beyond 120k RPM or 2 kHz) shown in Fig. 5.10b where multiple peaks of magnitude approximately of 0.3 are detected but they can be taken as ground noise because there are no relevant peak with higher magnitudes beyond 2 kHz. The second signal

analyzed using the methodology was from test 3 shown in Fig. 5.9 b) where almost all the peaks identified in test 2 were found; including 1x, 1.5x 2x of RPM and 1x *BPFI* and the 1.5x harmonic of RPM is the predominant frequency in this test too. Finally, the last signal analyzed using the methodology was from test 4 shown in Fig. 5.9 c) where the same peaks in the last two tests were identified as 1x, 1.5x and 2x harmonics of RPM and apparently 1x of *BPFI*, but in a more clear analysis that peak is out of the 1% of tolerance that [Randall, 2011] says so it not correspond to 1x *BPFI*.



(a) Zone B

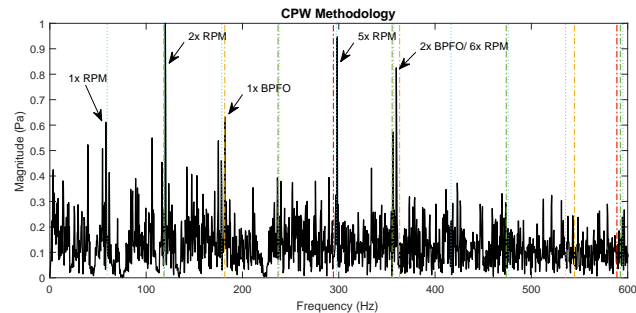


(b) Zone D (High frequencies)

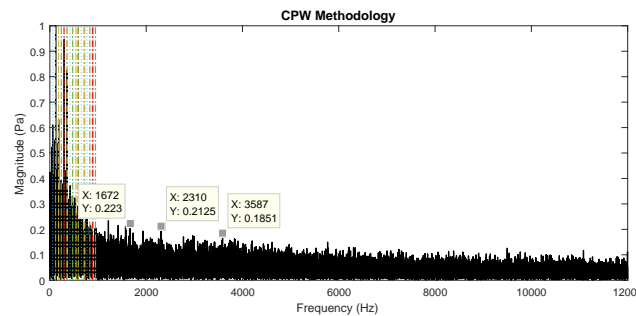
Figure 5.10: *IR* Test:2 *AE* signal.

**OR signals:** First, the results from the *OR* fault signal corresponding to test 1 shown in Fig. 5.11a was analyzed in detail using the *CPW* methodology, specifically in zone B (83.33 to 500 Hz), and the presence of multiple peaks is clearly notable; the most relevant peaks identified were from 2x and 5x of RPM and 1x and 2x of *BPFO* which means the presence of *UB* because of the magnitude of the harmonics of RPM and *BPFO* because the presence of 1x *BPFO* and its first harmonic; the predominant frequency in this case was from 5x of RPM. For the analysis in the zone D, shown in Fig. 5.11b, as in the *IR* case there are no significant peaks beyond 2 kHz that have more than 0.25 magnitude which can be taken as noise. The second signal analyzed using the methodology was from test 2 shown in Fig. 5.9 e) where all the peaks identified in test 1 were found; including 2x and 5x of RPM and 1x and 2x of *BPFO* and the predominant frequency is also 5x of RPM. Finally, the last signal analyzed using the methodology was from test 3 shown in Fig. 5.9 f) where

there same peaks from the last two tests were identified with the difference that 1x of RPM is also present and the Gaussian noise in this case is remarkable; the predominant frequency in this case is 1x of *BPFO* unlike the other cases.



(a) Zone B

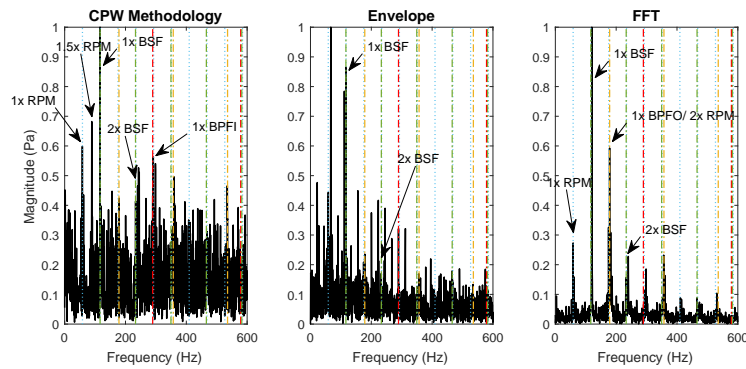


(b) Zone D (High frequencies)

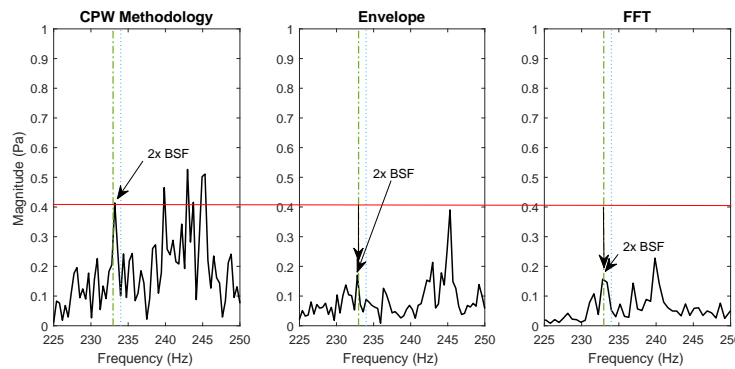
Figure 5.11: *OR* Test:1 *AE* signal

**RE signals:** First, the results from the *RE* fault signal corresponding to test 1 shown in Fig. 5.9 g) was analyzed using the methodology and the following peaks were identified: 1x, 5x and 6x of RPM and 1x of *BSF*; this means there is presence of *UB* due to the harmonics of the rotational speed with higher magnitudes compared to 1x RPM and there is no clear fault in *RE* diagnosable because the even harmonics of *BSF* have no peaks. The second signal analyzed using the methodology was from test 3 shown in Fig. 5.9 h) where the following peaks were identified: 3x RPM and 1x and 2x of *BSF* which means the presence of *UB* and *RE* fault because the first even harmonic is present in this case. Finally, the last signal analyzed using the methodology was from test 4 shown in Fig. 5.9 i) where the following peaks were identified: 1x and 1.5x of RPM and 1x and 2x of *BSF* which means there is shaft faults like: *UB* and *ML*. And *RE* fault because of the mentioned peaks respectively. The comparison between the *CPW* methodology, envelope + *FFT* and *FFT* spectra, for efficiency purposes, is presented in Fig. 5.12a using the signal from test 4 and analyzing them in the zone B (83.33 to 500 Hz) where the 2x *BSF* fault peak magnitude was compared in all the spectra; at first sight the peaks seems to be above 0.5 but doing a zoom to the spectrum at Fig. 5.12b the fault frequency is lower and is around 0.4 but still higher than in the other spectra. There is

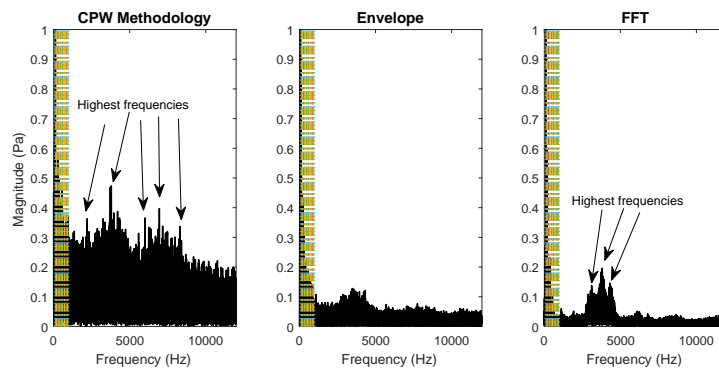
also some peaks that appear to be harmonics of the rotational speed at 6x RPM but, it corresponds to 1x *BPFI*. Another important fact in these analyzed signals is that 1x *BSF* is in all cases the *RE* frequency with higher magnitude compared to its harmonics. Finally, the high frequency analysis in zone D (beyond 2 kHz) is made into the comparison of all methodologies in Fig. 5.12c where the *CPW* methodology and *FFT* shows clear peaks in high frequency which are measured and compared to *BPFI*, *BPFO* and *BSF* in Table 5.4.



(a) Zone B



(b) Zoom at 2x BSF



(c) Zone D (High frequencies)

Figure 5.12: *RE* Test:4 *AE* signal method comparison.

The identification of fault components in the analyzed signals is an important feature that can be evaluated in the proposed methodology. For this evaluation Table 5.2 was made with information of the identification of fault components in the experimental system that summarize the name of signals, difficulty of diagnose, maximum magnitude in the spectrum, which is the reference for the normalization, amplitude of the expected faults and its first harmonic, localization of the maximum magnitude and fault components found that were different from the expected fault. The analyzed signals were labeled according the difficulty of the diagnosis in the same way as *CWRU* in subsection 5.2.

Table 5.2: Bearing fault results for experimental system's database

Database	Signal	Difficulty	Max mag. (g)	Fault amplitude normalized		Max amplitude	Additional significant peaks <sup>1</sup>
				Fault freq.	Harmonic		
Exp. System Vibration	<i>IR</i> Test 2	Easy	0.0010	0.4655	NA	1 (Shaft SH)	BPFI/ BSF/ Shaft
	<i>IR</i> Test 3	Easy	9.3304e-04	0.3819	NA	1 (Shaft SH)	<i>BPFI/ BPFO/</i> Shaft
	<i>IR</i> Test 4	Medium	7.5842e-04	0.5633	0.274	1 (Noise)	<i>BPFI/</i> Shaft H and SH
	<i>OR</i> Test 1	Medium	8.3762e-04	0.702	NA	1 (Noise)	<i>BPFO/ BSF</i> and H/ Shaft H
	<i>OR</i> Test 2	Medium	9.9131e-04	0.5241	0.3976	1 (Noise)	<i>BPFO/ BSF</i> and H/ Shaft H
	<i>OR</i> Test 3	Easy	9.3429e-04	0.6829	NA	1 (Noise)	<i>BPFO/ BSF/</i> Shaft
	<i>RE</i> Test 1	Medium	5.4423e-04	0.4988	NA	1 (1x Shaft)	<i>BSF H/ BPFI/</i> Shaft H
	<i>RE</i> Test 3	Medium	5.8755e-04	0.5766	NA	1 (1x <i>BSF</i> )	<i>BSF H/</i> Shaft H
	<i>RE</i> Test 4	Medium	4.1292e-04	0.7619	NA	1 (1x <i>BSF</i> )	<i>BSF H/</i> Shaft H and SH
Exp. System <i>AE</i>	<i>IR</i> Test 2	Easy	5.6836e-04	0.8911	NA	1 (1.5x Shaft SH)	<i>BPFI/ BSF/</i> Shaft H and SH
	<i>IR</i> Test 3	Medium	6.5332e-04	0.5352	NA	1 (1.5x Shaft SH)	<i>BPFI/ BSF H/</i> Shaft H and SH
	<i>IR</i> Test 4	Hard	5.4949e-04	NA	NA	1 (1.5x Shaft SH)	<i>BSF</i>
	<i>OR</i> Test 1	Medium	8.7464e-04	0.7448	0.8416	1 (5x Shaft)	<i>BPFO/</i> Shaft H
	<i>OR</i> Test 2	Medium	9.0393e-04	0.6879	0.8767	1 (5x Shaft)	<i>BPFO/ BSF H/</i> Shaft H
	<i>OR</i> Test 3	Easy	6.0526e-04	1	0.9509	1 (1x <i>BPFO</i> )	<i>BPFO/</i> Shaft H and SH
	<i>RE</i> Test 1	Medium	6.5875e-04	0.3646	NA	1 (5x Shaft)	<i>BSF</i> odd H/ <i>BPFI/</i> Shaft/ <i>BPFO H</i>
	<i>RE</i> Test 3	Medium	4.2121e-04	0.2659	NA	1 (1x <i>BSF</i> )	<i>BSF</i> odd H/ <i>BPFI/</i> Shaft
	<i>RE</i> Test 4	Medium	4.2313e-04	0.3958	NA	1 (1x <i>BSF</i> )	<i>BSF</i> even H/ <i>BPFI/</i> Shaft H and SH

SH = Half harmonic, H = Harmonics, NA= Not Available



## 5.4 Results discussion

This section presents the result discussion for the experimental case studied.

### 5.4.1 Experimental system discussion

The results obtained from vibration and *AE* signals analyzed in the low frequency band (Zone B) and the *AE* high frequency band (Zone D) are presented and compared in this section. The low frequency comparison between vibration and *AE* signals from the same tests of the Experimental System Database have two performance indicators: diagnose effectiveness and computational time needed to process the signals.

**Diagnostic effectiveness** is explained using two criteria with Table 5.3 information of zone B analyses; (1) considering the difficulty of diagnose, defined in section 5.2 with the *CWRU* database, the signal that is easier to detect and identify the specific fault frequency is the best, and (2) in case the difficulty is the same in both signals, the magnitude of frequency peaks is compared and the signal with the higher one is the best. In 6 from 9 tests vibration have a better result than *AE*, specifically in *IR* and *RE* faults, for the remaining tests that correspond to *OR* fault, *AE* have a better result in frequency peak magnitudes because the difficulty of diagnose were the same in all 3 tests.

Table 5.3: Experimental System results comparison

Signal	Vibration			Acoustic Emission			Best signal
	Difficulty	Fault amplitude normalized		Difficulty	Fault amplitude normalized		
		Fault. freq	Harmonic		Fault. freq	Harmonic	
IR Test 2	Easy	0.4655	NA	Easy	0.8911	NA	Vibration
IR Test 3	Easy	0.3819	NA	Medium	0.5352	NA	Vibration
IR Test 4	Medium	0.5633	0.274	Hard	NA	NA	Vibration
OR Test 1	Medium	0.702	NA	Medium	0.7448	0.8416	AE
OR Test 2	Medium	0.5241	0.3976	Medium	0.6879	0.8767	AE
OR Test 3	Easy	0.6829	NA	Easy	1	0.9509	AE
RE Test 1	Medium	0.4988	NA	Medium	0.3646	NA	Vibration
RE Test 3	Medium	0.5766	NA	Medium	0.2659	NA	Vibration
RE Test 4	Medium	0.7619	NA	Medium	0.3958	NA	Vibration

The high frequency band (zone D) the *AE* signals analyzed did not add value to the analysis expect for the signals of *RE* where peaks of frequency of notable magnitude were identified. Taking into account that the amount of peaks of frequency is much higher in high frequency bands than low ones, only the most relevant ones were identified in Table 5.4 to compare their frequencies with

*BPFI*, *BPFO* and *BSF* and RPM to see if they are harmonics of those frequencies or not. The values in Table 5.4 are obtained dividing the frequency detected by the rotational speed RPM, *BPFI*, *BPFO* and *BSF* specified in Table 5.1 and if the result have a 1-3% of error is highlighted. There are four remarked values corresponding to rounded values of 33x of *BPFO* in Test 4, 22x of *BPFO* in Test 1, 33x and 55x of *BSF* in Test 3; where Test 3 its the only test with close values to *RE* fault harmonics in high frequency band.

Table 5.4: High frequencies found in *AE* signals for *RE* fault

Signal	Frequency (Hz)	Magnitude	RPM	BPFI	BPFO	BSF
Test 4	3723	0.4683	62.31	12.59	20.42	31.29
	3793	0.4734	63.48	12.83	20.80	31.88
	2205	0.3627	36.90	7.46	12.09	18.53
	6016	0.3655	100.69	20.35	<b>32.99</b>	50.56
	6950	0.3967	116.32	23.51	38.11	58.42
	8293	0.337	138.79	28.05	45.48	69.70
	5584	0.3136	93.46	18.89	30.62	46.93
Test 1	3496	0.2575	58.51	11.83	19.17	29.38
	4008	0.2682	67.08	13.56	<b>21.98</b>	33.69
	3200	0.2615	53.56	10.82	17.55	26.90
Test 3	3923	0.4137	65.66	13.27	21.51	<b>32.97</b>
	4327	0.3554	72.42	14.64	23.73	36.37
	7403	0.3771	123.90	25.04	40.60	62.22
	6545	0.3017	109.54	22.14	35.89	<b>55.01</b>
	7705	0.3395	128.95	26.06	42.25	64.76
	3707	0.3566	62.04	12.54	20.33	31.16

**Computational time** is explained in Appendix C where it is clear that vibration signals requires less computational time than *AE* when applying the methodology in the *Experimental System Database*, this is because of the extra pre-processing required by the *AE* signals with the compression and RMS limit filters. Comparing times from *OR* tests from vibration (Table C.2) and *AE* (Table C.5) using 100 revolutions as window length; the mean time on vibration is 0.5073 secs and on *AE* is 0.9285 secs which is a 83% increased computational time. For *IR* and *RE* the same comparison was made given a 82% and 82.9% increased computational times which is consistent with the last value obtained for *IR* fault.

# Chapter 6

## Conclusions

*Spindle Condition Monitoring* have great importance in machining, it allows to acquire and identify valuable information that is not easily accessible to improve the efficiency of machining processes. Some of the multiple challenges in condition monitoring are the selection of the best feature extraction method to extract and identify the condition signature information and data acquisition instrument selection to help improve the information acquired, cost and accessibility of equipment. In this work, a methodology based on *CPW*, proposed by [Smith and Randall, 2015], for bearing condition detection is tested using two types of instruments currently used in the literature: vibration and acoustic emission in a self-made experimental system. This methodology allows to detect bearing faults in medium and late stages. First, the type of signal to analyze is selected between vibration and *AE*, for *AE* two extra filters are applied, first an *RMS* filter to erase the peaks over a multiple of the *RMS* value of the original audio signal and second, a compression filter that expands logarithmically the lower magnitude waveforms to reveal the bearing signature information. After that the *CPW* is applied to reveal bearing faults, envelope spectrum to identify them easier, trend removal to eliminate any present trend, *FFT* to transform the signal to the frequency domain and normalization to have a reference margin. Finally, for vibration signals the *CPW* methodology is applied the same from *CPW* to normalization with the same purposes.

For the 18 analyzed signals from the experimental system in low frequency zone, 9 were from vibration and 9 from acoustic emission, most of them have partially good results for bearing fault detection; in 5 signals the identification of fault components were easily made, in 12 signals the fault identification was possible; but there were peaks with similar amplitudes of the fault components and in 1 signal the identification of fault components was unsatisfactory because there was no peak that matches the bearing fault frequencies. A disadvantage was found when *CPW* is applied, causing it to add low frequency peaks in noisy signals that trend removal can't remove and makes diagnose harder. In the high frequency zone analysis made for *AE* signals the results were unsatisfactory for *IR* and *OR* because there were no relevant frequency peaks that stand out the background noise, but in the *RE* case there were notable peaks in frequencies above 2000 Hz

(Zone D), and just for 1 test from the 3 analyzed two harmonics of *BSF* were identified at 33x and 55x of *BSF*. Using low and high frequency analyses, the result from both is that *RE* faults are the most notable fault among the three, because there are information in both low and high frequency peaks that support the presence of a ball with damages in *AE* and just in low frequency for vibration.

## 6.1 Contributions

*Condition based monitoring* using *Fast Fourier Transform* based methodologies always have challenges with noise filtering, computational time reduction and data acquisition selection. The use of *Cepstrum Pre-Whitening* for bearing condition diagnose have been investigated by a few authors like [Smith and Randall, 2015] and [Fan and Li, 2015] only using vibration signals, on the other hand authors like [He *et al.*, 2016] used both vibration and *AE* signals in their investigation for bearing condition diagnose but using *Short Time Fourier Transform* which is a more basic frequency analysis technique in noise filtering. Also [Law *et al.*, 2012] used both vibration and *AE* in their investigation but focused into *MA* diagnose. A mainly contribution to literature is the application of *CPW* specially to *AE* signals and compare them with equivalent vibration signals. A methodology proposed to process only vibration from bearing faults using *CPW* and envelope spectrum is applied to both vibration and *AE* signals. The condition fault identification is made using the frequency spectrum obtained from the methodology and the comparison between both signals helps to identify the possible areas of opportunity and advantages that acoustic emission have in this field compared to the mainly used type signal that is vibration e.g the high frequency zone detection. Therefore, the methodology can detect bearing faults in medium and late stages with a good accuracy using both vibration and/or *AE* sensors.

## 6.2 Publications

One published conference paper was presented during this research.

- "Diagnostico de Fallas en Husillos usando la Transformada Rapida de Fourier". Appendix. G. National Congress of Automatic Control 2017 (04-06 October 2017, Monterrey, NL, Mexico)

## 6.3 Future work

This investigation made a contribution for a better spindle fault detection. In addition to this work some opportunities have been found:

- Further analysis can be made by using *AE* signals and taking this work as a base of research by attaching ultrasonic sensors to the Experimental system made for this research and study ultrasonic frequencies influence into bearing condition monitoring.
- This methodology can be used to create an hybrid methodology by its combination with a signal decomposition technique like *Empirical Mode Decomposition* or *Wavelet Transform* to eliminate noise from resonance frequency bands of the system.
- The implementation of intelligent classification methods as *Artificial Neural Networks*, *Support Vector Machines* and *Deep Learning* can be applied to classify the type of fault without a visual inspection.
- Further analysis can be made using the vibration signals from the electric motor recorded using correlation methods like *Coherence* or *Correlation Coefficients* to identify vibrations not transmitted by the toothed belt in the Experimental System.

# Bibliography

- [Abellan-Nebot and Subirón, 2010] Jose Vicente Abellan-Nebot and Fernando Romero Subirón. A Review of Machining Monitoring Systems based on Artificial Intelligence Process Models. *The Int J of Advanced Manufacturing Technology*, 47(1-4):237–257, 2010.
- [Attoui *et al.*, 2017] Issam Attoui, Nadir Fergani, Nadir Boutasseta, Brahim Oudjani, and Adel Deliou. A New Time-Frequency Method for Identification and Classification of Ball Bearing Faults. *Sound and Vibration*, 397:241–265, 2017.
- [Barbini *et al.*, 2016] L. Barbini, M. Eltabach, and J. Du Bois. Application of Cepstrum Pre-Whitening on Non-Stationary Signals. In *Int Congress on Technical Diagnostics and Condition Monitoring of Machinery in Non-Stationary Operations*, Sept 2016.
- [Bediaga *et al.*, 2013] I. Bediaga, X. Mendizabal, A. Arnaiz, and J. Munoa. Ball Bearing Damage Detection Using Traditional Signal Processing Algorithms. *IEEE Instrumentation Measurement Magazine*, 16(2):20–25, April 2013.
- [Bhuiyan and Choudhury, 2014] M.S.H. Bhuiyan and I.A. Choudhury. Review of Sensor Applications in Tool Condition Monitoring in Machining. *Comprehensive Materials Processing*, 13:539–569, 2014.
- [Boashash, 1992] Boualem Boashash. Estimating and interpreting the instantaneous frequency of a signal. ii. algorithms and applications. *Proc of the IEEE*, 80(4):540–568, 1992.
- [Boudiaf *et al.*, 2016] Adel Boudiaf, Abdelkrim Moussaoui, Amine Dahane, and Issam Atoui. A Comparative Study of Various Methods of Bearing Faults Diagnosis using the Case Western Reserve University Data. *J of Failure Analysis and Prevention*, 16(2):271–284, 2016.
- [Bujoreanu *et al.*, 2013] Carmen Bujoreanu, Vasile Horga, and Barbu Drăgan. Vibration Analysis Methods in Bearing Damage Detection. In *Applied Mechanics and Materials*, volume 371, pages 622–626. Trans Tech Publ, 2013.

- [Campos *et al.*, 2018] R. Campos, R. Morales-Menendez, A. Vallejo, and D. Ibarra. *Hilbert-Huang Transform based Methodology for Bearing Fault Detection*. PhD thesis, School of Engineering and Sciences. Instituto Tecnológico y de Estudios Superiores de Monterrey - ITESM, May 2018.
- [Cao and Altintas, 2007] Yuzhong Cao and Y Altintas. Modeling of Spindle-Bearing and Machine Tool Systems for Virtual Simulation of Milling Operations. *Int J of machine tools and manufacture*, 47(9):1342–1350, 2007.
- [Cao and Fan, 2011] Zhengjun Cao and Xiao Fan. A Heuristic Description of Fast Fourier Transform. *arXiv preprint arXiv:1110.5989*, 2011.
- [Chandra, 2016] AS Chandra, N Harish Sekhar. Fault Detection in Rotor Bearing Systems using Time Frequency Techniques. *Mechanical Systems and Signal Processing*, 72:105–133, 2016.
- [Choi and Kim, 2007] Young-Chul Choi and Yang-Hann Kim. Fault Detection in a Ball Bearing System using Minimum Variance Cepstrum. *Measurement Science and Technology*, 18(5):1433, 2007.
- [Cohen, 1989] Leon Cohen. Time-Frequency Distributions-a Review. *Proc of the IEEE*, 77(7):941–981, 1989.
- [Deris *et al.*, 2011] Ashanira Mat Deris, Azlan Mohd Zain, and Roselina Sallehuddin. Overview of Support Vector Machine in Modeling Machining Performances. *Procedia Eng*, 24:308–312, 2011.
- [Dimla, 2004] D.E. Dimla. The Impact of Cutting Conditions on Cutting Forces and Vibration Signals in Turning with Plane Face Geometry Inserts. *J of materials processing technology*, 155:1708–1715, 2004.
- [Fan and Li, 2015] Zhiqi Fan and Huaizhong Li. A Hybrid Approach for Fault Diagnosis of Planetary Bearings using an Internal Vibration Sensor. *Measurement*, 64:71–80, 2015.
- [Gowid *et al.*, 2015] S. Gowid, R. Dixon, and S. Ghani. A Novel Robust Automated FFT-based Segmentation and Features Selection Algorithm for Acoustic Emission Condition based Monitoring Systems. *Applied Acoustics*, 88:66–74, 2015.
- [Gu *et al.*, 2002] S. Gu, J. Ni, and J. Yuan. Non-Stationary Signal Analysis and Transient Machining Process Condition Monitoring. *Int J of Machine Tools and Manufacture*, 42(1):41–51, 2002.

- [Guo *et al.*, 2009] Lei Guo, Jin Chen, and Xinglin Li. Rolling Bearing Fault Classification based on Envelope Spectrum and Support Vector Machine. *J of Vibration and Control*, 15(9):1349–1363, 2009.
- [He and He, 2017] M. He and D. He. Deep Learning Based Approach for Bearing Fault Diagnosis. *IEEE Trans on Industry Applications*, 53(3):3057–3065, 2017.
- [He *et al.*, 2016] Miao He, David He, and Yongzhi Qu. A New Signal Processing and Feature Extraction Approach for Bearing Fault Diagnosis using AE Sensors. *J of Failure Analysis and Prevention*, 16(5):821–827, 2016.
- [Hemmati *et al.*, 2016] Farzad Hemmati, Wasim Orfali, and Mohamed S Gadala. Roller Bearing Acoustic Signature Extraction by Wavelet Packet Transform, Applications in Fault Detection and Size Estimation. *Applied Acoustics*, 104:101–118, 2016.
- [Ho and Randall, 2000] D Ho and RB Randall. Optimization of Bearing Diagnostic Techniques using Simulated and Actual Bearing Fault Signals. *Mechanical Systems and Signal Processing*, 14(5):763–788, 2000.
- [Hwang *et al.*, 2009] Yean-Ren Hwang, Kuo-Kuang Jen, and Yu-Ta Shen. Application of Cepstrum and Neural Network to Bearing Fault Detection. *J of Mechanical Science and Technology*, 23(10):2730–2737, 2009.
- [ITU, 1993] General Aspects of Digital Transmission Systems. Terminal Equipments. Pulse Code Modulation (PCM) of Voice Frequencies. pages 1–12, 1993.
- [Law *et al.*, 2012] L.S. Law, J.H. Kim, W.Y.H Liew, and S.K. Lee. An Approach based on Wavelet Packet Decomposition and Hilbert-Huang Transform (WPD-HHT) for Spindle Bearings Condition Monitoring. *Mechanical Systems and Signal Processing*, 33:197–211, 2012.
- [Lei, 2016] Yaguo Lei. *Intelligent Fault Diagnosis and Remaining Useful Life Prediction of Rotating Machinery*. Butterworth-Heinemann, 2016.
- [Lopez-Ramírez *et al.*, 2016] M. Lopez-Ramírez, R.J. Romero-Troncoso, D. Morinigo-Sotelo, O. Duque-Perez, L.M. Ledesma-Carrillo, D. Camarena-Martinez, and A. Garcia-Perez. Detection and Diagnosis of Lubrication and Faults in Bearing on Induction Motors through STFT. In *Int Conf on Electronics, Communications and Computers*, pages 13–18, 2016.
- [McFadden and Smith, 1984] PD McFadden and JD Smith. Model for the Vibration Produced by a Single Point Defect in a Rolling Element Bearing. *J of sound and vibration*, 96(1):69–82, 1984.



- [México, 2018] Pro México. ProMéxico, Informe de Autoevaluación Primer Semestre 2018, 2018.
- [Phadataré and B., 2016] H.P. Phadataré and Pratiher B. Nonlinear Frequencies and Unbalanced Response Analysis of High Speed Rotor-Bearing Systems. *Procedia Eng*, 144:801–809, 2016.
- [Quiroga *et al.*, 2012] Jabid E Quiroga, Gerson Trujillo, and Sergio Quintero. Estudio de Fallas Incipientes en Rodamientos Usando la Técnica de la Envolvente y Cepstrum. *Ingeniare. Revista Chilena de Ingeniería*, 20(3):350–359, 2012.
- [Randall and Sawalhi, 2011] Robert B Randall and Nader Sawalhi. A New Method for Separating Discrete Components from a Signal. *Sound and Vibration*, 45(5):6, 2011.
- [Randall, 2011] R.B. Randall. *Vibration-based Condition Monitoring: Industrial, Aerospace and Automotive Applications*. EBL-Schweitzer. John Wiley & Sons, 2011.
- [Scheffer and Girdhar, 2004] Cornelius Scheffer and Paresh Girdhar. *Practical Machinery Vibration Analysis and Predictive Maintenance*. Elsevier, 2004.
- [Sheen, 2007] Yuh-Tay Sheen. An Analysis Method for the Vibration Signal with Amplitude Modulation in a Bearing System. *J of Sound and Vibration*, 303(3-5):538–552, 2007.
- [Sinha, 2014] Jyoti Kumar Sinha. *Vibration Analysis, Instruments, and Signal Processing*. CRC Press, 2014.
- [Sklar, 2001] Bernard Sklar. *Digital Communications*, volume 2. Prentice Hall Upper Saddle River, 2001.
- [Smith and Randall, 2015] Wade A Smith and Robert B Randall. Rolling Element Bearing Diagnostics using the Case Western Reserve University Data: A Benchmark Study. *Mechanical Systems and Signal Processing*, 64:100–131, 2015.
- [Yan *et al.*, 2011] J. Yan, Ch. Guo, and X. Wang. A Dynamic Multi-Scale Markov Model based Methodology for Remaining Life Prediction. *Mechanical Systems and Signal Processing*, 25(4):1364–1376, 2011.

# Appendix A

## Acronyms and Variables Descriptions

Table A.1: Acronyms Definitions

<i>Acronyms</i>	<i>Description</i>	<i>Acronyms</i>	<i>Description</i>
AD	Amplitude Demodulation	IFFT	Inverse Fast Fourier Transform
AE	Acoustic Emission	IR	Inner Race
ANN	Artificial Neural Network	KLT	Karhunen Loeve Transformation
AR	Autoregressive	LDA	Linear Discriminant Analysis
BPFI	Ball-Passing Frequency Inner-Race	MA	Misalignment
BPFO	Ball-Passing Frequency Outer-Race	MED	Minimum Entropy Deconvolution
BPFR	Ball-Passing Frequency Roller	ML	Mechanical Looseness
BS	Bent Shaft	MVC	Minimum Variance Cepstrum
BSF	Ball Spin Frequency	OR	Outer Race
C	Cage	PCA	Principal Component Analysis
CA	Cepstrum Analysis	PSD	Power Spectral Density
CF	Crest Factor	PTP	Peak to Peak
CNC	Computer Numerical Control	PTV	Peak to Valley
COM	Centre of Mass	RE	Rolling Element
CWT	Continuous Wavelet Transform	SC	Shaft Crack
CPW	Cepstrum Pre-Whitening	SSA	Statistical Signal Analysis
DWT	Discrete Wavelet Transform	STFT	Short Time Fourier Transform
EA	Envelope Analysis	SK	Spectral Kurtosis
EM	Empirical Mode Decomposition	UB	Unbalance
FFT	Fast Fourier Transform	WPT	Wavelet Packet Transform

Table A.1: Acronyms Definitions (Continued)

<i>Acronyms</i>	<i>Description</i>	<i>Acronyms</i>	<i>Description</i>
FTF	Fundamental Train Frequency	WT	Wavelet Transform
HHT	Hilbert Huang Transform	WVD	Wigner-Ville Distribution
HSM	High Spindle Machining		

Table A.2: Algorithms. Variables Descriptions

<i>Variable</i>	<i>Description</i>	<i>Variable</i>	<i>Description</i>
$\phi$	Diameter of Bearing Fault	$h(n - mR)$	Short-Time Window
$F_{UB}$	Unbalance Force	$mR$	Overlap of Window
$M$	Mass of the Rotor	$\mathcal{F}(x)$	Fast Fourier Transform of x
$e$	Rotor's Radial Displacement	$\mathcal{F}^{-1}(x)$	Inverse Fast Fourier Transform of x
$\omega$	Shaft Rotation Speed	$H[T]$	Hilbert Transform of T
$n$	Number of Rolling Elements in Bearing	$E(t)$	Envelope Spectrum
$fr$	Shaft Speed Frequency	$X_{RMS}$	RMS Value of x
$d$	Rolling Element Diameter	$L$	Limit Value of RMS Limit Filter
$D$	Pitch Bearing Diameter	$A$	Compression Constant of Filter A-law
$\alpha$	Angle of the Load from Radial Plane	$\mu$	Compression Constant of Filter $\mu$ -law
$x(n)$	Discrete Vibration/Acoustic emission signal	$p_1, p_2$	Polynomial Constant of Trend Line
$\mathcal{F}_N(x)$	Fast Fourier Transform Normalized Spectrum		

# Appendix B

## Experimental system additional results

### B.1 Defects measurements

In the experimental system, properly described in section 4.2 with the technical specifications and design of experiments in subsection 4.2.2, the bearings used to simulate faults in the experimental system were damaged using wide grain sandpaper to sand the rolling elements, inner and outer race. The defects were measured using a stereo microscope Zeiss Discovery V8, the bearing were focused perpendicular for *RE* defect and in a  $30^\circ$  degree of inclination for the *IR* and *OR* defects then the defects areas were compared with the *CWRU* ones to have a reference margin of the severity of the faults in the experimental system. For this comparison the *CWRU* faults were assumed to have a circular shape to get their areas using the formula  $A = \pi * r^2$ , the values of them are presented in Table B.1. First of all, a comparison between a good and bad condition in every part of the bearing is made between a *RE*, *IR* and *OR* respectively in good and bad condition, where Fig. B.1a shows a *RE* in good condition with a few scratches and Fig. B.1b shows a *RE* in bad condition with several fissures present in all the ball area. In Fig. B.3a an *IR* in good condition is clearly visible without scratches and Fig. B.3b another *IR* in bad condition with some notable scratches and fissures is presented. Finally, in Fig. B.2a a *OR* in good condition is presented without any notable scratches, meanwhile in Fig. B.2b another *OR* in bad condition with some scratches is visible.

Table B.1: *CWRU* diameters and areas of available faults

Diameter (inch)	Diameter ( $\mu m$ )	Area ( $\mu m^2$ )
0.007	177.8	24,816
0.014	355.6	99,264
0.021	533.4	223,344
0.028	711.2	397,057

Using the stereo microscope software, the defect areas were measured, the first measured was the *RE* defect which raw image is shown in Fig. B.4a and next to it in Fig. B.4b some vertical defects are identified, quantified and measured. The clearest ones in the image were five and have the following areas from left to right:  $90,838.17 \mu m^2$ ,  $35,241.39 \mu m^2$ ,  $78,577.01 \mu m^2$ ,  $35,298.5 \mu m^2$  and  $23,485.57 \mu m^2$ . The second measurement made was the same image presented in Fig. B.5a, but analyzing horizontal defects in this case. The clearest defects in Fig. B.5b identified were five from top to bottom with the following areas:  $23,956.15 \mu m^2$ ,  $23,356.71 \mu m^2$ ,  $14,245.3 \mu m^2$ ,  $20,128.18$

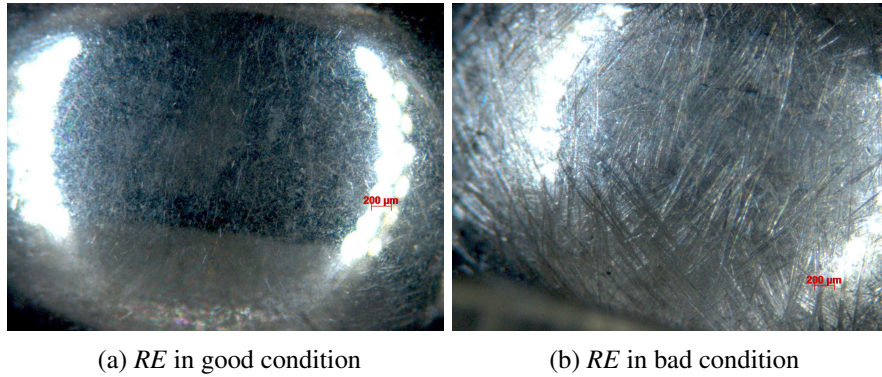


Figure B.1: *RE* condition comparison

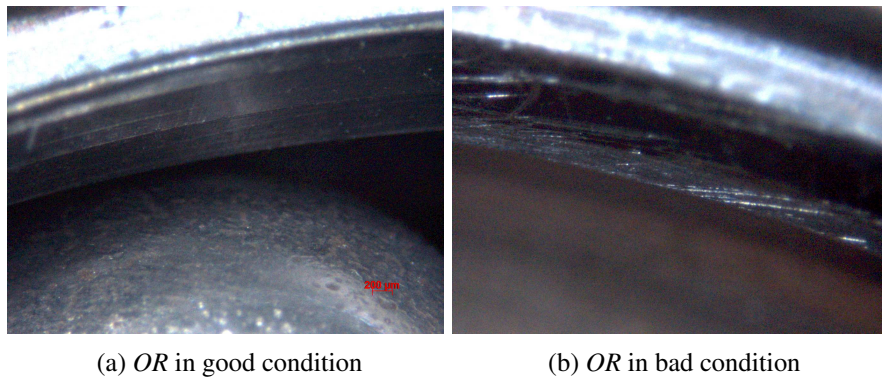


Figure B.2: *OR* condition comparison

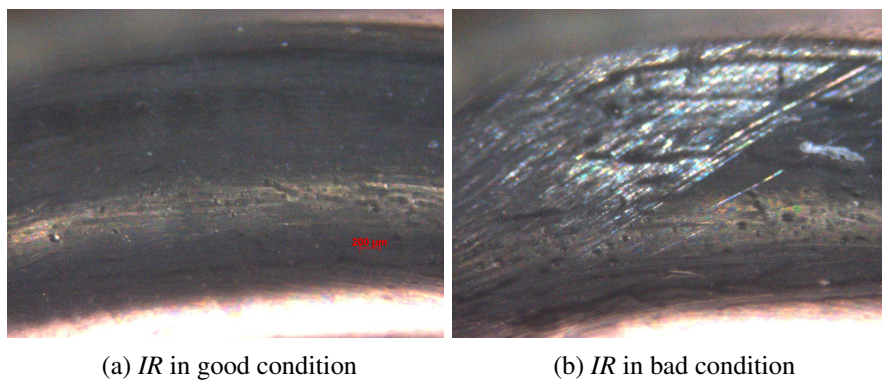


Figure B.3: *IR* condition comparison

$\mu m^2$  and  $20,863.23 \mu m^2$ . Every defect in the *RE* have areas lower than  $24,816 \mu m^2$  or between it and  $99,264 \mu m^2$  what correspond to defects with radius of 0.007 and 0.014 inch respectively; thus, the *RE* defect are between these two radius. The next defect measured is the *OR*, which raw images are shown in Fig. B.6a and B.7a and next to them in Fig. B.6b and B.7b a few defects were identified as notable scratches with the following areas:  $177,744.52 \mu m^2$ ,

36,606.01  $\mu\text{m}^2$ , 24,115.62  $\mu\text{m}^2$  and 33,687.28  $\mu\text{m}^2$ . Analyzing the defects, four were found in the *OR* located on the orthogonal side of the *OR* and the quantity of them are significant lower than the ones on *RE*, their areas are between 24,816 and 99,264  $\mu\text{m}^2$  so the defects should be in the 0.007 and 0.014 inch radius scale. The final defect measured is the *IR* defect, which raw image is shown in Fig. B.8a and next to it in Fig. B.8b some defects were identified, being three the most notable with the following areas: 43,969.98  $\mu\text{m}^2$ , 160,306  $\mu\text{m}^2$  and 635,439  $\mu\text{m}^2$ . The defects analyzed in the *IR* have areas between 24,816 and 223,344  $\mu\text{m}^2$  except from the last one, but the number of defects present in this part of the bearing is lower than the others. So, the defect on *IR* should be in a wide range specifically 0.007, 0.021 and 0.028 inch depending on each area.

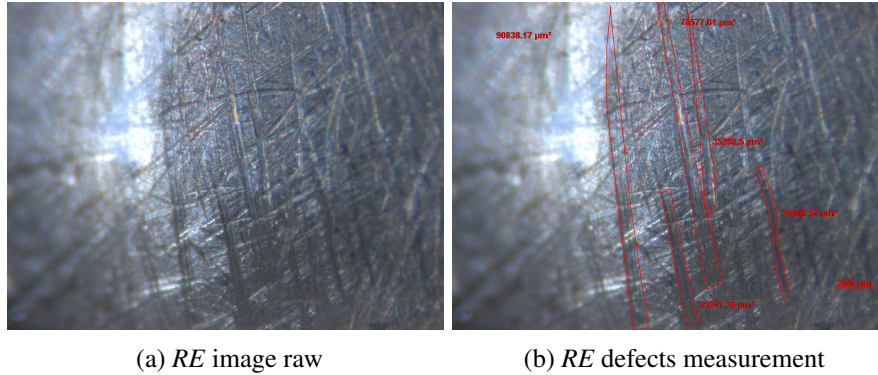


Figure B.4: *RE* vertical defects measurement

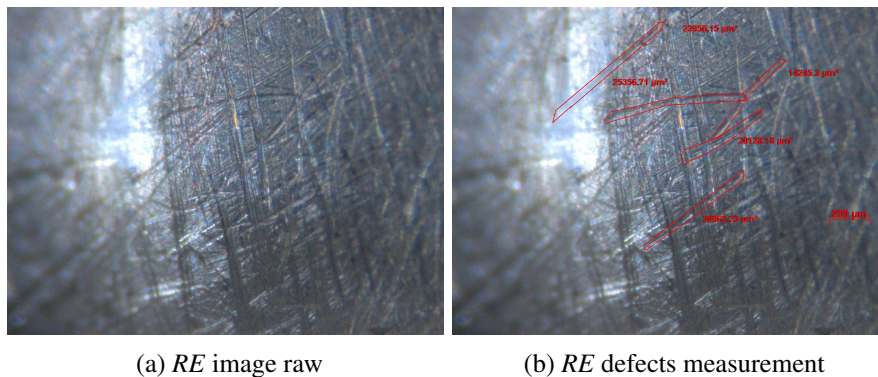
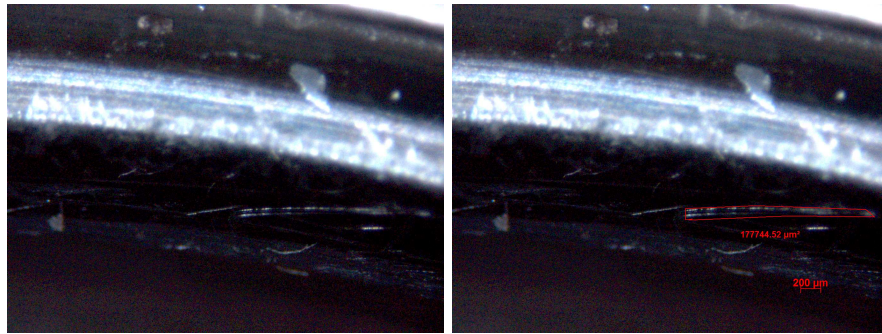


Figure B.5: *RE* horizontal defects measurement

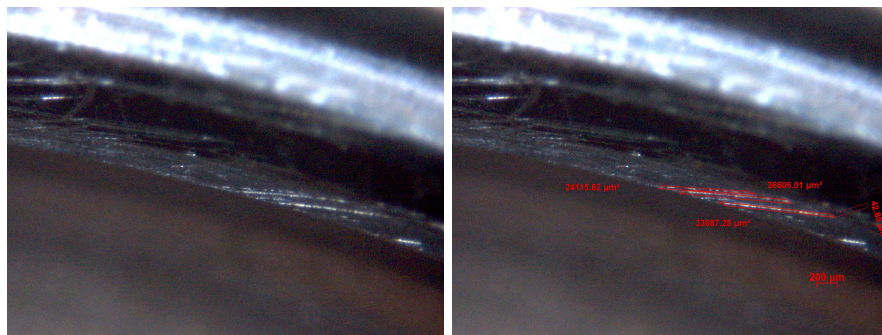
As a conclusion, it can be said that most of the defects are between 0.007 and 0.014 inch radius scale comparing them to the *CWRU* bearing defects and all the values without the decimal data were listed in Table 4.4 in subsection 4.2.1 to have a better perception of the experimental system severity of faults.



(a) *OR* image raw

(b) *OR* defects measurement

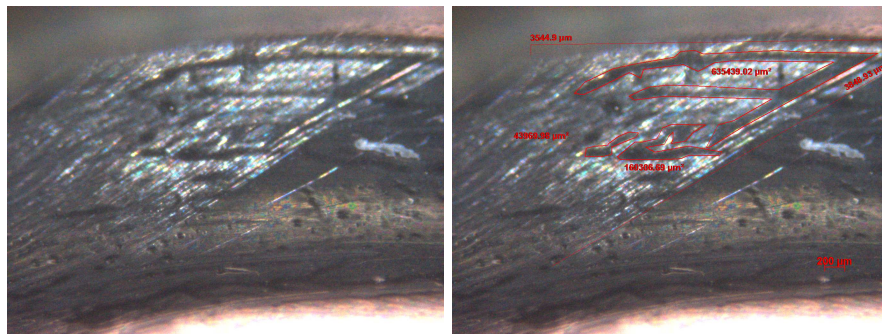
Figure B.6: *OR* 1st defects measurement



(a) *OR* image raw

(b) *OR* defects measurement

Figure B.7: *OR* 2nd defects measurement



(a) *IR* image raw

(b) *IR* defects measurement

Figure B.8: *IR* defects measurement

## B.2 Experimental results

The experimental tests recorded with the design of experiments described in subsection 4.2.2 are presented. Four tests were obtained with 4 different bearings: 1 new bearing to record the normal state (*NM*) of the machine and 1 with each know fault in bearings, *IR*, *OR* and *RE*. The *NM* signals for tests 1, 2, 3 and 4 are presented in Figs. B.9a and B.9b, *IR* signals for tests 1, 2, 3 and 4 in Figs. B.10a and B.10b, *OR* signals for tests 1, 2, 3 and 4 in Figs. B.11a and B.11b and *RE* signals for tests 1, 2, 3 and 4 in Figs. B.12a and B.12b.

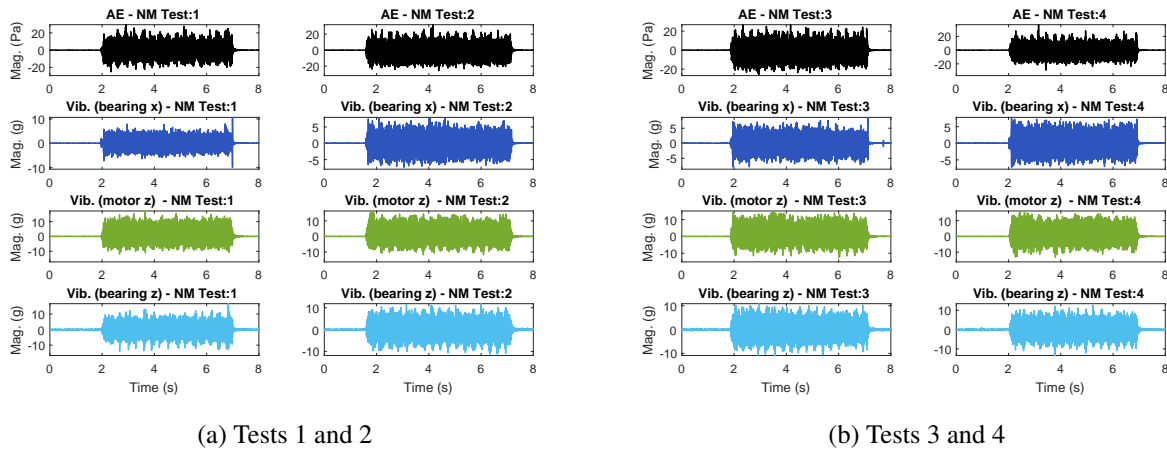


Figure B.9: Normal state AE and vibration signals

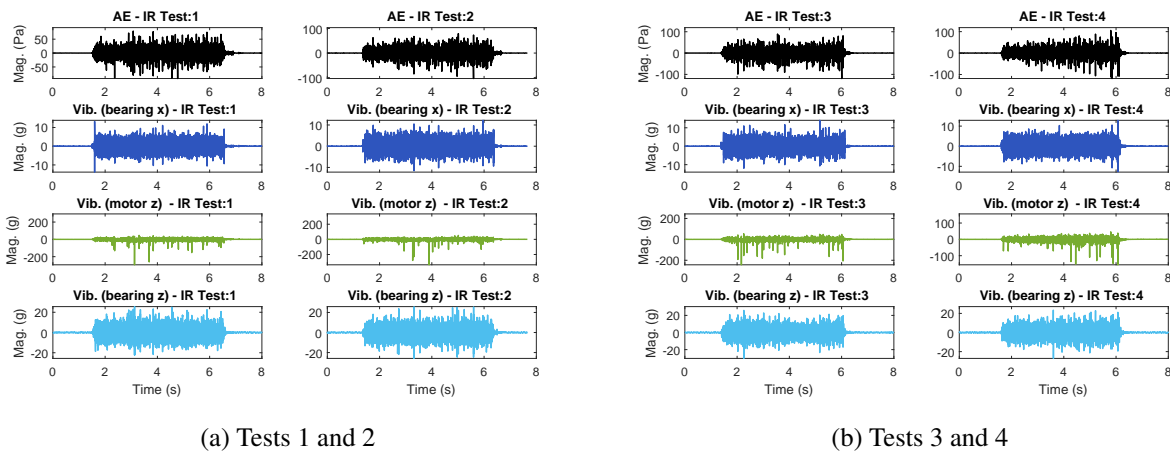


Figure B.10: Inner race AE and vibration signals



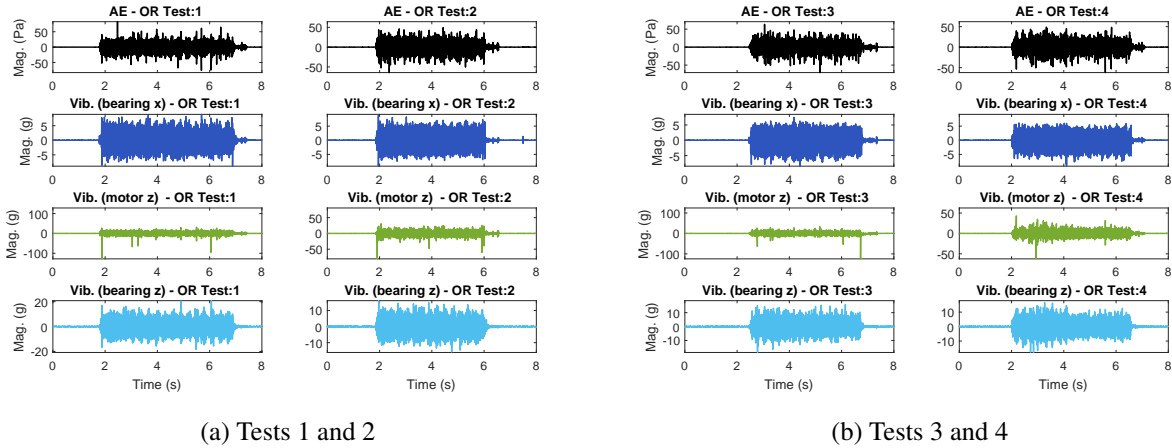


Figure B.11: Outer race AE and vibration signals

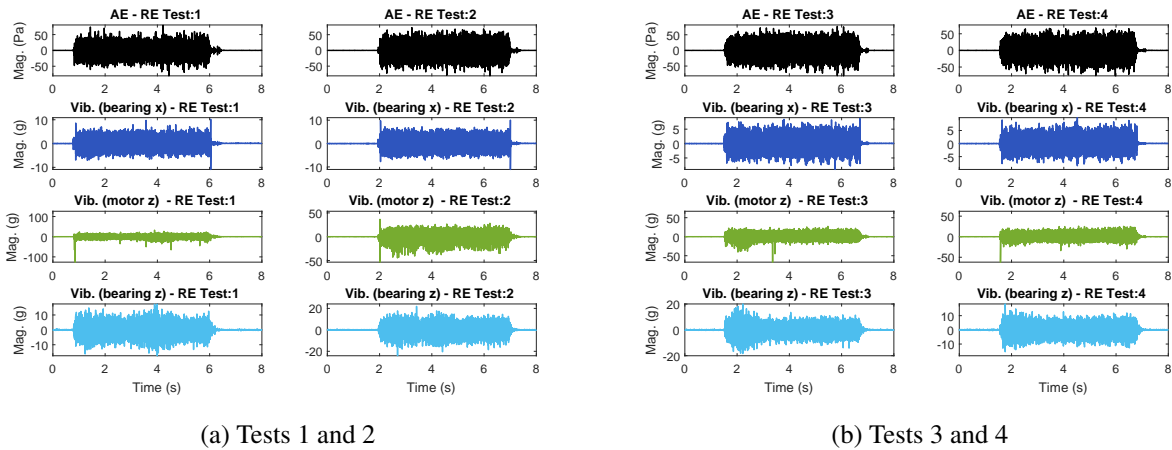


Figure B.12: Rolling element AE and vibration signals

# Appendix C

## Window size selection

In monitoring systems the two most important requirements are low computational time and good frequency spectrum resolution to identify machining condition components with the least possible resources. The methodology in this study is focused into vibration and acoustic emission application. For both type of signals, the *CPW* envelope spectrum, trend removal, *FFT* and normalization are applied in that order but, in the *AE* case two extra filters are applied before that are RMS and compression filters; for this reason the computational time of both type of signals in three different type of bearing with faults are measured to know the increase of computational time in percentage. Also, in both types of signals the envelope spectrum is used as the feature extraction method to identify bearing conditions; thus, if the envelope spectrum resolution is affected by the signal length (the larger the better spectrum resolution) that makes the diagnostic more difficult. The solution for one problem worsen the other problem, e.g. if a small sampling frequency is selected the computational time will be reduced, but the spectrum may not include fault frequencies or the resolution in the spectrum may not be appropriate to distinguish fault frequencies. This section is dedicated to analyze this problem, find an optimum window size for the methodology and accurately measure the increase of computational time that *AE* signals need. Test for *Experimental System* databases are based on revolutions of the shaft, and the optimum window selection is given in revolutions.

### C.1 *CWRU* Database

This database includes signals with speed fluctuations from 1,720 - 1,797 RPM (28.66 - 29.95 Hz). Envelope spectrum resolution was analyzed by [Campos *et al.*, 2018] to identify fault frequency components using envelope spectrum. He concluded that using a 5 revolution window was enough to get a good frequency resolution in *CWRU* signals. Based on that information, a few tests were made to analyze the minimum window size selection for these signals. Based on Table 4.2 it is observed that frequency factors are not integer multiples of the shaft rotational speed, and the identification of the fundamental fault frequencies in the spectrum should not be affected by the shaft frequency in the low harmonics of *BSF*, *BPFO* and *BPFI*.

### C.2 Experimental System Database

This database includes two type of signals with a constant speed of 3585 RPM (59.75 Hz). As tests are based on revolutions and the signals are recorded in time, to guarantee that the whole fault waveform is covered in all signals, a transient of 1 revolution of the speed was used ( $T = \frac{1}{f} = \frac{1}{59.75} = 0.0167$  sec). The signal's length used in these tests

is about 6-7 seconds with a sampling frequency of  $F_s = 25,600 \text{ Hz}$ , this makes  $\frac{F_s}{f_r} = \frac{25,600}{59.75} = 428 \text{ data/revolution}$ . A Table C.1 for experimental system data is presented based on Sinha's example (Sinha p. 151) [Sinha, 2014] and [Campos *et al.*, 2018] works for the number of revolutions used in the tests; to explore the maximum frequency and the envelope spectrum resolution for the selected revolutions, with the difference that in this case the minimum revolutions used are 10 because the sample frequency is more than the double than in *CWRU* database.

Table C.1: *Experimental system* envelope resolution based on shaft rev. and  $F_s = 25,6 \text{ kHz}$

$r$	$N$	$dt=1/F_s$	$T= N dt$	$df= 1/T$	$Fq= F_s/2$	$nf= N/2$
10	428	3.90625E-05	0.016719	59.81308	12800	214
25	10700	3.90625E-05	0.417969	2.392523	12800	5350
50	21400	3.90625E-05	0.835938	1.196262	12800	10700
100	42800	3.90625E-05	1.671875	0.598131	12800	21400

where  $r$  is the window size in revolutions,  $N$  is the number of data points,  $dt$  the time between two samples,  $T$  is the window size in seconds,  $df$  is the expected envelope spectrum resolution,  $Fq$  is maximum frequency in the spectrum based on Nyquist frequency, and  $nf$  is the number of lines in the spectrum plot. Based on Table 5.1 it is observed that frequency factors are close to be integer multiples of the shaft rotational speed, for that reason the identification of the fundamental fault frequencies in the spectrum should be heavily affected by the shaft frequency and its harmonics even in the low harmonics of *BSF*, *BPFO* and *BPFI*. For that reason, a good frequency resolution is strongly recommended in the Experimental System case specially when *RE* faults are diagnosed, e.g. the *RE* fundamental frequency = 118.97 Hz can be easily mistaken with the  $2^{nd}$  harmonic of the rotational speed = 119.5 Hz with a difference of 0.5 Hz which is really low and an important fact to take account in the analysis.

## C.2.1 Vibration

In Fig. C.1 it can be observed that the fundamental frequency of *BPFO* can be easily mistaken with the  $3^{rd}$  harmonic of the rotational speed using 10 revolutions, but in Fig. C.2 using 100 revolutions it is clear that the peak correspond to the fundamental frequency of *BPFO*. In terms of computational time based on Tables C.2, C.3 and C.4 it is clear that using 100 revolutions in *IR*, *OR* and *RE* increase the computational time compared to 10 revolutions in around 700% but using 10 revolution the  $df= 59 \text{ Hz}$  which is a bad frequency resolution; thus using 100 revolutions the  $df= 0.59$  which is the minimum to identify any bearing fault.

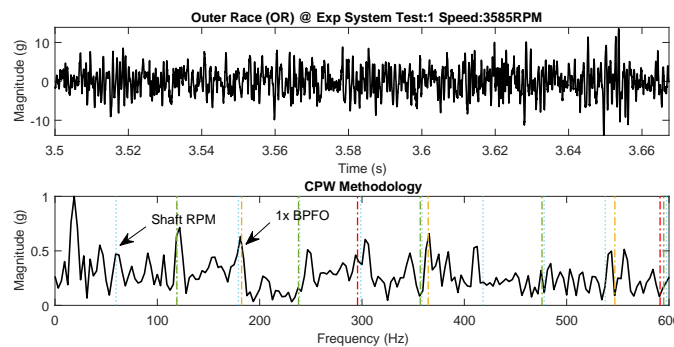
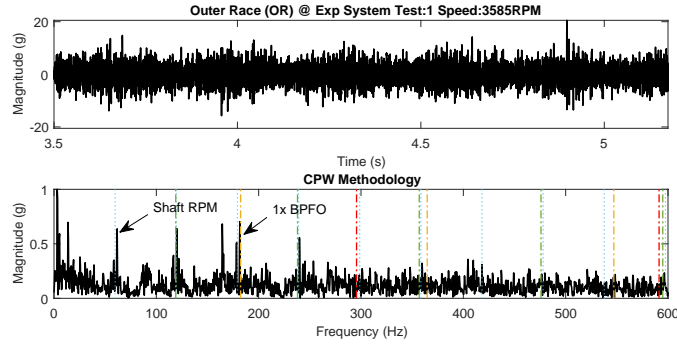


Figure C.1: Experimental system, *OR* vibration fault signal at window of 10 revolutions

Figure C.2: Experimental system, *OR* vibration fault signal at window of 100 revolutionsTable C.2: Experimental system *OR* vibration signals computational times at 10, 25, 50, 100 revs

Outer Race Fault Vibration Experimental System									
File	Test	TimeAvg_10	SD_10	TimeAvg_25	SD_25	TimeAvg_50	SD_50	TimeAvg_100	SD_100
Test_001_OR	0	0.05532	0.00272	0.07466	0.00189	0.16381	0.00153	0.47831	0.01697
Test_002_OR	1	0.05513	0.00137	0.0777	0.0009	0.1730	0.0086	0.4767	0.0034
Test_003_OR	2	0.0598	0.0034	0.0811	0.0011	0.1642	0.0016	0.4935	0.0125
Test_004_OR	3	0.0577	0.0018	0.0833	0.0038	0.1946	0.0072	0.5806	0.0158
Mean		0.0570	0.0023	0.0792	0.0019	0.1739	0.0048	0.5073	0.0122
Time increase compared to 10 rev				0.0222		0.1169		0.4503	
Time increase in % compared to 10 rev				38.96		205.17		790.24	

Table C.3: Experimental system *IR* vibration signals computational times at 10, 25, 50, 100 revs

Inner Race Fault Vibration Experimental System									
File	Test	TimeAvg_10	SD_10	TimeAvg_25	SD_25	TimeAvg_50	SD_50	TimeAvg_100	SD_100
Test_001_IR	0	0.0600	0.0219	0.0809	0.0215	0.1677	0.0244	0.4810	0.0231
Test_002_IR	1	0.0587	0.0207	0.0802	0.0216	0.1635	0.0209	0.4749	0.0233
Test_003_IR	2	0.0605	0.0218	0.0851	0.0211	0.1680	0.0185	0.4830	0.0215
Test_004_IR	3	0.0642	0.0041	0.0948	0.0082	0.1677	0.0216	0.4861	0.0229
Mean		0.0608	0.0171	0.0852	0.0181	0.1667	0.0213	0.4813	0.0227
Time increase compared to 10 rev				0.0244		0.1059		0.4204	
Time increase in % compared to 10 rev				40.12		174.07		691.14	

## C.2.2 Acoustic Emission

Acoustic emission signals according to the *CPW* methodology described in chapter 3, have two extra pre-processing filter (RMS and compression filters); therefore, in addition to selecting the optimal window for the frequency analysis, the computational time obtained applying the methodology in *AE* signals will be compared to the methodology applied to vibration signals to measure the percentage increase of computational time. In Fig. C.3 it can be observed that the fundamental frequency of *BPFO* can be easily mistaken with the 3<sup>rd</sup> harmonic of the rotational speed using 10 revolutions, but in Fig. C.4 using 100 revolutions it is clear that the peak correspond to the fundamental frequency of

Table C.4: Experimental system *RE* vibration signals computational times at 10, 25, 50, 100 revs

Rolling Element Fault Vibration Experimental System									
File	Test	TimeAvg_10	SD_10	TimeAvg_25	SD_25	TimeAvg_50	SD_50	TimeAvg_100	SD_100
Test_001_BD	0	0.0646	0.0254	0.0803	0.0227	0.2040	0.0293	0.4827	0.0225
Test_002_BD	1	0.0608	0.0236	0.0793	0.0219	0.1659	0.0254	0.5070	0.0263
Test_003_BD	2	0.0578	0.0212	0.0856	0.0257	0.1656	0.0229	0.4999	0.0261
Test_004_BD	3	0.0572	0.0209	0.0822	0.0208	0.1841	0.0322	0.4864	0.0228
Mean		0.0601	0.0228	0.0818	0.0228	0.1799	0.0274	0.4940	0.0244
Time increase compared to 10 rev				0.0217		0.1198		0.4339	
Time increase in % compared to 10 rev				36.14		199.28		721.72	

*BPFO*. In terms of computational time based on Tables C.5, C.6 and C.7 it is clear that using 100 revolutions in *IR*, *OR* and *RE* increase the computational time compared to 10 revolutions in around 400%, but using 10 revolution the  $df=59$  Hz which is a bad frequency resolution; thus, using 100 revolutions the  $df=0.59$  which is the minimum to identify any bearing fault.

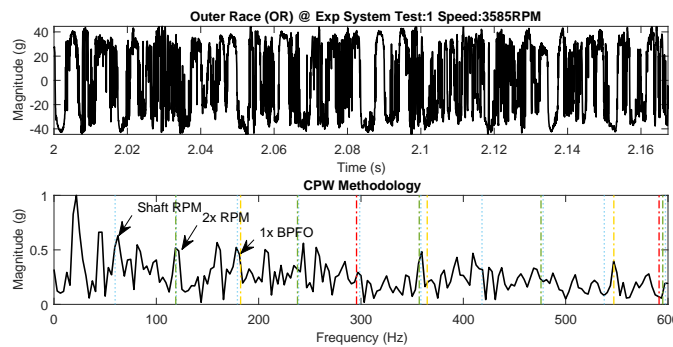


Figure C.3: Experimental system, *OR AE* fault signal at window of 10 revolutions

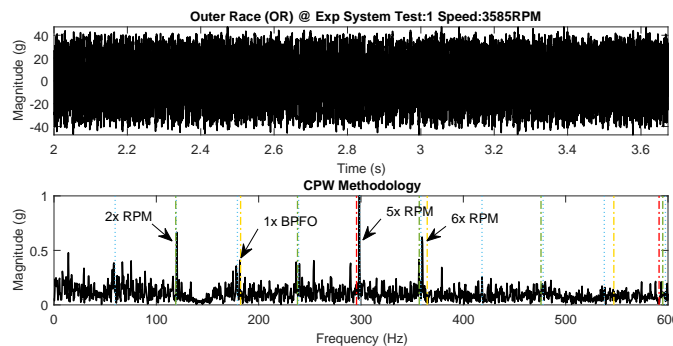


Figure C.4: Experimental system, *OR AE* fault signal at window of 100 revolutions

Table C.5: Experimental system *OR AE* signals computational times at 10, 25, 50, 100 revs

Outer Race Fault AE Experimental System									
File	Test	TimeAvg_10	SD_10	TimeAvg_25	SD_25	TimeAvg_50	SD_50	TimeAvg_100	SD_100
Test_001_OR	0	0.10222	0.05375	0.12468	0.05305	0.20639	0.05346	0.94741	0.10644
Test_002_OR	1	0.14710	0.11346	0.16565	0.07851	0.20988	0.05295	0.8968	0.04773
Test_003_OR	2	0.10351	0.05418	0.13794	0.05242	0.20682	0.05406	0.9719	0.06983
Test_004_OR	3	0.10308	0.05335	0.12148	0.05115	0.20650	0.05129	0.8978	0.06187
Mean		0.1140	0.0687	0.1374	0.0588	0.2074	0.0529	0.9285	0.0715
Time increase compared to 10 rev				0.0235		0.0934		0.8145	
Time increase in % compared to 10 rev				20.58		81.96		714.47	

Table C.6: Experimental system *IR AE* signals computational times at 10, 25, 50, 100 revs

Inner Race Fault AE Experimental System									
File	Test	TimeAvg_10	SD_10	TimeAvg_25	SD_25	TimeAvg_50	SD_50	TimeAvg_100	SD_100
Test_001_IR	0	0.16672	0.08914	0.22808	0.09968	0.73432	0.17969	0.88147	0.08799
Test_002_IR	1	0.17127	0.09696	0.20369	0.08750	0.34675	0.09033	0.88551	0.08957
Test_003_IR	2	0.17351	0.08662	0.20948	0.09120	0.37268	0.09115	0.86240	0.08018
Test_004_IR	3	0.15493	0.08439	0.19392	0.07791	0.33929	0.07992	0.87558	0.09096
Mean		0.1666	0.0893	0.2088	0.0891	0.4483	0.1103	0.8762	0.0872
Time increase compared to 10 rev				0.0422		0.2817		0.7096	
Time increase in % compared to 10 rev				25.32		169.05		425.93	

Table C.7: Experimental system *RE AE* signals computational times at 10, 25, 50, 100 revs

Rolling Element Fault AE Experimental System									
File	Test	TimeAvg_10	SD_10	TimeAvg_25	SD_25	TimeAvg_50	SD_50	TimeAvg_100	SD_100
Test_001_BD	0	0.16568	0.08407	0.21053	0.08712	0.38963	0.11143	0.90451	0.10216
Test_002_BD	1	0.16304	0.08535	0.20875	0.09088	0.38650	0.08779	0.88842	0.09500
Test_003_BD	2	0.17696	0.09480	0.22481	0.08927	0.43297	0.08984	0.90542	0.10733
Test_004_BD	3	0.17903	0.08848	0.21303	0.09672	0.40893	0.10064	0.91500	0.10515
Mean		0.1712	0.0882	0.2143	0.0910	0.4045	0.0974	0.9033	0.1024
Time increase compared to 10 rev				0.0431		0.2333		0.7322	
Time increase in % compared to 10 rev				25.18		136.31		427.72	

### C.2.3 Conclusions about window size selection

Comparing the Experimental System mean computational times using 100 revolutions, that will be the optimal window selected for resolution purposes, from Tables C.2, C.3 and C.4 for vibration the times are: 0.4503 for *OR*, 0.4204 for *IR* and 0.4339 for *RE*. And mean computational times using 100 revolutions from Tables C.5, C.6 and C.7 for *AE* the times are: 0.8145 for *OR*, 0.7096 for *IR* and 0.7322 for *RE*. Using that information it is clear that *AE* signals analyzed using the proposed methodology have more computational time than vibration ones in all bearing faults with, 83% for *OR*, 82% for *IR* and 82.9% for *RE*, which at the end gives a better result for vibration signals in terms of computational time.

# Appendix D

## CWRU Database validation

For validation of the proposed methodology, the *CWRU* vibration database was used analyzing three types of fault signals, *IR*, *OR* and *RE*, in three levels of diagnosable state: (*Y*) for easily diagnosable signals, (*P*) for partially diagnosable and (*N*) for no diagnosable signals following the criteria of [Smith and Randall, 2015] presented in Table 4.7. For the (*Y*) signals at Fig. D.1 a), b) the waveforms are clearly visible for *IR* and *OR* faults respectively, for the (*Y*) at Fig. D.1 c) the *RE* fault waveform is visible with noise not overwhelming the signal. Meanwhile (*P*) signals at Fig. D.1 b), e) and h) for *IR*, *OR* and *RE* faults respectively have a partially visible waveforms overwhelmed by noise with similar magnitude as (*Y*) signal for only the *IR* case. Finally the (*N*) signal at Fig. D.1 c) for *IR* fault its hard to distinguish the waveform despite having similar magnitudes as (*Y*) and (*P*) cases; the (*N*) signals at Fig. D.1 f) and i) for *OR* and *RE* faults have both hard to distinguish and non similar magnitudes characteristics compared to (*Y*) and (*P*) cases of the same faults.

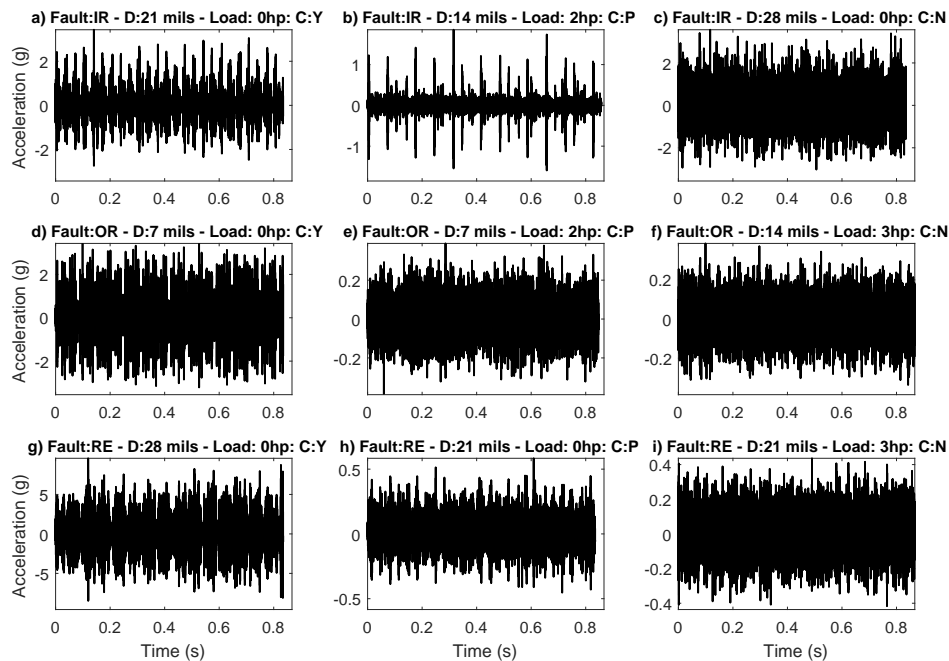


Figure D.1: *CWRU* analyzed signals used to validate the methodology



## D.1 CWRU Results

Figure D.2 show the results of methodology applied to the 9 signals selected in Fig. D.1 from *CWRU* database. Also, the Envelope and *FFT* spectrum were compared to the methodology to measure the maximum peaks values in each transform.

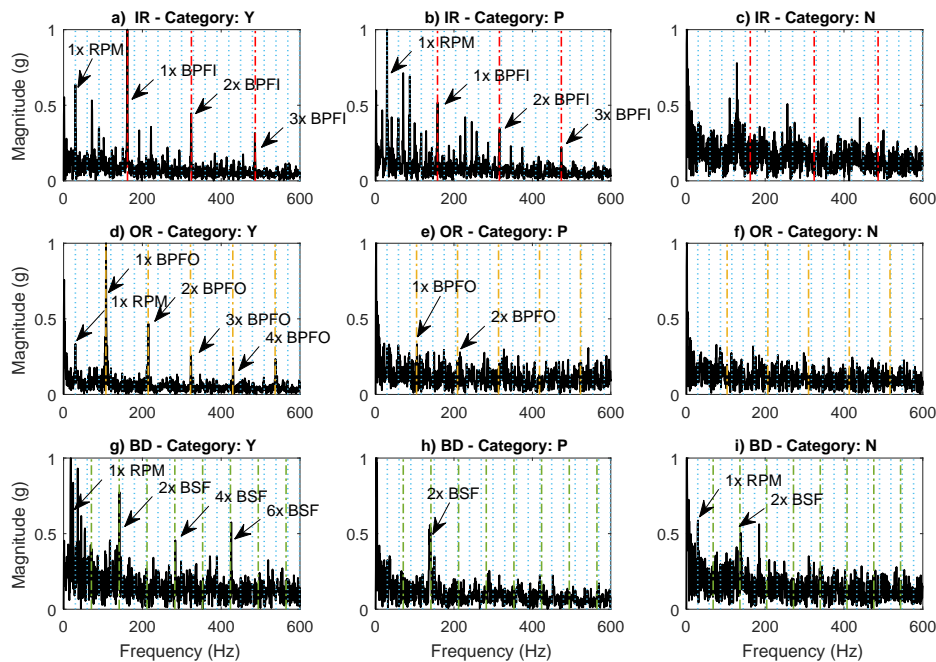
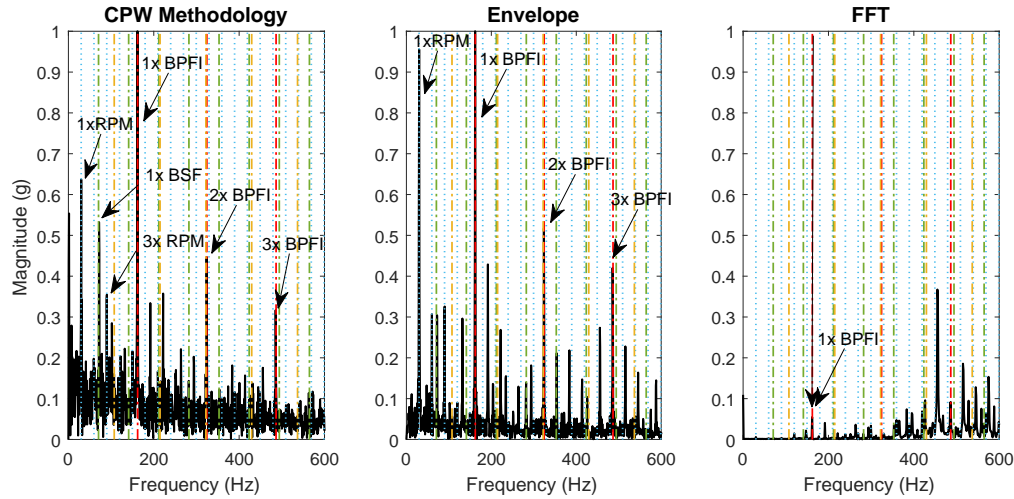
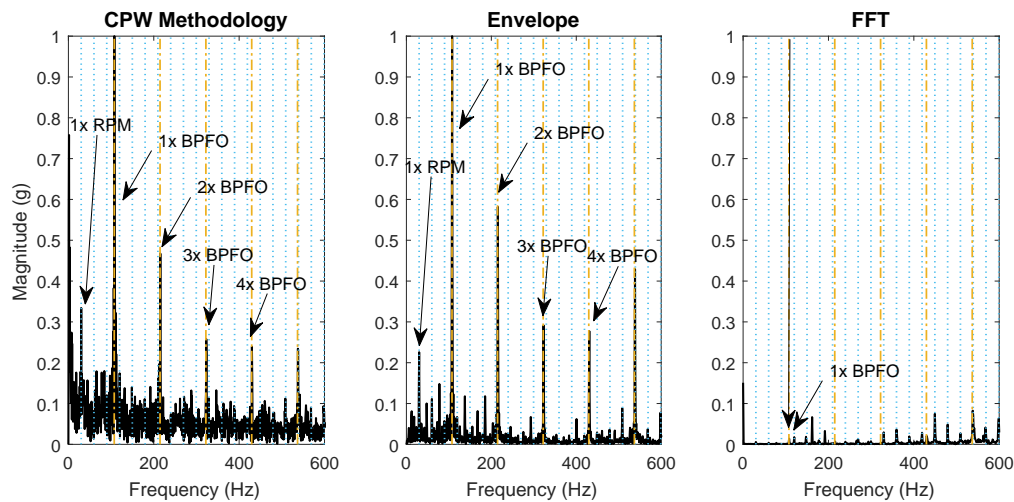


Figure D.2: *CWRU* signals after applying the proposed methodology

**IR signals:** First, the results from the (*Y*) clearly diagnosable signal shown in Fig. D.2 a) was successfully analyzed confirming the presence of the *BPF1* as the dominant frequency with a magnitude of 1 and 2 harmonics in a descendant pattern as expected. In addition to this, a peak in the *BSF* is present but no harmonics as Fig. D.3 show; this can't be taken as a *RE* fault because *BSF* in the Envelope spectrum are present in even harmonics because the fault strikes the same race (inner or outer) in every cycle, so there are two shocks per basic period [Randall, 2011]. In the (*P*) partially diagnosable signal shown in Fig. D.2 b) the fundamental frequency of the rotational speed is the dominant frequency in the spectra with a magnitude of 1 and some harmonics of it are present too; the presence of *BPF1* and the 2 following harmonics of it is confirmed with a lower magnitude than in the (*Y*) type signal. Finally, the (*N*) non diagnosable signal shown in Fig. D.2 c) confirmed that there are no peaks in *BPF1* or any of its harmonics and show a clear Gaussian noise. A comparison between the methodology, Envelope and *FFT* spectra is presented using the (*Y*) category signal in Fig. D.3 where the difference between the methodology and envelope spectra are minimal but mainly focused in the fact that *BPF1* in Envelope spectrum is not the dominant frequency exceeded by the first harmonic of the rotational speed. In the *FFT* comparison is clear that the dominant frequency are over the frequency limit of the graphic, so *BPF1* is almost totally suppressed by it because of the normalization.

Figure D.3: *IR (Y)* category signal method comparison (*CWRU*)

**OR signals:** The results obtained from the (*Y*) clearly diagnosable signal shown in Fig. D.2 d) as expected was easily diagnosable confirming the presence of the *BPFO* as the dominant frequency with a magnitude of 1 and 3 harmonics in a descendant pattern as expected. In the (*P*) partially diagnosable signal shown in Fig. D.2 e) the presence of *BPFO* is hardly remarkable, same as its harmonics and there is no presence of any remarkable frequency peak, so this signal can be barely diagnosable using the methodology. Finally, the (*N*) non diagnosable signal shown in Fig. D.2 f) have no remarkable peak for any *BPFO* peak or harmonic of it as expected. A comparison between the methodology, Envelope and *FFT* spectra is presented using the (*Y*) category signal in Fig. D.4 where there are no remarkable difference between the methodology and envelope spectra besides some Gaussian noise present in the methodology spectrum and the fact that *BPFO* harmonics only in the methodology spectrum have the descendant pattern expected. In the *FFT* comparison is clear that the dominant frequency are over the frequency limit of the graphic same as *IR* case, so *BPFO* is almost totally suppressed by it because of the normalization.

Figure D.4: *OR (Y)* category signal method comparison (*CWRU*)

**RE signals:** The results obtained from the (*Y*) clearly diagnosable signal shown in Fig. D.2 g) have some peak noises

at low frequencies around 1x RPM but the main feature of the signal that is the *BSF* at even harmonics 2x, 4x and 6x are remarkable in the signal, it's worth to repeat that *BSF* in Envelope spectrum is present in even harmonics because the fault strikes the same race (inner or outer) in every cycle [Randall, 2011], despite of not following the descendant pattern expected the signal in general is clearly diagnosable. In the (P) partially diagnosable signal shown in Fig. D.2 h) there are just one peak frequency at the second harmonic of *BSF* which confirm the fault but there is no peaks in the other even harmonics. Finally, the (N) non diagnosable signal shown in Fig. D.2 i) where a peak in 2x*BSF* is hardly remarkable because of the noise overwhelming it. The comparison between the methodology, Envelope and *FFT* spectra is presented using the (Y) category signal in Fig. D.5 where the maximum peak value for 2x*BSF* is compared in the three spectrum and its clear that the methodology have the higher value but in none of them that frequency is the dominant in the spectrum. Also the frequency peaks recognized as noise are identified in the methodology. Same as *IR* and *OR* in the *FFT* comparison is clear that the dominant frequency are over the frequency limit of the graphic, so *BSF* is almost totally suppressed by it because of the normalization.

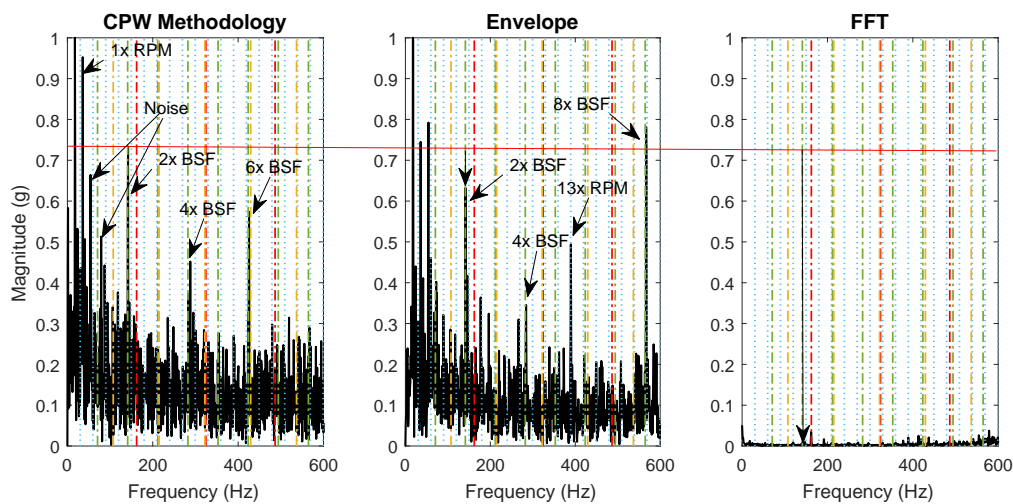


Figure D.5: *RE* (Y) category signal method comparison (*CWRU*)

Table D.1: Bearing fault results for *CWRU* database

Database	Signal	Difficulty	Max mag. (g)	Fault amplitude normalized		Max amplitude	Additional significant peaks <sup>a</sup>
				Fault freq.	Harmonic		
CWRU	IR (Y)	Easy	0.0057	0.4724	0.2109	1 (BPFI)	BPFI H/ Shaft
	IR (P)	Medium	0.0045	0.5584	0.3823	1 (1x Shaft)	BPFI H/ Shaft
	IR (N)	Hard	0.0028	NA	NA	1 (Noise)	Negligible
	OR (Y)	Easy	0.0069	1	0.4674	1 (1x BPFO)	BPFO H/ Shaft
	OR (P)	Medium	0.0023	0.3323	NA	1 (Noise)	BPFO
	OR (N)	Hard	0.0029	NA	NA	1 (Noise)	Negligible
	RE (Y)	Easy	0.0023	0.7736	0.4556	1 (0.5x Shaft)	BSF even H/ Shaft
	RE (P)	Easy	0.0042	0.5575	NA	1 (Noise)	BSF even H
RE (N)	Easy	0.0021	0.5053	NA	1 (Noise)	BSF even H/ Shaft	

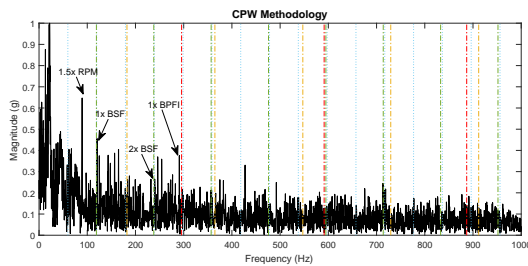
<sup>a</sup>SH = Half harmonic, H = Harmonics, NA= Not Available

# Appendix E

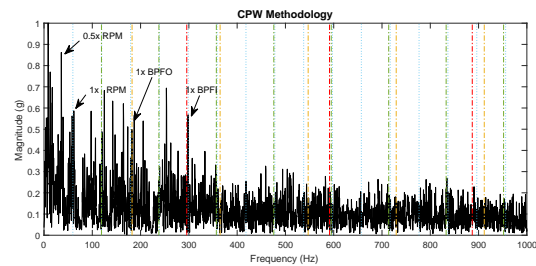
## Additional results

### E.1 Experimental system vibration results

The additional analysis for the experimental system vibration data is presented in this section; where Figs. E.1a, E.1b show the *IR* comparison of the methodology results with envelope and *FFT* for test 3 and 4 signals respectively. Figs. E.2a, E.2b show the *OR* comparison for partially test 2 and 3 signals respectively. Finally, Figs. E.3a, E.3b show the *RE* comparison for test 1 and 3 signals respectively. Table 5.2 show the relevant frequency peaks found in all the signals with the 1<sup>st</sup> and 2<sup>nd</sup> fault harmonic frequency magnitude and the difficulty of diagnosis of each signal.



(a) *IR* Test:3 vibration signal



(b) *IR* Test:4 vibration signal

Figure E.1: *IR* vibration signals

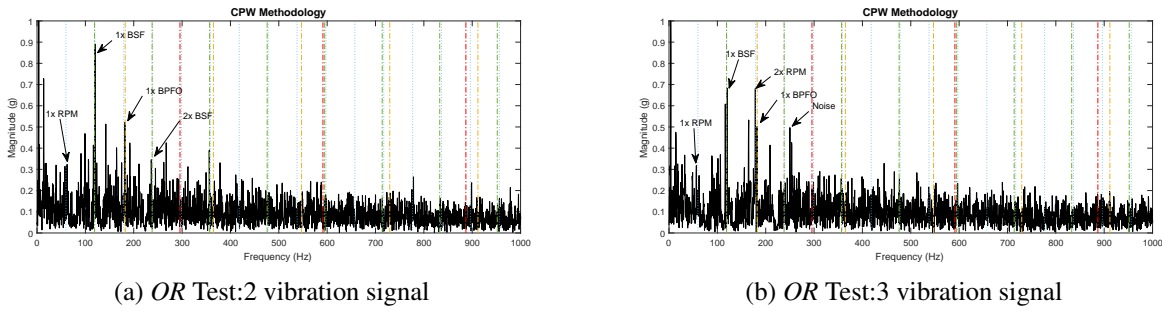


Figure E.2: *OR* vibration signals

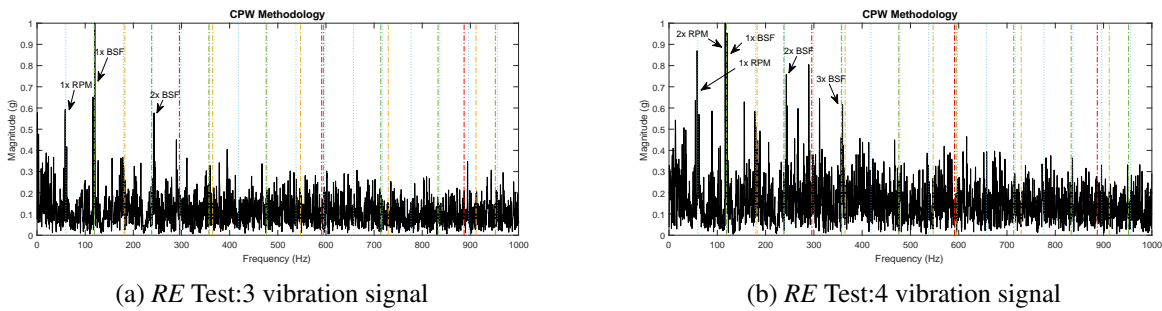


Figure E.3: *RE* vibration signals

## E.2 Experimental system acoustic results

The additional analysis for the experimental system about acoustic emission data is presented; where Figs. E.4a, E.4b show the *IR* comparison of the methodology results with envelope and *FFT* for test 3 and 4 signals respectively. Figs. E.5a, E.5b show the *OR* comparison for partially test 2 and 3 signals respectively. Finally, Figs. E.6a, E.6b show the *RE* comparison for test 1 and 4 signals respectively. Table 5.2 show the relevant frequency peaks found in all the signals with the 1<sup>st</sup> and 2<sup>nd</sup> fault harmonic frequency magnitude and the difficulty of diagnosis of each signal.

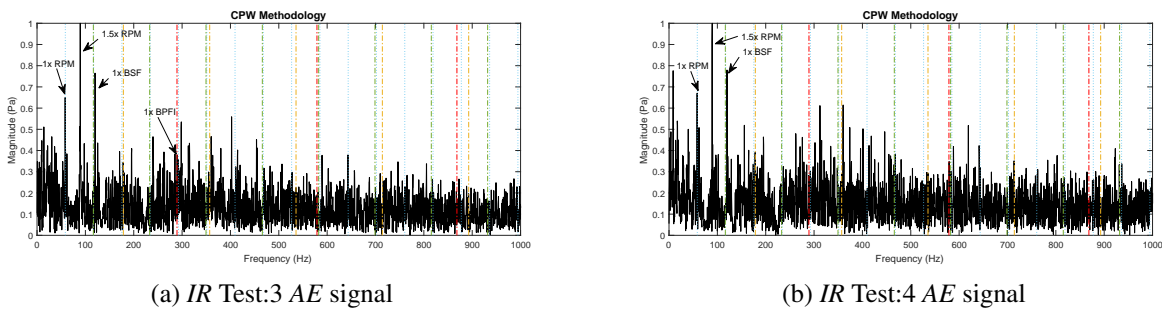
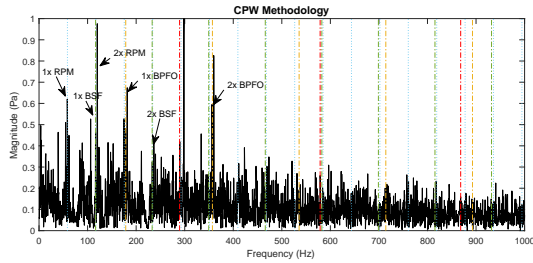
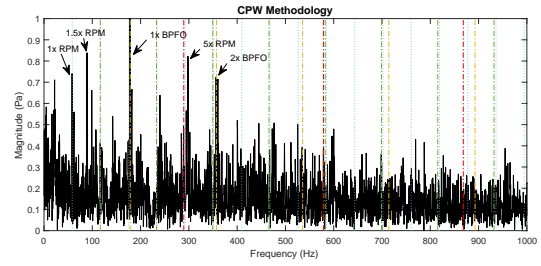
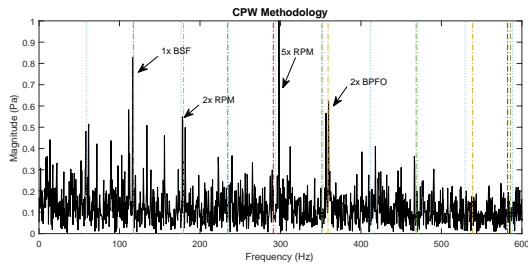
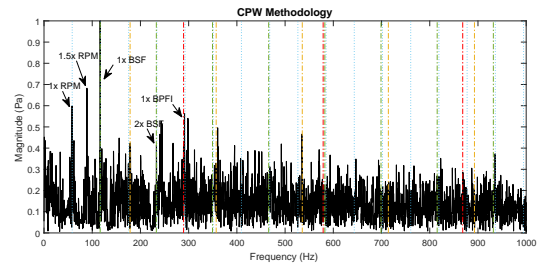


Figure E.4: *IR* AE signals

(a) *OR* Test:2 AE signal(b) *OR* Test:3 AE signalFigure E.5: *OR* AE signals(a) *RE* Test:1 AE signal(b) *RE* Test:4 AE signalFigure E.6: *RE* AE signals

# Appendix F

## Developed code

To implement the methodology four basic Matlab functions were developed, one function to trim the signal in a window defined by the user in seconds, one function to compute the *FFT* of a signal, one function to compute the envelope spectrum of a signal with trend removal included and one function to compute the *CPW* pre processing and frequency analysis with option for *FFT* or Envelope spectrum. The following codes is used to analyze the *CWRU* database with an easier selection using variables to avoid putting the name of the signals:

```
1 % Methodology for CWRU
2 % Oscar Tamayo P.      tamayo.oscar@hotmail.com
3 %
4 % This script is designed to analyze the signals from CWRU only.
5 %
6 clear all                %Clear existing data
7 %% ////////////////////////////////////////////////////////////////////
8 % Figure colors matrix
9 %//////////////////////////////////////////////////////////////////
10     0.000 0.000 0.000; % 1 Negro
11     1.000 0.141 0.420; % 2 Rosado
12     0.180 0.333 0.745; % 3 AzulCeleste
13     0.950 0.425 0.098; % 4 Naranja
14     0.466 0.674 0.188; % 5 VerdeC
15     0.929 0.694 0.125; % 6 Mostaza
16     0.301 0.745 0.933; % 7 Celeste
17     0.494 0.184 0.556; % 8 Morado
18     1.000 0.000 0.000; % 9 Rojo
19     0.000 0.800 0.500; % 10
20 ];
21 %% ////////////////////////////////////////////////////////////////////
22 % General variables
23 %//////////////////////////////////////////////////////////////////
24 Fs=12000;                %Sample frequency
25 lims=600;                %Superior limit for frequency spectrum
26 Ancho=5.5;              %Dimensions for figure plots
```

```

27 Alto=6.2;
28 th1=1.2;           %Signal plot thickness
29 th2=1;            %Guidelines plot thickness
30 %% ///////////////////////////////////////////////////////////////////
31 % Data import and selection for CWRU
32 %% ///////////////////////////////////////////////////////////////////
33 Sensor='DE_time';   % {DE (Drive End),FE (Fan End),BA (Base)}
34 faultSensor='DE12k'; % {DE12k, DE48k, FE12k}
35 Exper=0;           % Experiment load: [0,3]
36 faultMag=21;       % Fault magnitude {7,14,21,28}
37 addpath('Put here the route of the data');
38 arc_IR=strcat(faultSensor, '_', num2str(Exper), '_', num2str(faultMag, '%3.3u'), '_IR');
39 arc_B=strcat(faultSensor, '_', num2str(Exper), '_', num2str(faultMag, '%3.3u'), '_B');
40 arc_OR_C=strcat(faultSensor, '_', num2str(Exper), '_', num2str(faultMag, '%3.3u'), '_OR_C');
41 arc_OR_Op=strcat(faultSensor, '_', num2str(Exper), '_', num2str(faultMag, '%3.3u'), '_OR_Op');
42 arc_OR_Or=strcat(faultSensor, '_', num2str(Exper), '_', num2str(faultMag, '%3.3u'), '_OR_Or');
43 %% ///////////////////////////////////////////////////////////////////
44 % Bearing data 6205-2RS JEM SKF, deep groove ball bearing
45 %% ///////////////////////////////////////////////////////////////////
46 n=9;              %Number of balls
47 BD=0.3126;        %Rolling element diameter
48 PD=1.537;         %Pitch diameter
49 theta=0;          %Angle of the load from radial plane
50
51 switch Exper
52     case 0
53         frm=1797/60; % Rotor speed in Hz for each load
54     case 1
55         frm=1772/60;
56     case 2
57         frm=1750/60;
58     case 3
59         frm=1730/60;
60     otherwise
61         disp('Error!!');
62 end
63 f_OD=0.5*n*frm*(1-(BD/PD)*cos(theta)); %BPFO
64 f_ID=0.5*n*frm*(1+(BD/PD)*cos(theta)); %BPFI
65 f_CD=0.5*frm*(1-(BD/PD)*cos(theta)); %FTF
66 f_BD=0.5*(PD/BD)*frm*(1-(BD/PD)^2*cos(theta)^2); %BSF

```



```

67 %% //////////////////////////////////////////////////////////////////////////////////////////////////////////////////////////////////
68 % Methodology application
69 //////////////////////////////////////////////////////////////////////////////////////////////////////////////////////////////////
70 fault=5; %Fault type selection: 1 for IR, 2 for OR_C , 4 OR_Op, 5 OR_Or, 6 RE
71 ti=0; %Initial time value for time signal
72 tf=ti+(25/frm); %Final time value for time signal using 100 revolutions
73
74 switch fault
75     case 1 %Inner Race case
76         vars=whos('-file',strcat(arc_IR, '.mat')); %String for import IR
77         pos=0;
78         for ii=1:length([vars.size])/2
79             if length(strfind(vars(ii,1).name, 'DE_time'))>=1
80                 pos=ii;
81             end
82         end
83         if pos==0
84             disp('Error');
85         end
86         Data_IR=load(arc_IR, vars(pos,1).name); %Import data for IR
87         Data_Original=Data_IR.(vars(pos,1).name);
88         Data=Recortar(Data_Original, ti, tf, Fs); %Crooped signal
89
90         [freqFFT, FFT]= FFT_OTP(Data, Fs); %FFT with trend removal
91         [freqENV, ENV]= envolventeTrend(Data, Fs, 2); %Envelope with trend removal
92         [freqCPW, CPW]=cepstrumPWTrend(Data, Fs, 'envelope'); %CPW methodology
93
94         FFT_norm=Normalizar(FFT); %FFT normalization
95         ENV_norm=Normalizar(ENV); %Envelope normalization
96         CPW_norm=Normalizar(CPW); %CPW methodology normalization
97
98     case 2 %Central Outer Race case
99         vars=whos('-file',strcat(arc_OR_C, '.mat')); %String for import OR_C
100        pos=0;
101        for ii=1:length([vars.size])/2
102            if length(strfind(vars(ii,1).name, 'DE_time'))>=1
103                pos=ii;
104            end
105        end
106        if pos==0
107            disp('Error');
108        end
109        Data_OR_C=load(arc_OR_C, vars(pos,1).name); %Import data for OR_C
110        Data_Original=Data_OR_C.(vars(pos,1).name);
111        Data=Recortar(Data_Original, ti, tf, Fs); %Crooped signal

```

```

112
113     [freqFFT ,FFT]= FFT_OTP(Data ,Fs);           %FFT with trend removal
114     [freqENV ,ENV]= envolventeTrend (Data ,Fs ,2);%Envelope with trend removal
115     [freqCPW ,CPW]=cepstrumPWTrend (Data ,Fs , 'envelope');   %CPW methodology
116
117     FFT_norm=Normalizar (FFT);                 %FFT normalization
118     ENV_norm=Normalizar (ENV);                 %Envelope normalization
119     CPW_norm=Normalizar (CPW);                 %CPW methodology normalization
120
121     case 3                                     %Opposite Outer Race case
122         vars=whos ('-file ' ,strcat (arc_OR_Op , '.mat')); %String for import OR_Op
123         pos=0;
124         for ii =1:length ([ vars . size ])/2
125             if length (strfind (vars (ii ,1) .name , 'DE_time'))>=1
126                 pos=ii ;
127             end
128         end
129         if pos==0
130             disp ('Error');
131         end
132         Data_OR_Op=load (arc_OR_Op , vars (pos ,1) .name); %Import data for OR_Op
133         Data_Original=Data_OR_Op .( vars (pos ,1) .name);
134         Data=Recortar (Data_Original , ti , tf ,Fs); %Crooped signal
135
136         [freqFFT ,FFT]= FFT_OTP(Data ,Fs);           %FFT with trend removal
137         [freqENV ,ENV]= envolventeTrend (Data ,Fs ,2);%Envelope with trend removal
138         [freqCPW ,CPW]=cepstrumPWTrend (Data ,Fs , 'envelope');   %CPW methodology
139
140         FFT_norm=Normalizar (FFT);                 %FFT normalization
141         ENV_norm=Normalizar (ENV);                 %Envelope normalization
142         CPW_norm=Normalizar (CPW);                 %CPW methodology normalization
143
144     case 4                                     %Orthogonal Outer Race case
145         vars=whos ('-file ' ,strcat (arc_OR_Or , '.mat')); %String for import OR_Or
146         pos=0;
147         for ii =1:length ([ vars . size ])/2
148             if length (strfind (vars (ii ,1) .name , 'DE_time'))>=1
149                 pos=ii ;
150             end
151         end
152         if pos==0
153             disp ('Error');
154         end
155         Data_OR_Or=load (arc_OR_Or , vars (pos ,1) .name); %Import data for OR_Or
156         Data_Original=Data_OR_Or .( vars (pos ,1) .name);

```

```

157 Data=Recortar(Data_Original , ti , tf , Fs); %Crooped signal
158
159 [freqFFT ,FFT]= FFT_OTP(Data , Fs); %FFT with trend removal
160 [freqENV ,ENV]= envolventeTrend(Data ,Fs ,2);%Envelope with trend removal
161 [freqCPW ,CPW]=cepstrumPWTrend(Data ,Fs , 'envelope'); %CPW methodology
162
163 FFT_norm=Normalizar(FFT); %FFT normalization
164 ENV_norm=Normalizar(ENV); %Envelope normalization
165 CPW_norm=Normalizar(CPW); %CPW methodology normalization
166
167 case 5 %Rolling Element case
168 vars=whos('-file',strcat(arc_B , '.mat')); %String for import RE
169 pos=0;
170 for ii=1:length([vars.size])/2
171 if length(strfind(vars(ii,1).name , 'DE_time'))>=1
172 pos=ii;
173 end
174 end
175 if pos==0
176 disp('Error');
177 end
178 Data_B=load(arc_B , vars(pos,1).name); %Import data for RE fault
179 Data_Original=Data_B.(vars(pos,1).name);
180 Data=Recortar(Data_Original , ti , tf , Fs); %Crooped signal
181
182 [freqFFT ,FFT]= FFT_OTP(Data , Fs); %FFT with trend removal
183 [freqENV ,ENV]= envolventeTrend(Data ,Fs ,2);%Envelope with trend removal
184 [freqCPW ,CPW]=cepstrumPWTrend(Data ,Fs , 'envelope'); %CPW methodology
185
186 FFT_norm=Normalizar(FFT); %FFT normalization
187 ENV_norm=Normalizar(ENV); %Envelope normalization
188 CPW_norm=Normalizar(CPW); %CPW methodology normalization
189 end
190 %%%%%%%%%%%%%%%%%%%%%%%%%%%%%%%%%%%%%%%%%%%%%%%%%%%%%%%%%%%%%%%%%%%%%%%%%
191 % CPW Methodology comparison with Envelope and FFT of selected signal
192 %%%%%%%%%%%%%%%%%%%%%%%%%%%%%%%%%%%%%%%%%%%%%%%%%%%%%%%%%%%%%%%%%%%%%%%%%
193 figure('units','inches','Position',[3 0 Ancho*1.75 Alto*0.65])
194 subplot(1,3,3)
195 plot(freqFFT ,FFT_norm , 'Color',co(1,:) , 'LineWidth',th1); %FFT plot
196 hold on;
197 i=1;
198 while (i*frm)<lims
199 plot([i*frm i*frm],[ -2e6 2e6], 'LineStyle',':', 'Color',co(7,:) , '
lineWidth',th2); %RPM
200 i=i+1;

```

```

201     end
202     i=1;
203     while (i*f_ID)<lims
204         plot([i*f_ID i*f_ID],[-2e6 2e6], 'LineStyle', '-.', 'Color', co(9,:), '
lineWidth', th2); %BPFI
205         i=i+1;
206     end
207     i=1;
208     while (i*f_BD)<lims
209         plot([i*f_BD i*f_BD],[-2e6 2e6], 'LineStyle', '-.', 'Color', co(5,:), '
lineWidth', th2); %BSF
210         i=i+1;
211     end
212     i=1;
213     while (i*f_OD)<lims
214         plot([i*f_OD i*f_OD],[-2e6 2e6], 'LineStyle', '-.', 'Color', co(6,:), '
lineWidth', th2); %BPFO
215         i=i+1;
216     end
217     hold off;
218     xlabel('Frequency (Hz)');
219     title('FFT', 'FontSize', 12)
220     axis([0 lims 0 1])
221
222     subplot(1,3,1)
223     plot(freqCPW, CPW_norm, 'Color', co(1,:), 'LineWidth', th1); %CPW plot
224     hold on;
225     i=1;
226     while (i*frm)<lims
227         plot([i*frm i*frm],[-2e6 2e6], 'LineStyle', ':', 'Color', co(7,:), '
lineWidth', th2); %RPM
228         i=i+1;
229     end
230     i=1;
231     while (i*f_ID)<lims
232         plot([i*f_ID i*f_ID],[-2e6 2e6], 'LineStyle', '-.', 'Color', co(9,:), '
lineWidth', th2); %BPFI
233         i=i+1;
234     end
235     i=1;
236     while (i*f_BD)<lims
237         plot([i*f_BD i*f_BD],[-2e6 2e6], 'LineStyle', '-.', 'Color', co(5,:), '
lineWidth', th2); %BSF
238         i=i+1;
239     end

```

```

240     i=1;
241     while (i*f_OD)<lims
242         plot([i*f_OD i*f_OD],[-2e6 2e6], 'LineStyle','-.', 'Color',co(6,:), '
lineWidth',th2); %BPFO
243         i=i+1;
244     end
245     hold off
246     ylabel('Magnitude (g)');
247     xlabel('Frequency (Hz)');
248     title('CPW Methodology','FontSize',12)
249     axis([0 lims 0 1])
250
251     subplot(1,3,2)
252     plot(freqENV,ENV_norm, 'Color',co(1,:), 'LineWidth',th1);%Envelope plot
253     hold on;
254     i=1;
255     while (i*frm)<lims
256         plot([i*frm i*frm],[-2e6 2e6], 'LineStyle',':', 'Color',co(7,:), '
lineWidth',th2); %RPM
257         i=i+1;
258     end
259     i=1;
260     while (i*f_ID)<lims
261         plot([i*f_ID i*f_ID],[-2e6 2e6], 'LineStyle','-.', 'Color',co(9,:), '
lineWidth',th2); %BPFI
262         i=i+1;
263     end
264     i=1;
265     while (i*f_BD)<lims
266         plot([i*f_BD i*f_BD],[-2e6 2e6], 'LineStyle','-.', 'Color',co(5,:), '
lineWidth',th2); %BSF
267         i=i+1;
268     end
269     i=1;
270     while (i*f_OD)<lims
271         plot([i*f_OD i*f_OD],[-2e6 2e6], 'LineStyle','-.', 'Color',co(6,:), '
lineWidth',th2); %BPFO
272         i=i+1;
273     end
274     hold off;
275     title('Envelope','FontSize',12)
276     xlabel('Frequency (Hz)');
277     axis([0 lims 0 1])

```

The following codes is used to analyze the Experimental System database with an easier selection using variables to avoid putting the name of the signals:

```

1 % Methodology for Experimental System
2 % Oscar Tamayo P.      tamayo.oscar@hotmail.com
3 %
4 % This script is designed to analyze the signals from the experimental system
   only .
5 %
6 clear all                %Clear existing data
7 %%////////////////////////////////////////////////////////////////////////////////////////////////////////////////////////////////
8 % Figure colors matrix
9 %////////////////////////////////////////////////////////////////////////////////////////////////////////////////////////////////
10 co=[...
11     0.000 0.000 0.000; % 1 Negro
12     1.000 0.141 0.420; % 2 Rosado
13     0.180 0.333 0.745; % 3 AzulCeleste
14     0.950 0.425 0.098; % 4 Naranja
15     0.466 0.674 0.188; % 5 VerdeC
16     0.929 0.694 0.125; % 6 Mostaza
17     0.301 0.745 0.933; % 7 Celeste
18     0.494 0.184 0.556; % 8 Morado
19     1.000 0.000 0.000; % 9 Rojo
20     0.000 0.800 0.500; % 10
21 ];
22 %%////////////////////////////////////////////////////////////////////////////////////////////////////////////////////////////////
23 % General variables
24 %////////////////////////////////////////////////////////////////////////////////////////////////////////////////////////////////
25 Fs=25600;                %Sample frequency
26 lims=1000;              %Superior limit for frequency spectrum
27 Ancho=5.5;              %Dimensions for figure plots
28 Alto=6.2;
29 L=6;                    %Number of RMS multiples of RMS filter
30 th1=1.2;                %Signal plot thickness
31 th2=1;                  %Guidelines plot thickness
32 RatioExp=87.6;          %Expansion parameter
33 CompType='a/compressor'; %Compand type a or mu / expander or compressor
34 %%////////////////////////////////////////////////////////////////////////////////////////////////////////////////////////////////
35 % Bearing data 6204-2Z SKF, deep groove ball bearing
36 %////////////////////////////////////////////////////////////////////////////////////////////////////////////////////////////////
37 n=8;                    %Number of balls
38 BD=0.3126;              %Rolling element diameter
39 PD=1.319;               %Pitch diameter
40 theta=0;                %Angle of the load from radial plane
41 frm=3585/60;            %Rotor speed in Hz
42 f_OD=0.5*n*frm*(1-(BD/PD)*cos(theta)); %BPFO
43 f_ID=0.5*n*frm*(1+(BD/PD)*cos(theta)); %BPFI
44 f_CD=0.5*frm*(1-(BD/PD)*cos(theta)); %FTF

```

```

45 f_BD=0.5*(PD/BD)*frm*(1-(BD/PD)^2*cos(theta)^2); %BSF
46 %% //////////////////////////////////////////////////////////////////////////////////////////////////////////////////////////////////
47 % Data import for experimental system
48 %% //////////////////////////////////////////////////////////////////////////////////////////////////////////////////////////////////
49 Sensor=2; %Sensor signal: {3=Acc_x1, 4=Acc_z2, 5=Acc_z1, 2=AE}
50 fault=2; %Fault type: 1 for IR, 2 for OR, 3 for RE, 4 for NM
51 ti=3.5; %Initial time value for time signal
52 tf=ti+(100/frm); %Final time value for time signal using 100 revolutions
53 switch fault %Selection of fault for import data string
54     case 1
55         tit='Inner Race (IR) @';
56         cat='IR';
57     case 2
58         tit='Outer Race (OR) @';
59         cat='OR';
60     case 3
61         tit='Ball Defect (BD) @';
62         cat='BD';
63     case 4
64         tit='Normal State @';
65         cat='NM';
66 end
67 test='2'; %Selection of fault test for import data string
68 ExpSys_arc=strcat('test_00',num2str(test),'_',cat,'.lvm');%Import data string
69 ExpSys=importdata(ExpSys_arc); %Import data
70 %% //////////////////////////////////////////////////////////////////////////////////////////////////////////////////////////////////
71 % Methodology application for vibration
72 %% //////////////////////////////////////////////////////////////////////////////////////////////////////////////////////////////////
73 switch Sensor
74     case {3, 4, 5} % Vibration signals
75         Data=ExpSys(:, Sensor); %Selection of vibration data from structure
76         Data=Recortar(Data, ti, tf, Fs); %Crooped signal
77
78         [freqFFT, FFT]= FFT_OTP(Data, Fs); %FFT with trend removal
79         [freqENV, ENV]= envolventeTrend(Data, Fs, 2);%Envelope with trend removal
80         [freq_CPW, CPW]=cepstrumPWTrend(Data, Fs, 'envelope'); %CPW methodology
81
82         FFT_norm=Normalizar(FFT, Fs); %FFT normalization
83         ENV_norm=Normalizar(ENV, Fs); %Envelope normalization
84         CPW_norm=Normalizar(CPW, Fs); %CPW methodology normalization
85 %% //////////////////////////////////////////////////////////////////////////////////////////////////////////////////////////////////
86 % CPW Methodology comparison with Envelope and FFT (vibration)
87 %% //////////////////////////////////////////////////////////////////////////////////////////////////////////////////////////////////
88
89 figure('units','inches','Position',[3 0 Ancho*1.75 Alto*0.65])

```

```

90 subplot(1,3,3)
91 plot(freqFFT,FFT_norm,'Color',co(1,:), 'LineWidth',th1); %FFT plot
92 hold on;
93 i=1;
94 while (i*frm)<lims
95     plot([i*frm i*frm],[-2e6 2e6], 'LineStyle',':', 'Color',co(7,:), 'lineWidth',
96         th2); %RPM
97     i=i+1;
98 end
99 i=1;
100 while (i*f_ID)<lims
101     plot([i*f_ID i*f_ID],[-2e6 2e6], 'LineStyle','-.', 'Color',co(9,:), 'lineWidth',
102         ,th2); %BPFI
103     i=i+1;
104 end
105 i=1;
106 while (i*f_BD)<lims
107     plot([i*f_BD i*f_BD],[-2e6 2e6], 'LineStyle','-.', 'Color',co(5,:), 'lineWidth',
108         ,th2); %BSF
109     i=i+1;
110 end
111 i=1;
112 while (i*f_OD)<lims
113     plot([i*f_OD i*f_OD],[-2e6 2e6], 'LineStyle','-.', 'Color',co(6,:), 'lineWidth',
114         ,th2); %BPFO
115     i=i+1;
116 end
117 hold off;
118 xlabel('Frequency (Hz)');
119 title('FFT', 'FontSize',12)
120 axis([0 lims 0 1])
121
122 subplot(1,3,1)
123 plot(freq_CPW,CPW_norm,'Color',co(1,:), 'LineWidth',th1); %CPW plot
124 hold on;
125 i=1;
126 while (i*frm)<lims
127     plot([i*frm i*frm],[-2e6 2e6], 'LineStyle',':', 'Color',co(7,:), 'lineWidth',
128         th2); %RPM
129     i=i+1;
130 end
131 i=1;
132 while (i*f_ID)<lims
133     plot([i*f_ID i*f_ID],[-2e6 2e6], 'LineStyle','-.', 'Color',co(9,:), 'lineWidth',
134         ,th2); %BPFI

```



```

129     i=i+1;
130 end
131 i=1;
132 while (i*f_BD)<lims
133     plot([i*f_BD i*f_BD],[-2e6 2e6], 'LineStyle','-.', 'Color',co(5,:), 'lineWidth'
134         ,th2); %BSF
135     i=i+1;
136 end
137 i=1;
138 while (i*f_OD)<lims
139     plot([i*f_OD i*f_OD],[-2e6 2e6], 'LineStyle','-.', 'Color',co(6,:), 'lineWidth'
140         ,th2); %BPFO
141     i=i+1;
142 end
143 hold off
144 ylabel('Magnitude (g)');
145 xlabel('Frequency (Hz)');
146 title('CPW Methodology', 'FontSize',12)
147 axis([0 lims 0 1])
148
149 subplot(1,3,2)
150 plot(freqENV,ENV_norm, 'Color',co(1,:), 'LineWidth',th1); % Envelope plot
151 hold on;
152 i=1;
153 while (i*frm)<lims
154     plot([i*frm i*frm],[-2e6 2e6], 'LineStyle',':', 'Color',co(7,:), 'lineWidth',
155         ,th2); %RPM
156     i=i+1;
157 end
158 i=1;
159 while (i*f_ID)<lims
160     plot([i*f_ID i*f_ID],[-2e6 2e6], 'LineStyle','-.', 'Color',co(9,:), 'lineWidth'
161         ,th2); %BPFI
162     i=i+1;
163 end
164 i=1;
165 while (i*f_BD)<lims
166     plot([i*f_BD i*f_BD],[-2e6 2e6], 'LineStyle','-.', 'Color',co(5,:), 'lineWidth'
167         ,th2); %BSF
168     i=i+1;
169 end
170 i=1;
171 while (i*f_OD)<lims
172     plot([i*f_OD i*f_OD],[-2e6 2e6], 'LineStyle','-.', 'Color',co(6,:), 'lineWidth'
173         ,th2); %BPFO

```

```

168     i=i+1;
169 end
170 hold off;
171 title('Envelope','FontSize',12)
172 xlabel('Frequency (Hz)');
173 axis([0 lims 0 1])
174 %%%%%%%%%%%%%%%%%%%%%%%%%%%%%%%%%%%%%%%%%%%%%%%%%%%%%%%%%%%%%%%%%%%%%%%%%
175 % Methodology application for AE
176 %%%%%%%%%%%%%%%%%%%%%%%%%%%%%%%%%%%%%%%%%%%%%%%%%%%%%%%%%%%%%%%%%%%%%%%%%
177
178 case 2                                %Acoustic emission signals
179     Data=ExpSys(:,Sensor); %Selection of specific AE data from structure
180     Data=Recortar(Data,ti,tf,Fs); %Crooped signal
181     RMS=rms(Data); %RMS value of original signal
182
183     g=1; %RMS filter application
184     while g<=(length(Data))
185         if abs(Data(g))>RMS*L
186             if Data(g)>0
187                 Data(g)=RMS*L;
188             else
189                 Data(g)=-RMS*L;
190             end
191         end
192         g=g+1;
193     end
194
195     Data_Comp=compand(Data,RatioExp,(max(abs(RMS*L))),CompType); %Companding
196     [freqFFT_Comp,FFT_Comp]=FFT_OTP(Data_Comp,Fs);%FFT with trend removal
197     [freqENV_Comp,ENV_Comp]=envolventeTrend(Data_Comp,Fs,2); %Envelope with
198     trend removal
199     [freq_Comp,CPW_Comp]=cepstrumPWTrend(Data_Comp,Fs,'envelope');%CPW
200     methodology application
201
202     FFT_Comp_norm=Normalizar(FFT_Comp,Fs); %FFT normalization
203     ENV_Comp_norm=Normalizar(ENV_Comp,Fs); %Envelope normalization
204     CPW_Comp_norm=Normalizar(CPW_Comp,Fs); %CPW methodology normalization
205 %%%%%%%%%%%%%%%%%%%%%%%%%%%%%%%%%%%%%%%%%%%%%%%%%%%%%%%%%%%%%%%%%%%%%%%%%
206 % CPW Methodology comparison with Envelope and FFT (AE)
207 %%%%%%%%%%%%%%%%%%%%%%%%%%%%%%%%%%%%%%%%%%%%%%%%%%%%%%%%%%%%%%%%%%%%%%%%%
208 figure('units','inches','Position',[3 0 Ancho*1.75 Alto*0.65])
209 subplot(1,3,3)
210 plot(freqFFT_Comp,FFT_Comp_norm,'Color',co(1,:), 'LineWidth',th1);%FFT plot
211 hold on;
212 i=1;

```

```

211 while (i*frm)<lims
212     plot([i*frm i*frm],[-2e6 2e6], 'LineStyle',':', 'Color',co(7,:), 'lineWidth',
          th2); %RPM
213     i=i+1;
214 end
215 i=1;
216 while (i*f_ID)<lims
217     plot([i*f_ID i*f_ID],[-2e6 2e6], 'LineStyle','-.', 'Color',co(9,:), 'lineWidth',
          ,th2); %BPM
218     i=i+1;
219 end
220 i=1;
221 while (i*f_BD)<lims
222     plot([i*f_BD i*f_BD],[-2e6 2e6], 'LineStyle','-.', 'Color',co(5,:), 'lineWidth',
          ,th2); %BSF
223     i=i+1;
224 end
225 i=1;
226 while (i*f_OD)<lims
227     plot([i*f_OD i*f_OD],[-2e6 2e6], 'LineStyle','-.', 'Color',co(6,:), 'lineWidth',
          ,th2); %BPFO
228     i=i+1;
229 end
230 hold off;
231 xlabel('Frequency (Hz)');
232 title('FFT', 'FontSize',12)
233 axis([0 lims 0 1])
234
235 subplot(1,3,1)
236 plot(freq_Comp,CPW_Comp_norm, 'Color',co(1,:), 'LineWidth',th1); %CPW plot
237 hold on;
238 i=1;
239 while (i*frm)<lims
240     plot([i*frm i*frm],[-2e6 2e6], 'LineStyle',':', 'Color',co(7,:), 'lineWidth',
          th2); %RPM
241     i=i+1;
242 end
243 i=1;
244 while (i*f_ID)<lims
245     plot([i*f_ID i*f_ID],[-2e6 2e6], 'LineStyle','-.', 'Color',co(9,:), 'lineWidth',
          ,th2); %BPM
246     i=i+1;
247 end
248 i=1;
249 while (i*f_BD)<lims

```

```

250     plot([i*f_BD i*f_BD],[-2e6 2e6], 'LineStyle', '-.', 'Color', co(5,:), 'lineWidth'
        , th2); %BSF
251     i=i+1;
252 end
253 i=1;
254 while (i*f_OD)<lims
255     plot([i*f_OD i*f_OD],[-2e6 2e6], 'LineStyle', '-.', 'Color', co(6,:), 'lineWidth'
        , th2); %BPFO
256     i=i+1;
257 end
258 hold off
259 ylabel('Magnitude (Pa)');
260 xlabel('Frequency (Hz)');
261 title('CPW Methodology', 'FontSize', 12)
262 axis([0 lims 0 1])
263
264 subplot(1,3,2)
265 plot(freqENV_Comp, ENV_Comp_norm, 'Color', co(1,:), 'LineWidth', th1); %Envelop plot
266 hold on;
267 i=1;
268 while (i*frm)<lims
269     plot([i*frm i*frm],[-2e6 2e6], 'LineStyle', ':', 'Color', co(7,:), 'lineWidth',
        th2); %RPM
270     i=i+1;
271 end
272 i=1;
273 while (i*f_ID)<lims
274     plot([i*f_ID i*f_ID],[-2e6 2e6], 'LineStyle', '-.', 'Color', co(9,:), 'lineWidth'
        , th2); %BPFI
275     i=i+1;
276 end
277 i=1;
278 while (i*f_BD)<lims
279     plot([i*f_BD i*f_BD],[-2e6 2e6], 'LineStyle', '-.', 'Color', co(5,:), 'lineWidth'
        , th2); %BSF
280     i=i+1;
281 end
282 i=1;
283 while (i*f_OD)<lims
284     plot([i*f_OD i*f_OD],[-2e6 2e6], 'LineStyle', '-.', 'Color', co(6,:), 'lineWidth'
        , th2); %BPFO
285     i=i+1;
286 end
287 hold off;
288 title('Envelope', 'FontSize', 12)

```

```

289 xlabel('Frequency (Hz)');
290 axis([0 lims 0 1])
291 end

```

The functions used in the codes are:

```

1 % Oscar Tamayo P. tamayo.oscar@hotmail.com
2 % This function trim the signal for a given window size (s)
3 % t = Time vector
4 % signal = Original signal
5 % ti = Initial time (s)
6 % tf = Final time (s)
7 % Fs = Sampling frequency of the original signal
8 %
9 function Trim = Recortar(signal , ti , tf ,Fs)
10 t=(0:1/Fs:(length(signal)-1)/Fs);
11 i=1;
12 l=1;
13 Trim=zeros(1,length(signal));
14 while i<=length(signal)
15     if t(i)>=ti && t(i)<=tf
16         Trim(l)=signal(i);
17         l=l+1;
18         i=i+1;
19     else
20         i=i+1;
21     end
22 end
23 return

```

```

1 % Oscar Tamayo P. tamayo.oscar@hotmail.com
2 % This function compute the Fast Fourier Transform of a signal
3 % L = length of original signal array
4 % Signal = Original signal
5 % freqFFT= Frequency array for FFT Spectrum
6 % aux = Two-Sided Amplitude FFT Spectrum of the signal
7 % FFT = Single-Sided Amplitude FFT Spectrum of the signal
8 %
9 function [freqFFT ,FFT]= FFT_OTP(Signal ,Fs)
10 L=length(Signal);
11 freqFFT=Fs*(0:floor(L/2))/L;
12 aux = abs(fft(Signal)/L);
13 FFT= aux(1:floor(L/2)+1); FFT(2:end-1) = 2*FFT(2:end-1);
14 return

```

```

1 % Oscar Tamayo P. tamayo.oscar@hotmail.com
2 % This function computes the envelope of the signal by two different

```

```

3 % methods: Butterworth low pass filter and Hilbert Transform
4 %
5 %First Method: By using Low Pass Filter. The Signal is Squared, Passed
6 %through LPF and then taken square root.
7 %
8 %Second Method: Using Hilbert Transform. Hilbert Transform is taken using
9 %the inbuilt function in Matlab
10 %
11 %freq_s = Frequency array for reference
12 %Xmag_es = Envelope spectrum
13 %%%%%%%%%%%%%%%%%%%%%%%%%%%%%%%%%%%%%%%%%%%%%%%%%%%%%%%%%%%%%%%%%%%%%%%%%
14 function [freq_s ,Xmag_es]=envolventeTrend (signal ,Fs ,method)
15 n = length(signal); % Length of signal
16 NFFT = 2^nextpow2(n/1); % Next power of 2 from length of y
17 freq_s = Fs/2*linspace(0,1,NFFT/2+1); % Frequency array
18
19 switch method
20     case 1 %Low Pass Filter
21         %Envelope Detection based on Low pass filter and then FFT
22         [a,b]=butter(2,0.1); %Butterworth Filter of 2 poles and Wn=0.1
23         sig_sq=2*signal.* signal; % Squaring for rectifying
24         %gain of 2 for maintianing the same energy in the output
25         y_sq = filter(a,b, sig_sq); %Applying LPF
26         y1=sqrt(y_sq); %Taking Square root
27         t=(0:1/Fs:(length(y1)-1)/Fs); %Time array for trend removal
28         poly = fit(t',y1', 'poly1'); %Trend fit using polynomial approx
29         trend = poly.p1*t+poly.p2; %Trend of 2nd order
30         y2=y1-trend; %Subtraction of trend of the signal
31         X_es = fft(y2,NFFT); % FFT application
32         Xmag_es=2*abs(X_es(1:NFFT/2+1)/n);%Single-Sided Amplitude FFT Spectrum
33
34
35     case 2 %Hilbert Transform
36         %Envelope Detection based on Hilbert Transform and then FFT
37         analy=hilbert(signal); %Inbuilt function for Hilbert transform
38         y1=abs(analy+signal); %Sum of the characteristic function with
39         %original
40         t=(0:1/Fs:(length(y1)-1)/Fs); %Time array for trend removal
41         poly = fit(t',y1', 'poly1'); %Trend fit using polynomial approx
42         trend = poly.p1*t+poly.p2; %Trend of 2nd order
43         y2=y1-trend; %Subtraction of trend of the signal
44         X_es = fft(y2,NFFT); % FFT application
45         Xmag_es=2*abs(X_es(1:NFFT/2+1)/n); %Single-Sided FFT Spectrum
46 end
47 end

```

```

1 % Oscar Tamayo P. tamayo.oscar@hotmail.com
2 % This function computes the Cepstrum pre whitening pre processing of the
3 % signal with two frequency spectrum techniques: FFT and Envelope using
4 % Hilbert Transform
5 %
6 % freq_s = Frequency array for reference
7 % CPW_spectrum = CPW frequency spectrum
8 % CPW_time = Time signal with CPW processing done
9 %%%%%%%%%%%%%%%%%%%%%%%%%%%%%%%%%%%%%%%%%%%%%%%%%%%%%%%%%%%%%%%%%%%%%%%%%
10 function [freq_s ,CPW_spectrum , CPW_time]=cepstrumPWTrend( signal ,Fs ,method)
11
12 esp=fft( signal); %Cepstrum Pre Whitening pre processing
13 CPW_time = ifft( esp ./ abs(esp)); %CPW= ifft(fft(s)/|fft(s)|)
14
15 n = length( signal); % Length of signal
16 NFFT = 2^nextpow2(n/1); % Next power of 2 from length of y
17 freq_s = Fs/2* linspace( 0,1 ,NFFT/2+1); % Frequency array
18
19 switch method
20 case 'FFT' %CPW + FFT
21 X = fft( CPW_time ,NFFT); %FFT application
22 CPW_spectrum=2*abs(X(1:NFFT/2+1)/n); %Single-Sided FFT Spectrum
23
24 case 'envelope' %CPW + Envelope
25 analy=hilbert( CPW_time); %Inbuilt function for Hilbert transform
26 y1=abs( analy+CPW_time); %Sum of the characteristic function with
27 %original
28 t=(0:1/Fs:( length(y1)-1)/Fs); %Time array for trend removal
29 poly = fit( t',y1', 'poly1' ); %Trend fit using polynomial approx
30 trend = poly.p1*t+poly.p2; %Trend of 2nd order
31 y2=y1-trend; %Subtraction of trend of the signal
32 X_es = fft( y2 ,NFFT); % FFT application
33 CPW_spectrum=2*abs( X_es(1:NFFT/2+1)/n); %Single-Sided FFT Spectrum
34
35 end
36 end

```

# **Appendix G**

## **Published papers**



# Diagnóstico de Fallas en Husillos usando la Transformada Rápida de Fourier <sup>\*</sup>

Oscar Tamayo Pazos, Diana Hernández-Alcantara <sup>\*</sup>  
Antonio Jr Vallejo Guevara, David Ibarra Zarate <sup>\*</sup>  
Ruben Morales-Menendez <sup>\*</sup>

<sup>\*</sup> *Tecnológico de Monterrey, School of Engineering and Sciences  
Monterrey NL, México, {A01370447, dianahalc, avallejo, david.ibarra,  
rmm}@itesm.mx*

---

**Abstract:** El monitoreo de la condición de una máquina es indispensable en los centros de mecanizado para administrar el mantenimiento preventivo/correctivo. La calidad y la eficiencia dependen de las condiciones del husillo. Se presenta un análisis detallado de los métodos *Transformada Rápida de Fourier*, *Transformada Corta de Fourier*, usando una ventana *Hanning* con 50% de traslape y *Pre-blanqueamiento del Cepstrum* para la detección de fallas en los rodamientos de un husillo. La propuesta permite la detección de fallas del elemento rodante, de la pista interna y externa con buena precisión.

*Keywords:* Diagnóstico Fallas, Vibraciones, Husillos, Transformada Rápida de Fourier

---

## 1. INTRODUCCIÓN

En las industrias manufactureras que cuentan con centros de mecanizado, la confiabilidad es muy importante, no es suficiente lograr una alta disponibilidad, sino también minimizar la probabilidad de falla en las máquinas críticas, es decir, lograr una alta confiabilidad.

Las consecuencias de una falla pueden ir desde la pérdida de producción, horas-hombre de operación infructíferas, hasta la degradación y daño de las propias máquinas. Una gran disponibilidad no implica una gran confiabilidad, pero una gran confiabilidad sí involucra una buena disponibilidad y seguridad.

Teniendo en cuenta que la calidad de las piezas de los centros de mecanizado depende de su precisión dimensional, y ésta a su vez, no solo depende de la máquina herramienta, sino también de la condición del husillo.

Un sistema de monitoreo del husillo en tiempo real, además del reconocimiento temprano de las fallas, reduciría notablemente el número de piezas defectuosas y el posible tiempo de paro.

Existen dos grandes tipos de sistemas de monitoreo de husillos: los sistemas que miden con contacto físico y los que no. Los acelerómetros son un ejemplo del primer tipo, los sistemas ópticos y acústicos son ejemplos del segundo tipo.

Se presentará un análisis de las señales de vibración de rodamientos de un husillo usando algoritmos basados en la *Transformada Rápida de Fourier* (*FFT*, *Fast Fourier Transform*), *Transformada Corta de Fourier* (*STFT*, *Short Time Fourier Transform*) y *Cepstrum* para de-

tección/diagnóstico de fallas. La Tabla 1 resume los acrónimos utilizados.

La *FFT* es uno de los métodos de análisis de frecuencia más utilizado en el diagnóstico de fallas en equipos rotativos, por su capacidad de analizar señales transitorias y obtener información en el dominio de la frecuencia. Estas señales son generalmente vibraciones o emisiones acústicas las cuales encubren las fallas de la máquina. La *FFT* se basa en la *Transformada Discreta de Fourier* (*DFT*, *Discrete Fourier Transform*), siendo *FFT* una versión más eficiente de *DFT*. Esta versión de la *DFT* cuando la señal es discreta y finita, corresponde a las series de Fourier en que la transformada directa se divide por la longitud de la señal  $N$  para proporcionar componentes de la serie de Fourier correctamente escalados. Si se usa *DFT* en señales transitorias o estacionarias aleatorias, se debe ajustar el escalamiento siguiendo el criterio de Nyquist, Randall (2011).

Otro enfoque para analizar señales de vibración y/o de emisión acústica es la *Transformada de Tiempo Corto de Fourier* (*STFT*, *Short Time Fourier Transform*), la cual es ampliamente utilizada debido a su capacidad para analizar señales no estacionarias, Li (2002). Tradicionalmente, se utilizan las distribuciones tiempo-frecuencia para revelar los patrones de falla de rodamientos, que representan la energía de las señales en las funciones bidimensionales de tiempo y frecuencia. La *STFT* es una de las distribuciones de tiempo-frecuencia más populares. La idea básica es dividir la señal en segmentos con una ventana de tiempo corto, y luego aplicar *FFT* a cada segmento. La *STFT* de una señal es:

$$X_{STFT}(w) = \sum_{n=0}^{\infty} x(n)h(n - mR)e^{-jwn} \quad (1)$$

---

<sup>\*</sup> Los autores agradecen al Tecnológico de Monterrey y CONACyT por su apoyo parcial.

# Curriculum Vitae



*Oscar Darío Tamayo Pazos.* was born in Quito Ecuador on October 13<sup>th</sup>, 1993. He received the degree of Mechatronics Engineer from the Instituto Tecnológico de Monterrey Campus Estado de México in December 2016. He was part of Automotive Consortium research group, as member actively participated with the Bocar Group in the project named: Monitoring and Diagnosis of High Speed Machining Spindles. He pursuit a Master Degree in Science with Manufacturing Systems specialization at Tecnológico de Monterrey, Escuela de Ingeniería y Ciencias, Campus Monterrey from August 2016 to December 2018.

This document was typed in using L<sup>A</sup>T<sub>E</sub>X by Oscar Darío Tamayo Pazos.